National Library of Canada
Acquisitions and Bibliographic Services Branch
395 Wellington Street
Ottawa, Ontario
K1A 0N4

Bibliothèque nationale du Canada
Direction des acquisitions et des services bibliographiques
395, rue Wellington
Ottawa (Ontario)
K1A 0N4

Your file *Votre référence*

Our file *Notre référence*

NOTICE

The quality of this microform is heavily dependent upon the quality of the original thesis submitted for microfilming. Every effort has been made to ensure the highest quality of reproduction possible.

If pages are missing, contact the university which granted the degree.

Some pages may have indistinct print especially if the original pages were typed with a poor typewriter ribbon or if the university sent us an inferior photocopy.

Reproduction in full or in part of this microform is governed by the Canadian Copyright Act, R.S.C. 1970, c. C-30, and subsequent amendments.

AVIS

La qualité de cette microforme dépend grandement de la qualité de la thèse soumise au microfilmage. Nous avons tout fait pour assurer une qualité supérieure de reproduction.

S'il manque des pages, veuillez communiquer avec l'université qui a conféré le grade.

La qualité d'impression de certaines pages peut laisser à désirer, surtout si les pages originales ont été dactylographiées à l'aide d'un ruban usé ou si l'université nous a fait parvenir une photocopie de qualité inférieure.

La reproduction, même partielle, de cette microforme est soumise à la Loi canadienne sur le droit d'auteur, SRC 1970, c. C-30, et ses amendements subséquents.

Canada

UNIVERSITY OF ALBERTA

SIMULATION OF ULTRA SHORT LASER PULSES IN STEEP GRADIENT PLASMAS

by

CLARENCE KWOK-YAN KAN

A THESIS

SUBMITTED TO THE FACULTY OF GRADUATE STUDIES AND RESEARCH IN PARTIAL FULFILLMENT OF THE REQUIREMENTS FOR THE DEGREE OF MASTER OF SCIENCE

DEPARTMENT OF ELECTRICAL ENGINEERING

EDMONTON, ALBERTA

FALL, 1992

National Library of Canada
Bibliothèque nationale du Canada

Canadian Theses Service
Service des thèses canadiennes

Ottawa, Canada
K1A 0N4

The author has granted an irrevocable non-exclusive licence allowing the National Library of Canada to reproduce, loan, distribute or sell copies of his/her thesis by any means and in any form or format, making this thesis available to interested persons.

L'auteur a accordé une licence irrévocable et non exclusive permettant à la Bibliothèque nationale du Canada de reproduire, prêter, distribuer ou vendre des copies de sa thèse de quelque manière et sous quelque forme que ce soit pour mettre des exemplaires de cette thèse à la disposition des personnes intéressées.

The author retains ownership of the copyright in his/her thesis. Neither the thesis nor substantial extracts from it may be printed or otherwise reproduced without his/her permission.

L'auteur conserve la propriété du droit d'auteur qui protège sa thèse. Ni la thèse ni des extraits substantiels de celle-ci ne doivent être imprimés ou autrement reproduits sans son autorisation.

ISBN 0-315-77073-2

Canada

UNIVERSITY OF ALBERTA

RELEASE FORM

NAME OF AUTHOR: Clarence Kwok-Yan Kan

TITLE OF THESIS: Simulation of Ultra Short Laser Pulses in Steep Gradient Plasmas

DEGREE: Master of Science

YEAR THIS DEGREE GRANTED: FALL, 1992

Permission is hereby granted to the University of Alberta Library to reproduce single copies of this thesis and to lend or sell such copies for private, scholarly or scientific research purposes only.

The author reserves all other publication and other rights in association with the copyright in the thesis, and except as hereinbefore provided neither the thesis nor any substantial portion thereof may be printed or otherwise reproduced in any material form whatever without the author's prior written permission.

Clarence Kan

302-3915-107 ST

Edmonton, Alberta

Canada T6J 2N7

Date: September 30, 1992

UNIVERSITY OF ALBERTA

FACULTY OF GRADUATE STUDIES AND RESEARCH

The undersigned certify that they have read, and recommend to the Faculty of Graduate Studies and Research for acceptance, a thesis entitled Simulation of Ultra Short Laser Pulses in Steep Gradient Plasmas submitted by Clarence Kwok-Yan Kan in partial fulfillment of the requirements for the degree of Master of Science.

C.E. Capjack (supervisor)

R. Rankin (supervisor)

R. Fedosejevs (committee member)

G. Rostoker (external examiner)

Date: September 30, 1992

Dedication

To my parents.

Abstract

With recent advances of high power sub-picosecond laser technology, a new field of laser applications has been created. The irradiation of such intense laser light onto a solid target can produce ultra-short X-ray pulses [6,7,8] and the resulting plasma formed at the surface of the target can be used as a gain medium for X-ray lasers [8]. The study of the sub-picosecond interactions generally consists of experimental investigations, theoretical analysis and computer modelling of the interaction processes. In this thesis, one dimensional computer simulations are used to examine this type of laser-plasma interaction, with emphasis on the absorption of the laser light and the resulting hydrodynamic response of the plasma.

The modelling work undertaken in this project consists primarily of the development of a laser code and the incorporation of this code into an existing plasma fluid or hydro code. The laser code is designed to determine the electric field inside the plasma by numerically solving the wave equation for a plasma whose properties are assumed to vary in only one direction. The absorption of the laser light is then calculated from fundamental electromagnetic relations. The hydrodynamic response of the plasma due to absorption is obtained by a hydro-code which solves the energy and momentum equations for a two-fluid plasma. The laser code and hydro-code are coupled through an energy term in the fluid energy equation. The laser light absorption and the hydrodynamic response are then solved self-consistently.

Results obtained from the simulations include the time evolution of the plasma hydrodynamic behavior, the dependence of absorption on angle of laser incidence and the

sensitivity of plasma parameters to the angle of laser incidence. The calculated time response of the electron temperature is also compared with theoretical predictions.

Acknowledgement

The author would like to thank his supervisors, Dr. C.E. Capjack and Dr. R. Rankin, for their constant guidance and support. The author would also like to thank Dr. R. Fedosejevs for his constructive theoretical and simulation advice. Further thanks go to Dr. W. Rozmus and Dr. V. Tikhonchuk for their helpful discussion on their theoretical models on short-pulse laser-plasma interactions.

Table of Contents

Chapter	Page
1. Introduction	1
1.1 Physical Model	4
1.2 Computational Scheme	7
1.3 Four Simulation Features	9
1.4 Other Similar Modelling Approaches	10
2. The Laser Code	12
2.1 The Wave Equation	13
2.2 Zero Gradient Propagation Modes	18
2.3 Modelling of Damping Mechanisms	21
2.4 Boundary Conditions	27
2.5 Calculation of Absorption	34
2.6 Normalizing Equations	37
2.7 Value for the Ratio of Specific Heats	40
2.8 Numerical Scheme	40
2.9 Structure of Program	51
2.10 Summary	53
3. The Hydro-Code	54
3.1 Introduction to MEDUSA	54
3.2 Mathematical Model	55
3.2.1 Equation of Motion	58

3.2.2 Equation of State and Calculation of Ionization 59

3.2.3 Initial Conditions and Boundary Conditions 60

3.3 Numerical Scheme 60

3.3.1 Method of Solution 64

3.4 Interfacing between MEDUSA and EMREAB 65

3.4.1 MEDUSA's and EMREAB's Coordinate Systems 65

3.4.2 Input Conversion 66

3.4.3 Output Conversion 68

3.5 Summary 68

4. Simulation Results 71

4.1 Simulations with Fixed Profiles 73

4.1.1 Long Scale-Length Results 74

4.1.2 Short Scale-Length Results 76

4.2 Simulations with Time-Dependent Profiles 79

4.2.1 Typical Results 81

4.2.2 Angular Dependence of Absorption and Plasma Parameters 82

4.2.3 Comparison with Theoretical Predictions 86

4.3 Summary 87

5. Conclusions 104

References 106

Appendix A: The CRR Collisional Frequency 108

Appendix B: Listing of EMREAB 111

List of Tables

Table — Page

4.1 Calculated Plasma Parameters for $I_{max} = 10^{14}$ W/cm^2 84

4.2 Calculated Plasma Parameters for $I_{max} = 2.5 \cdot 10^{15}$ W/cm^2 85

List of Figures

Figure — Page

1.1 Physical Model 5

1.2 Computational Scheme 8

2.1 The Coulomb Logarithm 24

2.2 Collision Frequencies 26

2.3 Boundary Conditions at x = 0 30

2.4 The Staggered Mesh 42

2.5 Difference Scheme: a) j = odd; b) j = even 43

2.6 The Pentadiagonal Structure 48

2.7 Structure of Laser Code 52

3.1 MEDUSA's Lagrangian Grid 61

3.2 The Five Time Level Scheme 62

3.3 Input Profile Transformation 67

3.4 Output Profile Transformation 69

4.1 Electric field and absorption profiles calculated for a long scale-length linear density profile at zero angle of incidence 88

4.2 Electric field and absorption profiles calculated for a long scale-length exponential density profile at zero angle of incidence 89

4.3 Electric field and absorption profiles calculated for a long scale-length exponential density profile at angle of incidence = 20° 90

4.4 Angular dependence of total absorption fraction for a long scale-length linear density profile 91

4.5 Dependence of total absorption fraction on density scale-length 92

4.6 Electric field and absorption profiles calculated for a short scale-length linear density profile at zero angle of incidence 93

4.7 Electric field and absorption profiles calculated for a short scale-length exponential density profile at zero angle of incidence 94

4.8 Electric field and absorption profiles calculated for a short scale-length linear density profile at angle of incidence = 20° 95

4.9 Angular dependence of total absorption fraction for a short scale-length linear density profile 96

4.10 Time evolution of electron density, electron temperature, ionization level and absorption at zero angle of incidence 97

4.11 Time-dependent absorption fraction at zero angle of incidence 98

4.12 Time evolution of electron density, electron temperature, ionization level and absorption at angle of incidence = 40° 99

4.13 Time-dependent absorption fraction at angle of incidence = 40° 100

4.14 Angular dependence of time-integrated absorption for $I_{max} = 10^{14}$ W/cm^2 . . 101

4.15 Angular dependence of time-integrated absorption for $I_{max} = 2.5 \cdot 10^{15}$ W/cm^2 102

4.16 Electron temperature at maximum local absorption 103

List of Symbols

Symbols	Definition
$\mathbf{A}_i$	amplitude of incoming electromagnetic wave at low density boundary
$\mathbf{B}$	magnetic field
$\mathbf{B}_i$	amplitude of outgoing electromagnetic wave at low density boundary
CRR	Cauble, Rogers and Rozmus
c	speed of light in vacuum
$\mathbf{D}_p$	amplitude of plasma wave at low density boundary
dM	mass in each hydro-cell
EM	electromagnetic
$\mathbf{E}$	electric field
$\mathbf{E}_{em}$	electromagnetic wave
$\mathbf{E}_{es}$	electrostatic or plasma wave
Eq.	equation
e	elementary charge
FWHM	full width at half maximum
fs	femtosecond
H	heat flow
I_{ej}	total absorption as calculated by Eq. (2.80)
I_s	total absorption as calculated by Eq. (2.84)
I_i	intensity of incident laser
I_{max}	maximum laser intensity

$\mathbf{J}$	current density
J	rate of bremsstrahlung emission
K	rate of exchange of energy between ions and electrons
K_B	Boltzmann constant
$\mathbf{k}_o$	wavevector of incident laser
k_y	component of k_o in the y-direction
$\mathbf{k}_{em}$	wavevector of electromagnetic wave
$\mathbf{k}_{es}$	wavevector of electrostatic wave
L	density scale-length
$\ln\Lambda$	Coulomb logarithm
m	atomic mass number
m_e	mass of electron
m_H	mass of proton
n_i	total ion number density
n_e	total electron number density
$\langle n_i \rangle$	hydrodynamic ion number density
$\langle n_e \rangle$, n_o	hydrodynamic electron number density
n_i'	perturbed ion number density
n_e'	perturbed electron number density
p	hydrodynamic pressure
p_i	ion pressure
p_e	electron pressure
ps	picosecond

Q	rate of viscous shock heating
q	artificial viscous pressure
R	hydro-code coordinates
S	Poynting vector
$\langle S \rangle$	average Poynting vector
T_i	ion temperature
T_e	electron temperature
U_i	internal energy for ions
U_e	internal energy for electrons
u	electromagnetic field energy
V	specific volume
V_i	total ion velocity
V_e	total electron velocity
$\langle V_i \rangle$	hydrodynamic ion velocity
$\langle V_e \rangle$	hydrodynamic electron velocity
V_i'	perturbed ion velocity
V_e'	perturbed electron velocity
V_{th}	electron thermal velocity
W_{ej}	local absorption as calculated by Eq. (2.75)
$\langle W_{ej} \rangle$	time average of $\langle W_{ej} \rangle$
W_s	absorption as calculated by Eq. (2.85)
$\langle W_s \rangle$	time average of $\langle W_s \rangle$
X	rate of laser absorption

x	laser code coordinates
Z	ionic charge number
$\langle Z \rangle$	average ionization number
α	absorption fraction
α_T	time-integrated absorption fraction
γ	ratio of specific heats
λ_o	wavelength of incident laser
ν	damping rate
ν_c	collisional frequency
ν_l	collisionless or Landau damping rate
ω	frequency of incident laser
ω_p	plasma frequency
ρ	plasma mass density
θ	angle of laser incidence
θ_p	angle of propagation of plasma wave

Chapter 1. Introduction

A plasma is essentially a gas of particles with some or all of the electrons stripped off from the atoms. It is approximately electrically neutral overall and its elements can exhibit non-local interactions with one another [1,2]. Plasmas are said to constitute about ninety-nine percent of the matter in the known universe [1]. Common places where they can be found in nature include the earth's upper atmosphere, interplanetary space, and stellar interiors [3]. On earth, plasmas can also be produced artificially. For example, one way of creating a plasma is through the electrical breakdown of gases. An example is the plasma found inside a neon tube where the electrons of the neon gas are removed from the atoms by electrons constituting an electric current. Another way of producing a plasma involves the irradiation of a target material such as aluminum with energetic and highly coherent monochromatic radiation, namely laser light.

This latter method of generating plasmas and the resulting laser-plasma interaction has received tremendous attention from the scientific world in the past few decades. This is mainly due to a number of important potential applications. The foremost plausible application is the fulfillment of laser fusion in which the laser induced plasma is heated and compressed to an extent that thermonuclear fusion can take place. Thermonuclear fusion is the mechanism by which the sun obtains its energy and is thought to be the ultimate energy source of the future due to the relatively inexhaustible supply of fuel [4]. Some of the other major applications of laser-plasma interactions include laser material processing in which substances can be drilled, welded or cut. Another example is laser

micro-lithography in which microelectronic circuits with very small feature sizes can be fabricated [5].

Recently a new regime of laser plasma interaction has been under vigorous investigation using advanced picosecond and subpicosecond laser technology. In this regime the target material is heated by a very short duration laser pulse with a time duration in the pico- or subpicosecond range. It is thought that such an interaction can be used as a source for high energy ultra-short X-ray pulses [6-8]. It is also believed that after the picosecond laser has been switched off, the rapidly cooled plasma can be utilized as a gain medium for the production of X-ray lasers [6,8]. One application of high energy X-ray pulses is X-ray lithography. Compared to conventional optical lithography, X-ray lithography can be used to fabricate micro-electronic circuits with much smaller feature sizes [9]. X-ray sources produced by a picosecond laser-plasma interaction is also thought to be much more economical than the conventional source -- the synchrotron -- which can cost millions of dollars to build [9]. X-ray lasers, as discussed in [10], also have a number of important applications. These applications include the creation of high resolution holograms of micro-biological elements such as the structure of key proteins and the DNA structure; and the inspection and production of very high density plasmas which can mimic the sun's interior where thermonuclear fusion takes place.

An important aspect of the study of picosecond laser plasma interactions is the computer modelling of the absorption of the incident laser light and the resulting plasma dynamics. The modelling of the absorption of the incident laser light and the resulting plasma dynamics is of particular importance because the absorption of the laser energy

and the evolution of the state of the target material are the primary manifestations of the laser plasma interaction. Without a knowledge of these two mechanisms, it is impossible to correctly predict other important quantities or processes, such as the ionization of the atoms, the distribution of the electrons in various energy levels, the transport of radiation, and the emission of X-rays.

In the past twenty years, the use of digital computers to study physical phenomena has increased rapidly and steadily. This is in part due to advances in computer technology. Very powerful computers have been built in which millions of calculations can now be performed in a matter of seconds. Such computers enable investigators to readily solve many complex mathematical equations depicting physical phenomena. An agreement between simulation and experimental results contributes to and adds confidence to the choice for the theoretical models employed in the simulation, which in turn sheds light on the actual physical processes involved. Moreover, a successful computer simulation can often be utilized to help design further experiments so that a deeper understanding of the phenomenon can be obtained.

The goal of this project is to develop a computer simulation code which is capable of modelling and predicting the absorption of laser light and the resulting plasma dynamics during a high power short-pulsed laser plasma interaction. This will enhance the understanding of the laser plasma interaction phenomenon when ultra-short pulses are involved.

The remainder of this thesis is divided as follows. The rest of this chapter will give a more specific physical description of the problem to be addressed and an outline

of the computational method used to solve it. This is followed by a discussion of the basic features of the simulations considered in this project and modelling schemes used by other research groups. Chapters two and three will detail the computer codes used in the simulations and the mathematical models and numerical methods involved. Chapter four will present the simulation results. The final chapter will deliver some concluding remarks and propose future enhancements to the simulations.

1.1. Physical Model

The geometry of the model is illustrated schematically in figure 1.1. The incident laser light is modeled as an electromagnetic plane wave propagating in the x-direction and impinging at an angle to the surface of the target material. The wave is assumed to be p-polarized meaning that the electric field associated with the wave is parallel to the plane of incidence and perpendicular to the direction of the wave propagation. For pulsed laser light, the intensity of the incident light is a function of time. The target material is assumed to be situated in a vacuum. The target and laser beam dimensions in the y- and z-directions are assumed sufficiently large so that only variations in the x-direction are significant. In figure 1.1 it is assumed that the target can be decomposed into two regions in the x-direction. The plasma region on the right is produced by laser heating. This is where the laser plasma interaction takes place. The region on the left is considered to be solid. As time progresses, part of this region will melt and eventually turn into a plasma due to the heat flow from the plasma region. Also, it is assumed that the target material in the positive x direction is sufficiently thick that there is no penetration of the laser light

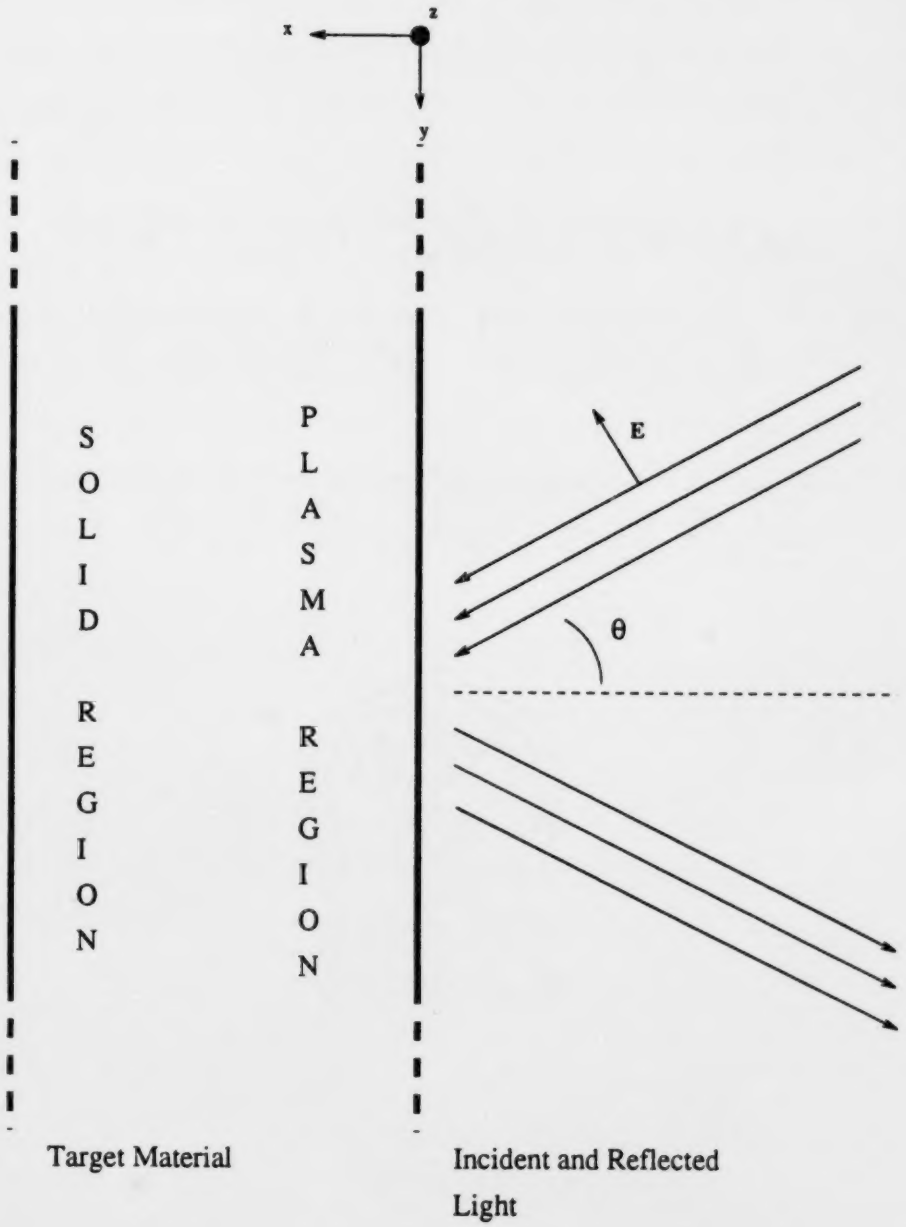

Figure 1.1: Physical Model.

through the target. In other words, the light is either absorbed or reflected.

The laser-plasma interaction itself can be decomposed into two processes. The first is the propagation and absorption of the incident light. The second is the hydrodynamics of the plasma.

The absorption of the incident electromagnetic (or EM) wave inside the plasma is manifested by the damping of the wave. As the wave propagates through the plasma, energy is transferred from the EM field to the plasma. Two damping mechanisms are considered in this model: collisional damping and collisionless or Landau damping. Collisional damping is caused by electron-ion collisions in the plasma. When electrons oscillate back and forth due to the presence of a periodic EM field and collide with the heavier ions, it is known [11] that the EM wave will experience an effective damping. Hence energy is transferred from the wave to the plasma. Landau damping arises primarily from the distribution of the electron velocities [1]. Kinetic theory indicates that electrons in a plasma do not all have the same velocity but rather have a distribution of velocities. When the distribution is such that there are more electrons travelling slower than the wave's phase velocity than those travelling faster than the wave's phase velocity (which is the case for a Maxwellian plasma), more electrons are accelerated than are slowed down. Since acceleration of electrons takes energy from the field and their deceleration adds energy to the field, the net outcome is that the electromagnetic wave is damped and loses its energy to the plasma.

As energy is fed into the plasma its hydrodynamic and thermodynamic properties change. The plasma will expand, its temperature and pressure will rise and its density

will change. Heat will flow from the high temperature plasma region to the low temperature solid region and thus energy will be transported to regions where the laser light cannot penetrate.

Although the laser-plasma interaction can be broken into two parts, the absorption of the laser light and the hydrodynamics of the plasma are two interdependent processes. The absorption of the laser light depends upon parameters such as the density and temperature of the plasma while the hydrodynamics of the plasma also depends on how much energy is being absorbed.

1.2. Computational Scheme

In light of the physical model just described, it is seen that the computational structure of the simulations can be decomposed into two components with one calculating the absorption of the laser energy and the other predicting the hydrodynamics of the plasma. In fact, as illustrated in figure 1.2, the overall computational approach used here utilizes two separate yet interdependent computer codes to realize the simulation model. The laser code is used to model the propagation and absorption of the incident laser light while the hydro-code is use to predict the target material's hydrodynamic response and thermodynamic properties. Note that while the laser code is to be developed in this project, an existing computer program MEDUSA will be modified and used for describing the hydrodynamics in the simulations.

The overall computational scheme can be described briefly as follows. At time equal to zero, a set of initial conditions such as the target's initial temperature and density

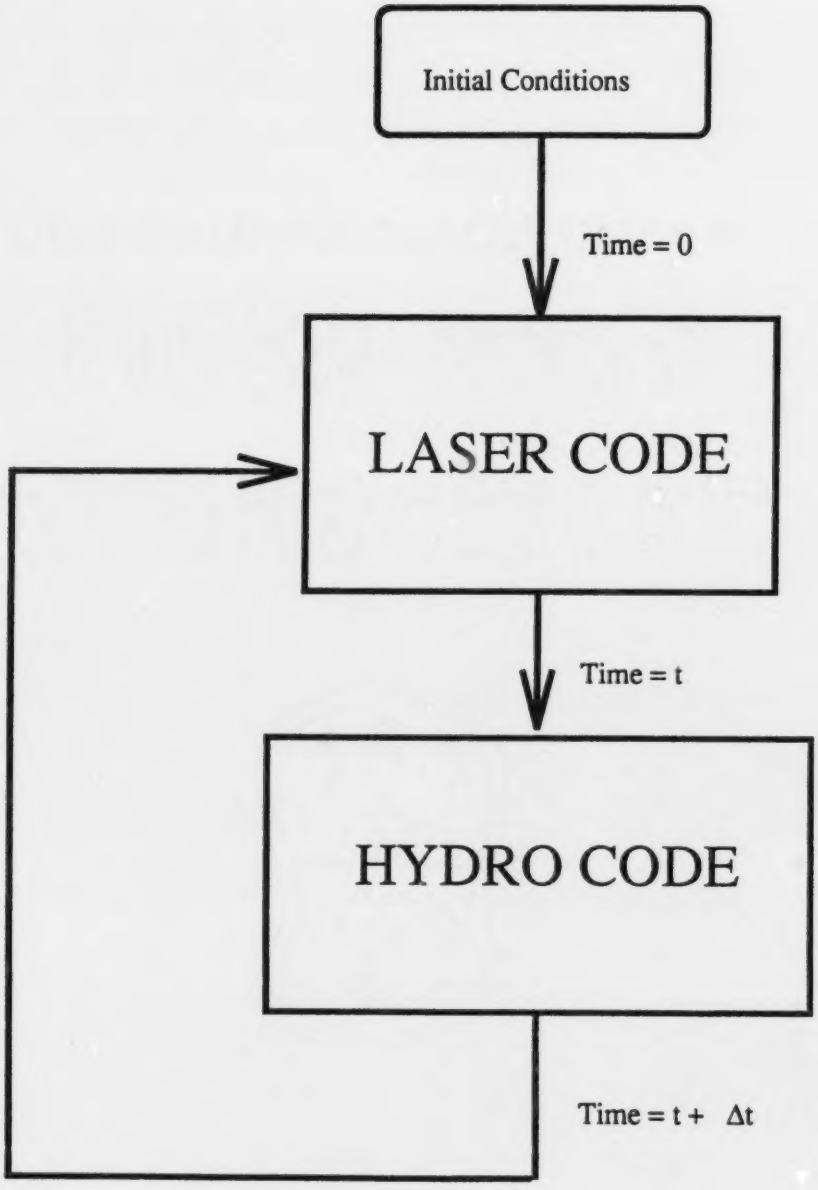

Figure 1.2: Computational Scheme.

and the laser light field are imposed. A time stepping procedure is then employed. The laser code is used to compute the propagation and absorption of the laser light based on these conditions. Next, the hydro-code calculates a new set of target hydrodynamic and thermodynamic properties due to the absorption just determined. Now time is advanced. For a pulsed laser, the intensity is also changed according to a preset function of time. The new set of target properties are then fed back into the laser code and the calculation cycle continues until the end of the simulation is reached.

1.3. Four Simulation Features

The first two related features of the simulations considered in this investigation are the one dimensional nature of the problem and the ultra-short duration of the laser pulse. An ultra-short laser pulse refers to a pulsed laser light with duration in the picosecond or sub-picosecond range. To date, laser systems have been developed which are capable of generating pulses ranging from 1 picosecond down to 250 femtosecond [6-8]. In such a short time scale, it is believed that the interaction is essentially one dimensional due to the limited hydrodynamic motion of the plasma [6]. A one dimensional interaction means that all the interacting variables, such as the amount of absorption, plasma density and temperature, can be considered as varying only in one direction -- the x-direction as in the simulations considered in this study.

The third feature is the intensity of the incident laser light. The intensity is a measure of the power per unit area carried by the EM wave. The intensity associated with a pulsed laser usually refers to the intensity at the peak of the laser pulse or the

maximum intensity. As discussed in [8], the intensity level can be categorized into three domains according to the laser plasma interaction regimes involved. At low laser intensity the target material remains a solid and absorption arises from the skin depth effect which is examined, for example, in [12]. At high intensities a very thin film of plasma is formed at the plasma vacuum boundary and the absorption is thought to be caused by the various wave damping mechanisms. At still higher intensities, nonlinear mechanisms are involved in the interaction and anomalous absorption occurs. In this investigation, the high intensity linear regime is considered.

The fourth feature of the simulations is the density gradient of the plasma. In the high intensity regime the plasma formed at the surface does not have uniform density. The density of the plasma usually goes from nearly zero at the plasma-vacuum boundary to solid density at the plasma-solid boundary. A very steep density gradient means that the density scale length, which is a measure of the transition from nearly zero density to solid density, is very short and can be of the order of a fraction of the incident laser wavelength.

1.4. Other Similar Modelling Approaches

The absorption of laser light by steep density gradient plasmas has also been investigated theoretically by a number of research groups [6-8]. Fedosejevs et al [6] and Kieffer et al [8] independently used similar modelling approaches. They both calculated the absorption by first solving the propagation of the laser light in a plasma with a presumed linear or exponential density profile. Only the collisional damping mechanism

was considered and the hydrodynamic motion of the plasma was neglected. In addition, the collision frequency, which is a measure of the amount of collisional damping, was assumed to be directly proportional to the density. To compare their theoretical predictions for the absorption with their experimental results, they had to infer the density scale length and the collision frequency from the experiments and use them as parameters for the calculation of absorption. Chaker et at [7] went further to incorporate the propagation and absorption solver into a one dimensional hydro-code to calculate the absorption as well as the evolution of the hydrodynamic and thermodynamic variables. However the simulation was done only at zero laser incident angle and the angular dependence of the absorption was not determined.

In the simulations proposed for this study, the absorption of laser energy and the time evolution of the plasma will be solved self-consistently. That is, the evolution of the plasma thermodynamic and hydrodynamic variables and the absorption of the laser light will all be calculated by solving the relevant mathematical equations from the beginning of the simulation to the end. The angle of incidence can vary from zero to ninety degrees in order that the angular dependence of the absorption can be obtained. Finally it is believed that instead of having to acquire the density scale length and collisional frequency from experiments, the simulation can predict these quantities from the calculations.

Chapter 2. The Laser Code

As in all computer modelling of physical phenomena, the simulation process involves obtaining solutions to the mathematical equations that depict the particular phenomena. With no exception, the laser code described herein determines the propagation and absorption of the incident laser light by numerically solving the wave equation inside the plasma. The wave equation is a second order vector differential equation describing the behavior of the electric field inside the plasma. It can be solved by employing appropriate boundary conditions and utilizing relevant numerical methods. Once the electric field is found, quantities such as the magnetic field, the current density, the energy flux as well as the absorption can also be determined from fundamental electromagnetic relations.

This chapter details the development of a laser code that can be used to describe the wave propagation in steep density gradients. The derivation of the wave equation is given first. This is followed by a discussion of the two propagating modes found in low density and low gradient plasmas and the modelling of the damping mechanisms. Next the appropriate boundary conditions are derived. Then the normalization of the equations and the numerical scheme are discussed. Lastly, the structure of the code is described.

It should be noted that all of the equations and quantities used in the laser code are expressed in Gaussian units.

2.1 The Wave Equation

The derivation of the wave equation begins with a number of observations and assumptions. The electric and magnetic fields inside the plasma are assumed to oscillate with the same frequency ω as the driving incident wave and have a temporal dependence of $e^{-i\omega t}$. The electron and ion motion is assumed to consist of two parts. The hydrodynamic or background motion arises from the expansion of the plasma while the oscillatory or perturbed motion which also varies as $e^{-i\omega t}$ is due to the ambient oscillatory EM field. The magnitudes of the hydrodynamic velocities of the ions and electrons are assumed to be negligible when compared with their oscillatory motions. This can be justified by considering the time scale over which the plasma would expand and the corresponding oscillatory time for electrons. Normally the electrons will oscillate many times before the plasma can expand to just a fraction of its size. Furthermore the perturbed ion motion is neglected in comparison with the electron motion. This is due to the fact that ions are much heavier than the electrons and therefore react much more slowly to the EM field than the electrons. Furthermore, ω is assumed to be the dominant frequency. In any calculations, terms that vary with different frequencies are assumed to have negligible amplitudes and are ignored.

The fundamental equations describing electromagnetic fields in a plasma medium are the Maxwell equations:

$$\nabla \cdot \boldsymbol{E} = 4\pi (Zn_i - n_e)e \qquad (2.1)$$

$$\nabla \cdot \boldsymbol{B}=0 \tag{2.2}$$

$$\nabla \times \boldsymbol{E}=-\frac{1}{c}\frac{\partial \boldsymbol{B}}{\partial t} \tag{2.3}$$

$$\nabla \times \boldsymbol{B}=\frac{4\pi}{c}\boldsymbol{J}+\frac{1}{c}\frac{\partial \boldsymbol{E}}{\partial t} \tag{2.4}$$

where **E** and **B** are the electric and magnetic fields respectively, **J** is the current density, Z is the ionic charge number, n_i and n_e are the ion and electron number densities respectively, e is the elementary charge and c is the speed of light in vacuum. The general wave propagation equation in matter is readily obtained by taking the curl of Eq. (2.3) and substituting for $\nabla \times \mathbf{B}$ by using Eq. (2.4) to give:

$$\nabla^2 \boldsymbol{E}-\nabla(\nabla \cdot \boldsymbol{E})-\frac{1}{c^2}\frac{\partial^2 \boldsymbol{E}}{\partial t^2}=\frac{4\pi}{c^2}\frac{\partial \boldsymbol{J}}{\partial t} \tag{2.5}$$

In deriving Eq. (2.5) two mathematical identities were used. The first was the vector identity $\nabla \times (\nabla \times \mathbf{A}) = \nabla(\nabla \cdot \mathbf{A}) - \nabla^2 \mathbf{A}$. The second was that the operators $\nabla \times \partial/\partial t$ and $\partial/\partial t \nabla \times$ are equivalent because time and space coordinates are independent variables. The current density is defined as:

$$\boldsymbol{J}=Zn_i e\boldsymbol{V}_i-n_e e\boldsymbol{V}_e \tag{2.6}$$

where $\mathbf{V}_i$ and $\mathbf{V}_e$ are the ion and electron velocities. By denoting hydrodynamic quantities by a < > term and the perturbed quantities with a prime (′), the velocities and densities can be expressed as:

$$V_i=\langle V_i\rangle+V_i'\approx 0+0=0 \tag{2.7}$$

$$n_i=\langle n_i\rangle+n_i'\approx\langle n_i\rangle \tag{2.8}$$

$$V_e=\langle V_e\rangle+V_e'\approx V_e' \tag{2.9}$$

$$n_e=\langle n_e\rangle+n_e' \tag{2.10}$$

Here the ion and electron's hydrodynamic velocities and the ion's perturbed motion have been neglected according to the assumptions made at the beginning of this section. Moreover the perturbed ion density has also been ignored. This is because the perturbed ion motion is so small that the resulting contribution to the ion's density should be negligible. However the hydrodynamic density contributions have been retained because, unlike the hydrodynamic velocities, they are usually much larger than their oscillatory counterparts. The perturbed electron density has also been retained due to the non-vanishing electron oscillation. In the simulations, plasma quasi-electrical-neutrality will be assumed. That is:

$$\langle n_e\rangle=Z\langle n_i\rangle=n_o \tag{2.11}$$

Hence the current density for the plasma is given by:

$$J=0-e(\langle n_e\rangle+n_e')V_e'\approx -e\langle n_e\rangle V_e'=-en_oV_e' \tag{2.12}$$

where the second order term $n_e'V_e'$ which varies as $e^{-i2\omega t}$ has been ignored and the hydrodynamic electron density is now written as n_o.

The fluid equation for electron momentum transport is given by:

$$m_e n_e\left(\frac{\partial V_e}{\partial t}+V_e\cdot\nabla V_e\right)=-en_e(E+\frac{V_e}{c}\times B)-\nabla p_e-m_e n_e \nu V_e \tag{2.13}$$

where m_e is the electron's mass, p_e is the electron pressure, ν is a damping frequency used to model the absorption mechanisms. The momentum equation essentially states that the change in momentum per unit volume for a fluid element of electrons with mass density $m_e n_e$ is due to the Lorentz force per unit volume $-en_e(\mathbf{E}+(\mathbf{V}_e/c)\times\mathbf{B})$, the negative of the pressure gradient ∇p_e and the dissipative force per unit volume $-m_e n_e \nu \mathbf{V}_e$. Assuming an adiabatic equation of state for the electrons, the electron pressure gradient can be expressed in terms of the density gradient and temperature as:

$$\nabla p_e=\gamma K_B T_e \nabla n_e \tag{2.14}$$

where K_B is the Boltzmann constant, T_e is the electron temperature and γ is the ratio of specific heats. Setting the second order terms $\mathbf{V}_e\cdot\nabla\mathbf{V}_e$ and $(\mathbf{V}_e'/c)\times\mathbf{B}$ in Eq. (2.13) to zero and using Eq. (2.9) and Eq. (2.14), Eq. (2.13) becomes:

$$\frac{\partial V_e'}{\partial t}=-\frac{e}{m}E-\frac{\gamma K_B T_e}{m_e}\frac{\nabla n_e}{n_e}-\nu V_e' \tag{2.15}$$

Furthermore, the density gradient term can be written as:

$$\frac{\nabla n_e}{n_e}=\frac{\nabla(n_o+n_e')}{n_o+n_e'}=\frac{1}{n_o}\left(\frac{1}{1+n_e'/n_o}\right)\nabla(n_o+n_e') \tag{2.16}$$

Assuming $n_e' \ll n_o$:

$$\frac{\nabla n_e}{n_e} \approx \frac{1}{n_o}\left(1-\frac{n_e'}{n_o}\right)\nabla(n_o+n_e) = \frac{1}{n_o}\left(\nabla n_o + \nabla n_e' - \frac{n_e'}{n_o}\nabla n_o - \frac{n_e'}{n_o}\nabla n_e'\right) \tag{2.17}$$

Eq. (2.17) is then linearized by neglecting the d.c. term ∇n_o and the second harmonic term $(n_e'/n_o)\nabla n_e'$ to give:

$$\frac{\nabla n_e}{n_e} \approx \frac{\nabla n_e'}{n_o} - \frac{n_e'\nabla n_o}{n_o^2} \tag{2.18}$$

Now using Eq (2.1), n_e' can be expressed in terms of **E** as:

$$\nabla\cdot\boldsymbol{E} = 4\pi e(Zn_i - n_e) = 4\pi e(Z\langle n_i\rangle - (\langle n_e\rangle + n_e')) = 4\pi e(n_o - n_o - n_e') = -4\pi e n_e' \tag{2.19}$$

or

$$n_e' = \frac{-\nabla\cdot\boldsymbol{E}}{4\pi e} \tag{2.20}$$

Hence the electron momentum equation becomes:

$$\frac{\partial \boldsymbol{V}_e'}{\partial t} = -\frac{e}{m}\boldsymbol{E} + \frac{\gamma V_{th}^2}{4\pi e n_o}\left(\nabla(\nabla\cdot\boldsymbol{E}) + (\nabla\cdot\boldsymbol{E})\frac{\nabla n_o}{n_o}\right) - \nu \boldsymbol{V}_e' \tag{2.21}$$

where

$$V_{th} \equiv \sqrt{\frac{K_B T_e}{m_e}} \tag{2.22}$$

is called the electron thermal velocity. Since all the terms on the right hand side of Eq. (2.21) vary as $e^{-i\omega t}$, $\partial/\partial t$ can be replaced by $-i\omega$. Rearranging terms in (2.21), $\mathbf{V}_e'$ can be expressed as:

$$\boldsymbol{V}_e' = -\frac{i}{\omega(1+i\nu/\omega)}\frac{e}{m}\boldsymbol{E} + \frac{i}{\omega(1+i\nu/\omega)}\frac{\gamma V_{th}^2}{4\pi e n_o}\left(\nabla(\nabla\cdot\boldsymbol{E}) + (\nabla\cdot\boldsymbol{E})\frac{\nabla n_o}{n_o}\right) \tag{2.23}$$

Finally, the wave equation can be obtained by using Eqs. (2.12) and (2.23) in relation (2.5):

$$\nabla^2\boldsymbol{E} - \nabla(\nabla\cdot\boldsymbol{E}) + \frac{\omega^2}{c^2}\left(1 - \frac{\omega_p^2}{\omega^2}\left(\frac{1}{1+i\nu/\omega}\right)\right)\boldsymbol{E} + \frac{\gamma V_{th}^2/c^2}{(1+i\nu/\omega)}\left(\nabla(\nabla\cdot\boldsymbol{E}) + (\nabla\cdot\boldsymbol{E})\frac{\nabla n_o}{n_o}\right) = 0 \tag{2.24}$$

where

$$\omega_p \equiv \sqrt{\frac{4\pi n_o e^2}{m_e}} \tag{2.25}$$

is defined as the electron plasma frequency.

2.2 Zero Gradient Propagation Modes

In the simulations it is assumed that after the density has just plunged very rapidly

from solid density to very low density near the plasma vacuum interface, it decreases much more slowly as it approaches vacuum. In other words, the density profile has a slow varying low density leading edge at the plasma vacuum boundary. In this region

$$\nabla n_o \approx 0 \tag{2.26}$$

and the wave equation can then be rewritten as:

$$\nabla^2 \boldsymbol{E} + k_o^2 \left(1 - \frac{\omega_p^2}{\omega^2} \frac{1}{1 + i\nu/\omega}\right) \boldsymbol{E} - \left(1 - \gamma \frac{V_{th}^2}{c^2} \frac{1}{1 + i\nu/\omega}\right) \nabla(\nabla \cdot \boldsymbol{E}) = 0 \tag{2.27}$$

where $k_o = \omega/c$ is the incident wave vector and is related to the laser wavelength λ_o by:

$$k_o \equiv \frac{2\pi}{\lambda_o} \tag{2.28}$$

Now it is assumed that the electric field can be decoupled into electromagnetic ($\mathbf{E}_{em}$) and electrostatic ($\mathbf{E}_{es}$) waves:

$$\boldsymbol{E} = \boldsymbol{E}_{em} + \boldsymbol{E}_{es} \tag{2.29}$$

Further, $\mathbf{E}_{em}$ and $\mathbf{E}_{es}$ are given by:

$$\boldsymbol{E}_{em} = [\boldsymbol{E}_{em}] \exp(i\boldsymbol{k}_{em} \cdot \boldsymbol{r}) \tag{2.30}$$

$$\boldsymbol{E}_{es} = [\boldsymbol{E}_{es}] \exp(i\boldsymbol{k}_{es} \cdot \boldsymbol{r}) \tag{2.31}$$

where [ ] denotes the amplitude of the field and **r** is the coordinate vector. It is further assumed that the directions of the wave vectors $\mathbf{k}_{em}$ and $\mathbf{k}_{es}$ are such that $\mathbf{k}_{em}$ is perpendicular to $\mathbf{E}_{em}$ and $\mathbf{k}_{es}$ is parallel to $\mathbf{E}_{es}$. Therefore from vector calculus and using Eqs. (2.30) and (2.31) it is found that:

$$\nabla^2 \boldsymbol{E}_{em} = -k_{em}^2 \boldsymbol{E}_{em} \tag{2.32}$$

$$\nabla(\nabla \cdot \boldsymbol{E}_{em}) = \nabla(i\boldsymbol{k}_{em} \cdot \boldsymbol{E}_{em}) = \nabla(0) = 0 \tag{2.33}$$

$$\nabla^2 \boldsymbol{E}_{es} = -k_{es}^2 \boldsymbol{E}_{es} \tag{2.34}$$

$$\nabla(\nabla \cdot \boldsymbol{E}_{es}) = -k_{es}^2 \boldsymbol{E}_{es} \tag{2.35}$$

Hence Eq. (2.27) becomes:

$$\left[-k_{em}^2 + k_o^2\left(1 - \frac{\omega_p^2}{\omega^2}\frac{1}{1+i\nu/\omega}\right)\right]\boldsymbol{E}_{em} + \left[-k_{es}^2\gamma\frac{V_{th}^2}{c^2}\frac{1}{1+i\nu/\omega} + k_o^2\left(1 - \frac{\omega_p^2}{\omega^2}\frac{1}{1+i\nu/\omega}\right)\right]\boldsymbol{E}_{es} = 0 \tag{2.36}$$

For Eq. (2.36) to be satisfied everywhere inside the plasma with non-vanishing **E** field, it requires:

$$k_{em}^2 = k_o^2\left(1 - \frac{\omega_p^2}{\omega^2}\frac{1}{1+i\nu/\omega}\right) \tag{2.37}$$

and

$$k_{es}^2 = k_o^2\frac{\left(1 - \frac{\omega_p^2}{\omega^2}\frac{1}{1+i\nu/\omega}\right)}{\gamma\frac{V_{th}^2}{c^2}\frac{1}{1+i\nu/\omega}} \tag{2.38}$$

which are the dispersion relations for the electromagnetic and electrostatic waves, respectively. Hence at the plasma vacuum boundary where the density gradient is small, the electric field can be approximately described by two waves propagating independent of each other. Nonetheless, when the density starts to rise rapidly, $\nabla n_o/n_o >> 1$, these two waves are strongly coupled and the electric field cannot be decomposed into the forms given above. Actually for an incident transverse wave it has been shown that the creation of $\mathbf{E}_{es}$ is due to linear mode conversion (for example, see [13]) at the critical density where the plasma frequency equals the laser frequency. Finally by noting that:

$$\nabla \times \boldsymbol{E}_{em} = i\boldsymbol{k}_{em} \times \boldsymbol{E}_{em} = ik_{em} E_{em} \neq 0 \tag{2.39}$$

$$\nabla \times \boldsymbol{E}_{es} = i\boldsymbol{k}_{es} \times \boldsymbol{E}_{es} = 0 \tag{2.40}$$

and examining Eq. (2.3), it is clear that $\mathbf{E}_{em}$ has a magnetic field associated with it but $\mathbf{E}_{es}$ does not. This is the reason why $\mathbf{E}_{em}$ is called the electromagnetic wave whereas $\mathbf{E}_{es}$ is referred to as the electrostatic or plasma wave.

2.3 Modelling of Damping Mechanisms

Collisional damping can be modeled by introducing a dissipative term into the momentum equation (2.13) (as discussed in section 2.1):

$$-m_e n_e \nu \boldsymbol{V}_e \tag{2.41}$$

which is proportional the electron velocity. The proportionality constant ν is called the collisional frequency and has units of t^{-1}. The usual form of ν is derived for weakly coupled plasmas in which the temperature is high and the density is low. It is given by [14]:

$$\nu=\frac{4(2\pi)^{1/2}}{3}\frac{Zn_e e^4\ln\Lambda}{m_e^{1/2}(K_B T_e)^{3/2}} \tag{2.42}$$

where lnΛ is called the Coulomb logarithm and has different complicated analytical expressions [14] depending on the electron temperature and the laser wavelength. One way of expressing lnΛ in a simple way is by fitting a second degree polynomial to the various expressions [15]:

$$\ln\Lambda\approx\sum_{i=1}^{3}\sum_{j=1}^{3}a_{ij}X^{i-1}Yj-1 \tag{2.43}$$

where

$$\begin{aligned} X&=\log_{10}(0.01\lambda_o Z^2)-1.5\\ Y&=\log_{10}(T_e/Z^2)-2 \end{aligned} \tag{2.44}$$

and

$$a_{ij}=\begin{bmatrix} 8.00715 & 2.703057 & 0.103552\\ 2.230034 & 0.314866 & -0.120930\\ 0.126149 & -0.078457 & 0.006118 \end{bmatrix} \tag{2.45}$$

For λ_o = 0.25 μm and Z = 4, a plot of $\ln\Lambda$ versus T_e in electron volt (eV) is shown on figure 2.1.

For strongly coupled plasmas in which the temperature is low and the density is high, Eq. (2.42) is no longer valid. This can been seen from an examination of the dispersion relation Eq. (2.37) for a cold plasma having a near solid density. At low temperatures the Coulomb logarithm as given by Eq. (2.43) becomes a constant. Hence the collision frequency is proportional to $n_e/T_e^{3/2}$. For large n_e and small T_e, ν is very large. Since the square of the plasma frequency is proportional to density, the second term in Eq. (2.37) can then be written as:

$$\frac{\omega_p^2}{\omega}\frac{1}{1+i\nu/\omega} \approx -i\frac{\omega_p^2}{\nu} \propto \frac{n_e}{n_e/T_e^{3/2}} = T_e^{3/2} \tag{2.46}$$

which vanishes for small temperatures. Hence the dispersion relation becomes:

$$k_{em} = k_o \tag{2.47}$$

which implies that the EM wave is propagating unattenuated. This is a contradictory result because the absorption of the EM wave is proportional to the collisional frequency (see for example, [1,11]) and a large collision frequency should simply imply a strong attenuation of the wave. Therefore, for the simulations proposed for this study, in which the target material can have a cold dense region (the solid-plasma transition region), a proper expression for the collision frequency which is also valid for strongly coupled plasmas is used.

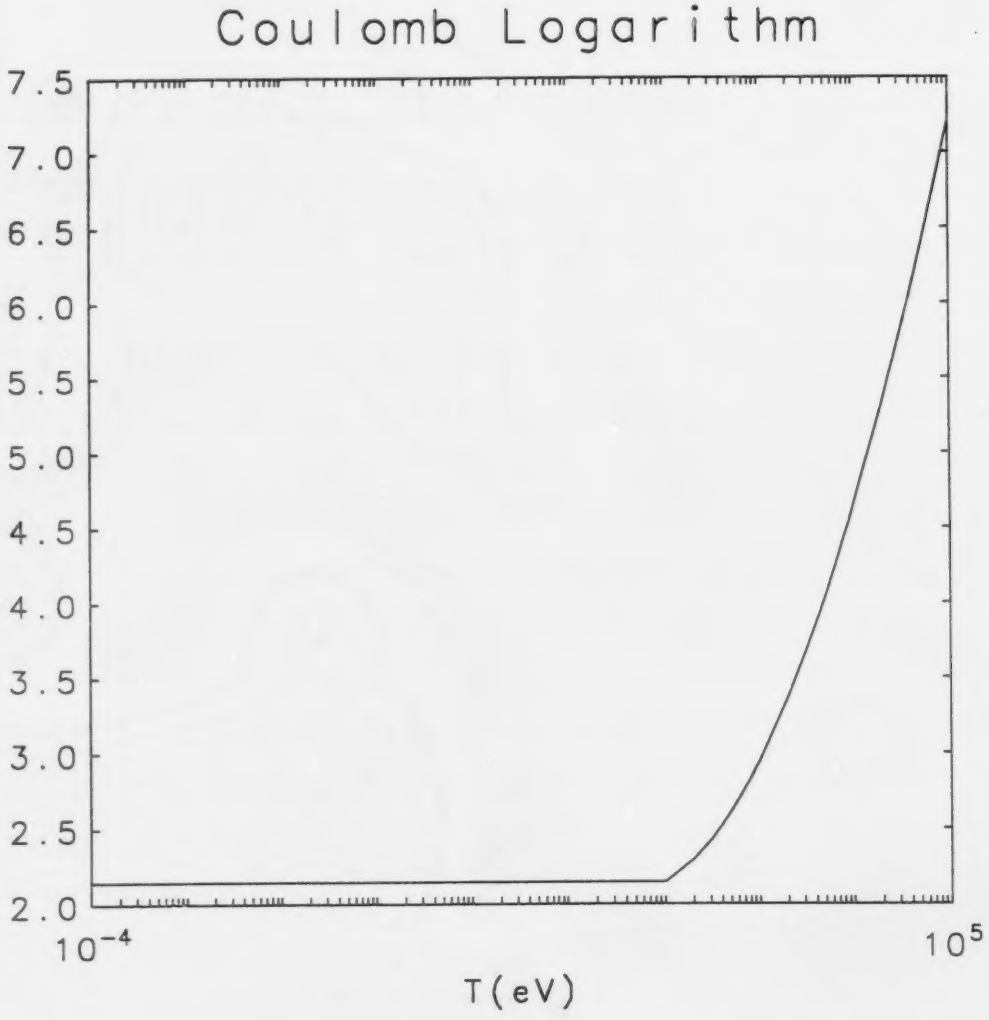

Figure 2.1: The Coulomb Logarithm.

Recently a theoretical study conducted by Cauble et al [16] has resulted in an expression for the collision frequency (ν_{CRR}) in a strongly coupled plasma. They started by considering the phase space particle-particle correlation for electrons and ions. The collision frequency was derived from the collision term in the spatially Fourier-transformed correlation function. The collision frequency was then expressed in terms of the momentum matrix elements of the collision term:

$$\nu_{CRR}=f[M] \tag{2.48}$$

where **M** is a 3×3 matrix and the form of ν_{CRR} is given explicitly in Appendix A. As a comparison, the collisional frequencies as computed by Eq. (2.42) (the dashed line) and Eq. (2.48) (the solid line) are plotted together in figure 2.2 as a function of electron temperature for λ_o = 0.25 μm, Z = 4 and $n_o = n_c$. It is seen that at high temperatures the CRR model converges to that given by Eq. (2.42). However, at low temperatures the CRR collisional frequency approaches zero. Then according to the Eq. (2.37) with $\omega_p^2 >> \omega$ (as in a dense plasma) the wavevector k_{em} for the EM wave has a large imaginary part and the wave is evanescent. Physically this means that, since there is no absorption (because $\nu \approx 0$), the EM wave is totally reflected from the cold solid region. Since the penetration of laser light into a thick cold solid has never been observed, the CRR collisional frequency appears to be a more physical model. Consequently the CRR formula will be used in the laser code to model the collisional processes.

To model Landau damping, Forslund et al [17] suggested that the collisional frequency in the last term on the left of the wave equation (2.24) be replaced by a

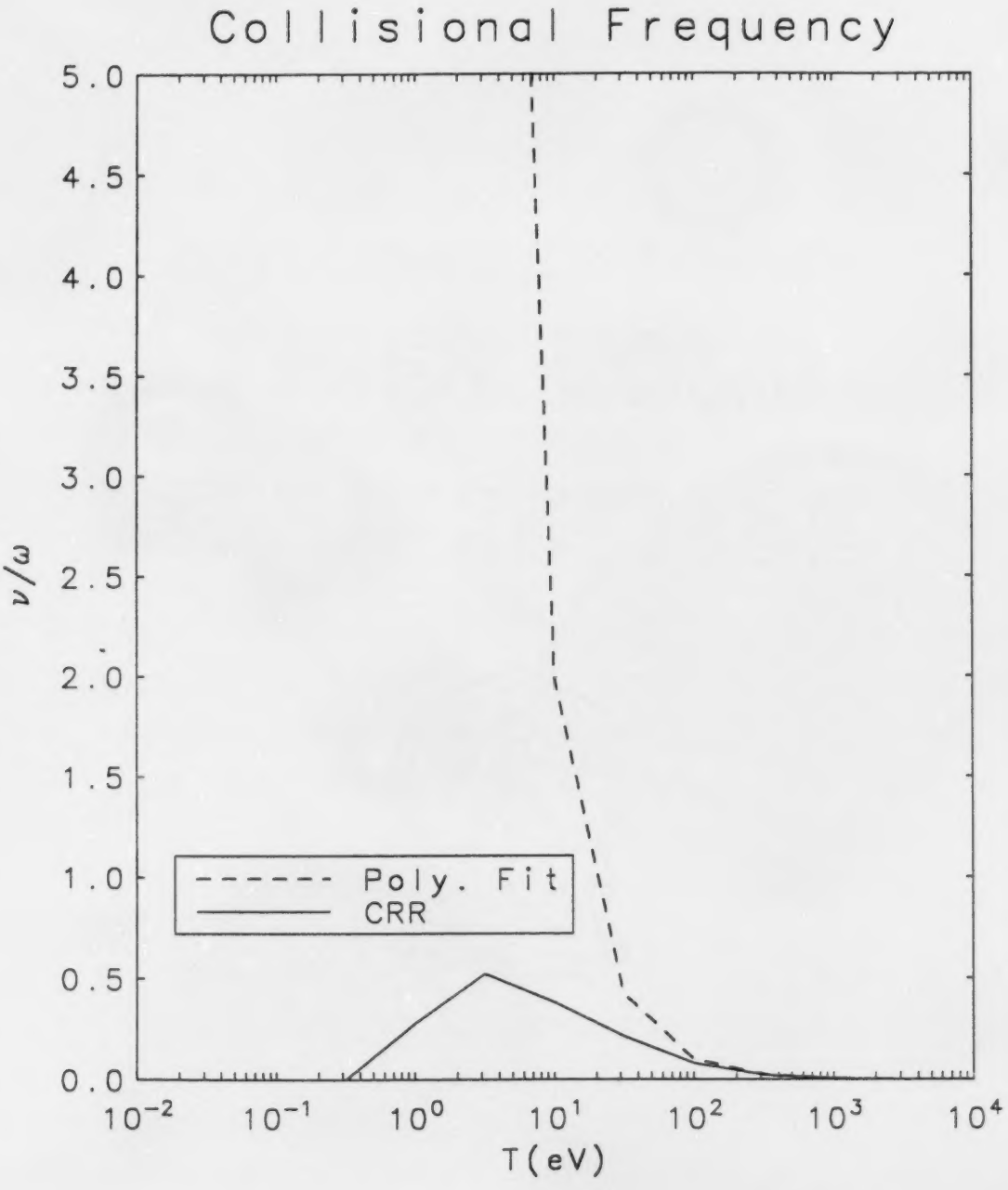

Figure 2.2: Collision Frequencies.

phenomenological damping rate:

$$\frac{\nu_l}{\omega}=\left(\frac{1}{8}\pi\right)^{1/2}\left(\frac{\gamma}{\varepsilon}\right)^{5/2}e^{-\gamma/\varepsilon}\ ;\quad (\omega^2>\omega_p^2) \tag{2.49}$$

where

$$\frac{1}{\varepsilon}=\frac{\omega^2}{\omega^2-\omega_p^2} \tag{2.50}$$

This damping term has the effect of heavily attenuating the plasma wave at the plasma-vacuum boundary and thus preventing the plasma wave from reflecting back from the boundary [17].

2.4 Boundary Conditions

From the geometry of the problem (see figure 1.1) it is seen that the electric field inside the plasma should not have a component in the z-direction. That is,

$$E_z=0 \tag{2.51}$$

Also it is assumed that, because the plasma properties are only dependent on the x-coordinate, the electric field inside the plasma should vary periodically in the y-direction. Therefore the electric field is assumed to have the form:

$$\boldsymbol{E}=(\hat{\boldsymbol{x}}E_x(x)+\hat{\boldsymbol{y}}E_y(x))e^{ik_y y}e^{-i\omega t} \tag{2.52}$$

where $\hat{\mathbf{x}}$ and $\hat{\mathbf{y}}$ are the unit vectors along the x- and y-directions respectively; and k_y is the y-component of the incident wave vector $\mathbf{k}_o$. Using Eq. (2.52) and denoting respectively the CRR collision frequency and Landau damping rate by ν_c and ν_l, the wave equations Eqs. (2.24) in component form are:

$$\frac{\gamma V_{th}^2/c^2}{1+\nu_l/\omega}\frac{d^2E_x}{dx^2}+k_o^2\left[1-\frac{\omega_p^2/\omega^2}{1+i\nu_c/\omega}-\frac{k_y^2}{k_o^2}\right]E_x+\left[\frac{\gamma V_{th}^2/c^2}{1+i\nu_l/\omega}-1\right]ik_y\frac{dE_y}{dx} \\ -\frac{\gamma V_{th}^2/c^2}{1+i\nu_l/\omega}\left[\frac{dE_x}{dx}+ik_yE_y\right]\frac{\frac{dn_o}{dx}}{n_o}=0 \tag{2.53}$$

$$\frac{d^2E_y}{dx^2}+k_o^2\left[1-\frac{\omega_p^2/\omega^2}{1+i\nu_c/\omega}-\frac{\gamma V_{th}^2/c^2}{1+i\nu_l/\omega}\frac{k_y^2}{k_o^2}\right]E_y+\left[\frac{\gamma V_{th}^2/c^2}{1+i\nu_l/\omega}-1\right]ik_y\frac{dE_x}{dx}=0 \tag{2.54}$$

which are two coupled second order ordinary differential equations in E_x and E_y.

Since Eqs. (2.53) and (2.54) are of second order, four boundary conditions are needed in solving these equations. These boundary conditions may be derived as follows. First, because it is assumed that the laser light cannot penetrate through the target, the boundary conditions at $x = +\infty$ are:

$$E_x=E_y=0 \tag{2.55}$$

At x = 0 it is assumed that the density gradient is small so that the electric field just inside the plasma is composed of (see figure 2.3) an incoming electromagnetic wave (the incident laser light), an outgoing electromagnetic wave (the reflected laser light) and an outgoing electrostatic or plasma wave (driven by linear mode conversion of the electromagnetic wave at the critical density):

$$E=E_{in}+E_{out}+E_p=A_i e^{ik_{i-}\cdot r}+B_r e^{ik_{r-}\cdot r}+D_p e^{ik_p\cdot r} \tag{2.56}$$

where $\mathbf{A}_i$ is the known incident EM wave amplitude, and $\mathbf{B}_r$ and $\mathbf{D}_p$ are respectively the amplitudes for the reflected EM wave and the ES wave. The latter two quantities are to be determined from the simulation. The wave vectors are given by:

$$\begin{aligned} k_{t+}&=\hat{x}k_{tx}+\hat{y}k_y \\ k_{t-}&=-\hat{x}k_{tx}+\hat{y}k_y \end{aligned} \tag{2.57}$$

$$k_p=-\hat{x}k_{px}+\hat{y}k_y \tag{2.58}$$

where the dispersion relations given in Eqs. (2.37) and (2.38) are used:

$$k_t^2=k_o^2\left(1-\frac{\omega_p^2}{\omega^2}\frac{1}{1+i\nu_e/\omega}\right) \tag{2.59}$$

and,

$$k_{tx}^2=k_t^2-k_y^2$$

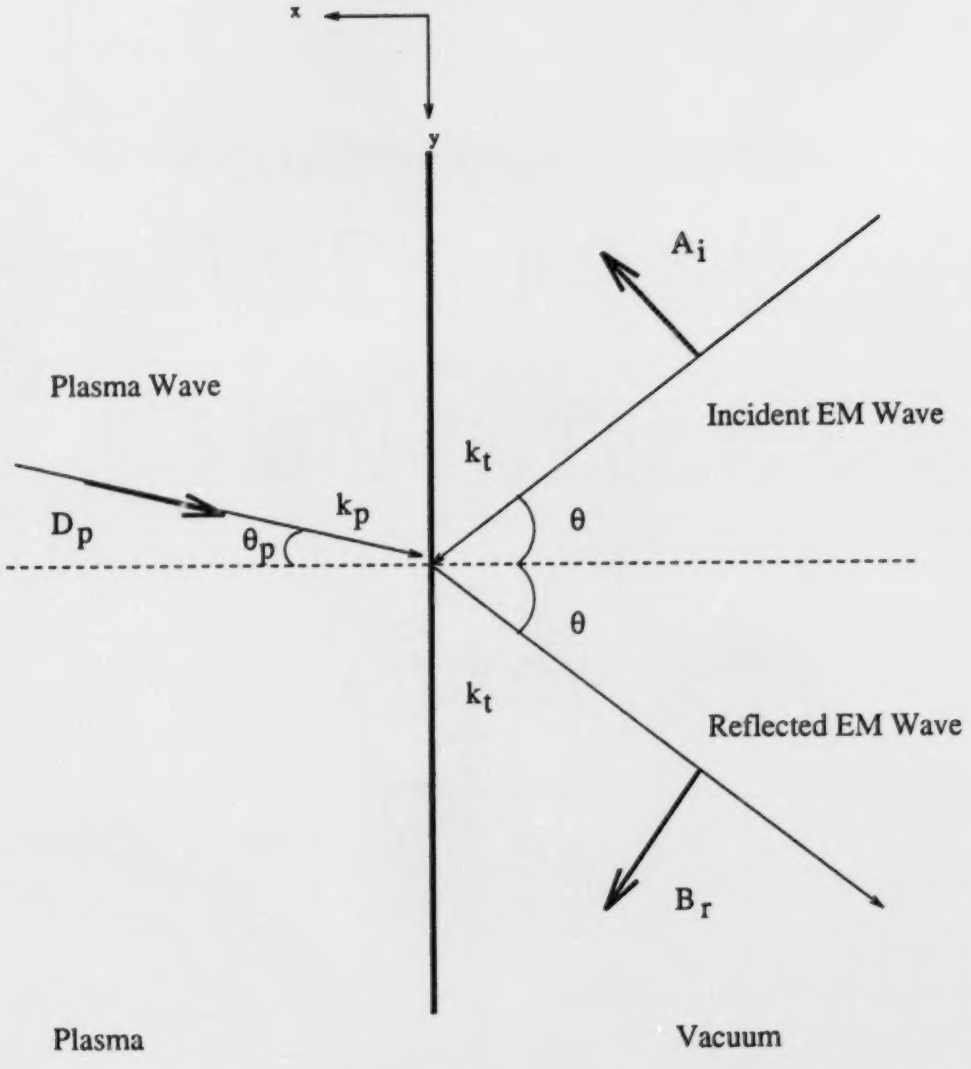

Figure 2.3: Boundary Conditions at x = 0.

$$k_p^2=k_o^2\left(\frac{1-\frac{\omega_p^2}{\omega^2}\frac{1}{1+i\nu_c/\omega}}{\gamma\frac{V_{th}^2}{c^2}\frac{1}{1+i\nu_c/\omega}}\right) \tag{2.60}$$

and,

$$k_{px}^2=k_p^2-k_y^2$$

Note that because of the periodic boundary condition imposed on the y-direction, k_y is the same for all three waves. This is a consequence of Snell's Law.

The electric fields at the entrance to the plasma in component form are then given by:

$$E_x=A_i\sin\theta+B_r\sin\theta-D_p\cos\theta_p \tag{2.61}$$

$$E_y=-A_i\cos\theta+B_r\cos\theta+D_p\sin\theta_p \tag{2.62}$$

where the angles are related to the wave vectors by:

$$\sin\theta=\frac{k_y}{\sqrt{k_y^2+k_{txr}^2}} \tag{2.63}$$

$$\cos\theta=\frac{k_{txr}}{\sqrt{k_y^2+k_{txr}^2}} \tag{2.64}$$

$$\sin\theta_p = \frac{k_y}{\sqrt{k_y^2 + k_{pxr}^2}} \tag{2.65}$$

$$\cos\theta_p = \frac{k_{pxr}}{\sqrt{k_y^2 + k_{pxr}^2}} \tag{2.66}$$

Here k_{txr} and k_{pxr} are the real parts of k_{tx} and k_{px} respectively. To obtain boundary conditions that are independent of the unknown amplitudes B_r and D_p, two more equations are introduced. These equations are found by differentiating Eqs. (2.61) and (2.62) with respect to x and ignoring the weak dependence of the angles on x:

$$\frac{dE_x}{dx} = ik_{tx}A_i\sin\theta - ik_{tx}B_r\sin\theta + ik_{px}D_p\cos\theta_p \tag{2.67}$$

$$\frac{dE_y}{dx} = -ik_{tx}A_i\cos\theta - ik_{tx}B_r\cos\theta - ik_{px}D_p\sin\theta_p \tag{2.68}$$

Eliminating B_r and D_p from Eqs. (2.61), (2.62), (2.67) and (2.68) the boundary conditions at x = 0 are:

$$\frac{dE_x}{dx} + \varepsilon_1 E_x + \varepsilon_2 E_y = \varepsilon_3 \tag{2.69}$$

$$\frac{dE_y}{dx} + \zeta_1 E_y + \zeta_2 E_x = \zeta_3 \tag{2.70}$$

where

$$\varepsilon_1 = i\frac{k_{px}k_{pxr}k_{txr}+k_{tx}k_y^2}{k_{pxr}k_{txr}+k_y^2}$$

$$\varepsilon_2 = -i\frac{k_y k_{pxr}(k_{px}-k_{tx})}{k_{pxr}k_{txr}+k_y^2} \qquad (2.71)$$

$$\varepsilon_3 = 2i\frac{k_y}{\sqrt{k_{txr}^2+k_y^2}}\frac{k_{px}k_{pxr}k_{txr}+k_{tx}k_y^2}{k_{pxr}k_{txr}+k_y^2}A_i$$

and

$$\zeta_1 = i\frac{k_{px}k_y^2+k_{tx}k_{pxr}k_{txr}}{k_{pxr}k_{txr}+k_y^2}$$

$$\zeta_2 = -i\frac{k_y k_{txr}(k_{px}-k_{tx})}{k_{pxr}k_{txr}+k_y^2} \qquad (2.72)$$

$$\zeta_3 = -2i\frac{k_{txr}}{\sqrt{k_y^2+k_{txr}^2}}\frac{k_{px}k_y^2+k_{tx}k_{pxr}k_{txr}}{k_{pxr}k_{txr}+k_y^2}A_i$$

Using Eqs. (2.61) and (2.62) B_r and D_p can be expressed in terms of A_i, E_x and E_y as:

$$B_r = \frac{1}{k_y^2+k_{txr}k_{pxr}}\left[\sqrt{k_y^2+k_{txr}^2}\,(E_x k_y+E_y k_{pxr})-A_i(k_y^2-k_{txr}k_{pxr})\right] \qquad (2.73)$$

$$D_p = \frac{1}{k_y^2+k_{txr}k_{pxr}}\frac{\sqrt{k_y^2+k_{pxr}^2}}{\sqrt{k_y^2+k_{txr}^2}}\left[\sqrt{k_y^2+k_{txr}^2}\,(-E_x k_{txr}+E_y k_y)+2A_i k_{txr}k_y\right] \qquad (2.74)$$

Hence, once the electric field is found, B_r and D_p can be readily determined.

2.5 Calculation of Absorption

From electromagnetic theory the power per unit volume dissipated from the electromagnetic fields to a distribution of charge and current is:

$$W_{oj}=\boldsymbol{E}\cdot\boldsymbol{J} \tag{2.75}$$

For complex harmonic fields the average power dissipated per unit volume is given by:

$$\langle W_{oj}\rangle=\frac{1}{2}\mathrm{Re}[\boldsymbol{E}^{*}\cdot\boldsymbol{J}] \tag{2.76}$$

where Re[ψ] signifies the real part of ψ and a (*) denotes the complex conjugate. The current density expressed in terms of **E** can be found by substituting Eq. (2.23) into (2.12). In component form the current density is given by:

$$J_x=\frac{i\omega}{4\pi}\left[\frac{\omega_p^2/\omega^2}{1+i\nu_c/\omega}E_x-\frac{\gamma V_{th}^2/c^2}{1+i\nu_c/\omega}\frac{1}{k_o^2}\left(\frac{d^2E_x}{dx^2}+ik_y\frac{dE_y}{dx}-\left(\frac{dE_x}{dx}+ik_yE_y\right)\frac{\frac{dn_o}{dx}}{n_o}\right)\right] \tag{2.77}$$

$$J_y=\frac{i\omega}{4\pi}\left[\frac{\omega_p^2/\omega^2}{1+i\nu_c/\omega}E_y-\frac{\gamma V_{th}^2/c^2}{1+i\nu_c/\omega}\frac{1}{k_o^2}\left(ik_y\frac{dE_x}{dx}-k_y^2E_y\right)\right] \tag{2.78}$$

Hence the expression for the average power absorbed per unit volume according to Eq. (2.76) is then:

$$\langle W_{ej}\rangle=\frac{\omega}{8\pi}\mathrm{Re}\left[i\frac{\omega_p^2/\omega^2}{1+\nu_e/\omega}|E_x^2+E_y^2|\right]$$

$$+\frac{\omega}{8\pi}\mathrm{Re}\left[-i\frac{\gamma V_{th}^2/c^2}{1+\nu_e/\omega}\frac{1}{k_o^2}\left(E_x^*\frac{d^2E_x}{dx^2}+ik_yE_x^*\frac{dE_y}{dx}+ik_yE_y^*\frac{dE_x}{dx}-k_y^2|E_y^2|-E_x^*\left(\frac{dE_x}{dx}+ik_yE_y\right)\frac{\frac{dn_o}{dx}}{n_o}\right)\right] \tag{2.79}$$

where $|\psi|$ denotes the magnitude of the complex number ψ. The total power per unit area absorbed by the plasma can be obtained by integrating Eq. (2.79) over the x-axis:

$$I_{ej}=\int_0^\infty\langle W_{ej}\rangle dx \tag{2.80}$$

Another way of calculating the absorption is to utilize the Poynting theorem:

$$\frac{\partial u}{\partial t}+\nabla\cdot\boldsymbol{S}=-\boldsymbol{J}\cdot\boldsymbol{E} \tag{2.81}$$

where u is the total field energy density given by:

$$u=\frac{1}{8\pi}(\boldsymbol{E}\cdot\boldsymbol{E}^*+\boldsymbol{B}\cdot\boldsymbol{B}^*) \tag{2.82}$$

and the Poynting vector **S** is:

$$\boldsymbol{S}=\frac{c}{4\pi}(\boldsymbol{E}\times\boldsymbol{B}) \tag{2.83}$$

which represents the energy flux (power/area). The Poynting theorem essentially states that the decrease in the field energy in an elementary volume is equal to the energy flowing out of the volume plus the work done by the field on the charges within the volume. For steady state harmonic fields, u is constant when averaged over time. The time averaged Poynting theorem gives:

$$\langle W_s\rangle \equiv -\nabla\cdot\langle \boldsymbol{S}\rangle = \langle W_{ej}\rangle \tag{2.84}$$

and **<S>** is given by:

$$\langle \boldsymbol{S}\rangle=\frac{c}{8\pi}\mathrm{Re}[\boldsymbol{E}^{*}\times\boldsymbol{B}] \tag{2.85}$$

The magnetic field is readily obtained by substituting Eq.s (2.52) into (2.3):

$$\boldsymbol{B}=\hat{z}\frac{-i}{k_o}\left(\frac{\mathrm{d}E_y}{\mathrm{d}x}-ik_yE_x\right) \tag{2.86}$$

Hence **<S>** in component form is given by:

$$\langle S_x\rangle=\frac{c}{8\pi}\frac{1}{k_o}\mathrm{Re}\left[-i\left(E_y^{*}\frac{\mathrm{d}E_y}{\mathrm{d}x}-ik_yE_y^{*}E_x\right)\right] \tag{2.87}$$

$$\langle S_y\rangle=-\frac{c}{8\pi}\frac{1}{k_o}\mathrm{Re}\left[-i\left(E_x\frac{dE_y}{dx}-ik_y|E_x^2|\right)\right] \tag{2.88}$$

And the absorption as calculated from the Poynting vector is:

$$\langle W_s\rangle=-\frac{\partial\langle S_x\rangle}{\partial x}-\frac{\partial\langle S_y\rangle}{\partial y}=-\frac{d\langle S_x\rangle}{dx}=-\frac{c}{8\pi}\frac{1}{k_o}\frac{d}{dx}\mathrm{Re}\left[-i\left(E_y^*\frac{dE_y}{dx}-ik_yE_y^*E_x\right)\right] \tag{2.89}$$

Here since $\mathrm{Re}[S_y]$ has a $\cos^2(k_y y+\omega t)$ dependence, it loses its y dependence when averaged over time. Therefore $\partial\langle S_y\rangle/\partial y = 0$. As before the total power per unit area absorbed by the plasma can be calculated by integrating $\langle W_s\rangle$ over the x-axis:

$$I_s=\int_0^\infty\langle W_s\rangle dx=\int_0^\infty-\frac{d\langle S_x\rangle}{dx}dx=\langle S_x(0)\rangle-\langle S_x(\infty)\rangle \tag{2.90}$$

However at $x = \infty$ all fields are assumed to be zero, thus:

$$I_s=\langle S_x(0)\rangle \tag{2.91}$$

Finally although Eqs. (2.79), (2.80), (2.89) and (2.91) will give the same results for absorption, it is seen that the latter two equations have simpler expressions and thus are preferable when used in calculating the absorption.

2.6 Normalizing Equations

The equations derived in the previous sections can be expressed in simpler forms before they are used for numerical evaluation. This is done by substituting normalized

variables into the equations. Defining:

$$\hat{E} \equiv \frac{E}{A_l} \tag{2.92}$$

$$\hat{x} \equiv 2\pi \frac{x}{\lambda} = x k_o \tag{2.93}$$

$$\hat{V}_{th}^2 \equiv \frac{V_{th}^2}{c^2} \tag{2.94}$$

$$\hat{k}_y \equiv \frac{k_y}{k_o}; \quad \hat{k}_{tx} \equiv \frac{k_{tx}}{k_o}; \quad \hat{k}_{px} \equiv \frac{k_{px}}{k_o} \tag{2.95}$$

$$\begin{aligned} \Diamond_c &\equiv \frac{\nu_c}{\omega} \\ \Diamond_l &\equiv \frac{\nu_l}{\omega} \end{aligned} \tag{2.96}$$

$$\hat{n}_o \equiv \frac{n_o}{n_c} \tag{2.97}$$

the wave equations become:

$$\frac{\gamma \hat{V}_{th}^2}{1+i\Diamond_u} \frac{d^2\hat{E}_x}{d\hat{x}^2} + \left[1 - \frac{\hat{n}_o}{1+i\Diamond_c} - \hat{k}_y^2\right] \hat{E}_x + \left[\frac{\gamma \hat{V}_{th}^2}{1+i\Diamond_l} - 1\right] i\hat{k}_y \frac{d\hat{E}_y}{d\hat{x}} - \frac{\gamma \hat{V}_{th}^2}{1+i\Diamond_l} \left[\frac{d\hat{E}_x}{d\hat{x}} + i\hat{k}_y \hat{E}_y\right] \frac{d\hat{n}_o}{d\hat{x}} = 0 \tag{2.98}$$

$$\frac{d^2\hat{E}_y}{d\hat{\ell}^2}+\left[1-\frac{\hat{\omega}_p^2}{1+i\hat{\nu}_e}-\frac{\gamma\hat{V}_{th}^2}{1+i\hat{\nu}_i}\hat{k}_y^2\right]\hat{E}_y+\left[\frac{\gamma\hat{V}_{th}^2}{1+i\hat{\nu}_i}-1\right]\hat{k}_y\frac{d\hat{E}_x}{d\hat{\ell}}=0 \tag{2.99}$$

where n_c is the critical density defined by:

$$n_c\equiv\frac{\omega^2 m_e}{4\pi e^2} \tag{2.100}$$

Note that the relation:

$$\frac{\omega_p^2}{\omega^2}=\hat{n}_o \tag{2.101}$$

can be obtained by comparing Eq. (2.100) with Eq. (2.25).

The plasma vacuum boundary conditions are now given by:

$$\frac{d\hat{E}_x}{d\hat{\ell}}+\hat{\varepsilon}_1\hat{E}_x+\hat{\varepsilon}_2\hat{E}_y=\hat{\varepsilon}_3 \tag{2.102}$$

$$\frac{d\hat{E}_y}{d\hat{\ell}}+\zeta_1\hat{E}_y+\zeta_2\hat{E}_x=\zeta_3 \tag{2.103}$$

where the normalized ε's and ζ's can be obtained from Eqs. (2.71) and (2.72) by setting A_i to unity and replacing the k's by their corresponding normalized values as given in Eq. (2.95).

The normalized energy flux is:

$$\langle \hat{S}_x \rangle \equiv \frac{\langle S_x \rangle}{I_i} = -\mathrm{Re}\left[\hat{E}_y^* \left(\hat{k}_y \hat{E}_x + i\frac{d\hat{E}_y}{d\hat{\xi}}\right)\right] \tag{2.104}$$

and from Eq. (2.91) the total absorption fraction is:

$$\alpha = \frac{I_s}{I_i} = \frac{\langle S_x(0) \rangle}{I_i} = \langle \hat{S}_x(0) \rangle \tag{2.105}$$

where I_i is the incident laser intensity:

$$I_i = \frac{c}{8\pi} A_i^2 \tag{2.106}$$

2.7 Value for the Ratio of Specific Heats

For adiabatic compression the value of γ is given by [1]:

$$\gamma = \frac{2+N}{N} \tag{2.107}$$

where N is the number of degrees of freedom. Since the electrons have only translational motion (V_x, V_y, V_z), N is equal to 3 and γ therefore has a value of 5/3.

2.8 Numerical Scheme

The normalized wave equations (2.98) and (2.99) are solved numerically using the following finite difference scheme. First the derivatives in these equations are

approximated by the finite difference formulae:

$$\frac{dF[x]}{dx} \approx \frac{F[x+\Delta x]-F[x-\Delta x']}{\Delta x+\Delta x'} \tag{2.108}$$

$$\frac{d^2F[x]}{dx^2} \approx \frac{\Delta x' F[x+\Delta x]+\Delta x F[x-\Delta x']-(\Delta x+\Delta x')F[x]}{\frac{1}{2}\Delta x\Delta x'(\Delta x+\Delta x')} \tag{2.109}$$

where $\Delta x \neq \Delta x'$ allows for non-uniform grid spacing. These formulae are then applied to the 'staggered' mesh as shown in figure 2.4. The advantage of using such mesh is that the resulting difference equations constitute a pentadiagonal matrix structure which can be solved by a method (as will be discussed later in this section) relatively more efficient than the standard Gaussian Elimination procedure. The mesh has J grid points where J is an even number. The distance between adjacent grid points is:

$$\Delta x_j = \hat{x}_{j+1} - \hat{x}_j \tag{2.110}$$

The electric field values E_j to be determined at the odd grid points corresponding to the E_x values and those to be determined at the even grid points corresponding to the E_y values. Eqs. (2.98) and (2.99) are then applied alternately at each consecutive point from the right boundary (j=1) to the left boundary (j=J). Since Eq. (2.98) has a second derivative in E_x, it is more convenient to apply this equation at the odd grid points. By looking at figure 2.5a and using the difference formulae given in Eqs. (2.108) and (2.109), the values of E_x, E_y and their derivatives as expressed in terms of E_i are given by:

$$\hat{E}_x = E_j \tag{2.111}$$

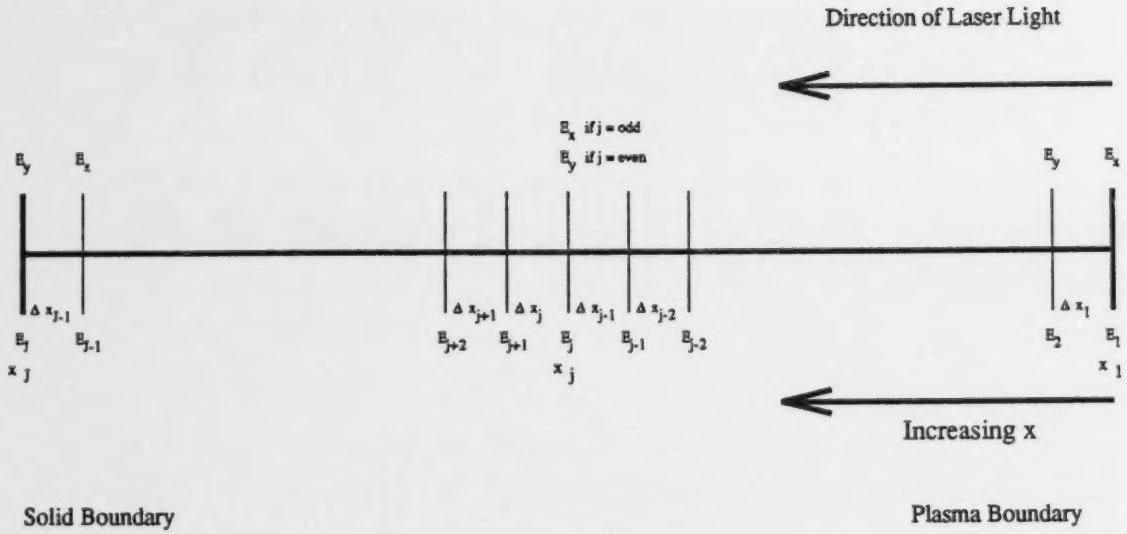

Figure 2.4: The Staggered Mesh.

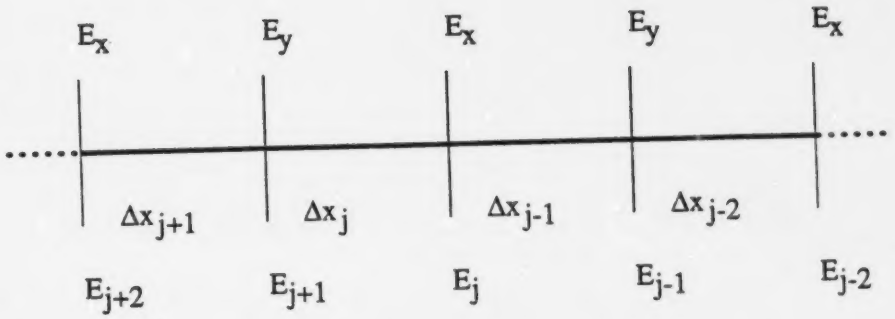

a)

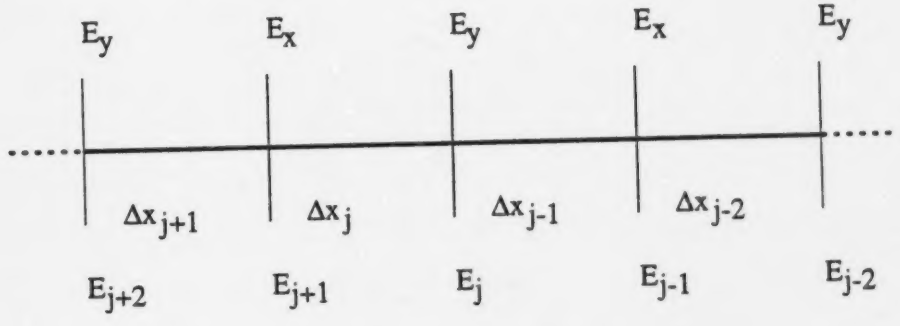

b)

Figure 2.5: Difference Scheme: a) j = odd; b) j = even.

$$\hat{E}_y=\frac{E_{j-1}\Delta x_j+E_{j+1}\Delta x_{j-1}}{\Delta x_{j-1}+\Delta x_j} \tag{2.112}$$

$$\frac{d^2\hat{E}_x}{d\ell^2}=\frac{E_{j-2}(\Delta x_{j-2}+\Delta x_{j-1})+E_{j-2}(\Delta x_j+\Delta x_{j+1})-E_j(\Delta x_{j-2}+\Delta x_{j-1}+\Delta x_j+\Delta x_{j+1})}{\frac{1}{2}(\Delta x_{j-2}+\Delta x_{j-1})(\Delta x_j+\Delta x_{j+1})(\Delta x_{j-2}+\Delta x_{j-1}+\Delta x_j+\Delta x_{j+1})} \tag{2.113}$$

$$\frac{d\hat{E}_x}{d\ell}=\frac{E_{j+2}-E_{j-2}}{\Delta x_{j-2}+\Delta x_{j-1}+\Delta x_j+\Delta x_{j+1}} \tag{2.114}$$

$$\frac{d\hat{E}_y}{d\ell}=\frac{E_{j+1}-E_{j-1}}{\Delta x_{j-1}+\Delta x_j} \tag{2.115}$$

Note that the E_y at the odd grid points are taken as the average of the E_y at adjacent even grid points. Similarly Eq. (2.99) has a second derivative in E_y and is therefore applied at the even grid points (see figure 2.5b) where:

$$\hat{E}_y=E_j \tag{2.116}$$

$$\frac{d^2\hat{E}_y}{d\ell^2}=\frac{E_{j-2}(\Delta x_{j-2}+\Delta x_{j-1})+E_{j-2}(\Delta x_j+\Delta x_{j+1})-E_i(\Delta x_{j-2}+\Delta x_{j-1}+\Delta x_j+\Delta x_{j+1})}{\frac{1}{2}(\Delta x_{j-2}+\Delta x_{j-1})(\Delta x_j+\Delta x_{j+1})(\Delta x_{j-2}+\Delta x_{j-1}+\Delta x_j+\Delta x_{j+1})} \tag{2.117}$$

$$\frac{d\hat{E}_x}{\hat{d}x}=\frac{E_{j+1}-E_{j-1}}{\Delta x_{j-1}+\Delta x_j} \tag{2.118}$$

Substituting Eqs. (2.111) through (2.115) back to Eq. (2.98) and Eqs. (2.116) through (2.118) back to Eq. (2.99), a system of difference equations is obtained:

$$P_1^jE_{i+2}+P_2^jE_{i+1}+P_3^jE_i+P_4^jE_{j-1}+P_5^jE_{j-2}=P_6^j\ ;\quad 3\le j\le J-2 \tag{2.119}$$

where for <u>odd</u> values of j, the coefficients P_i^j are given by:

$$P_1^j=\gamma\frac{\hat{V}_{th}^2}{1+i\hat{\nu}_l}\frac{1}{\Delta x_{j-2}+\Delta x_{j-1}+\Delta x_j+\Delta x_{j+1}+\Delta x_{j+2}}\left[\frac{1}{\frac{1}{2}(\Delta x_j+\Delta x_{j+1})}-\frac{\frac{d\hat{n}_o}{d\hat{\ell}}}{\hat{n}_o}\right] \tag{2.120}$$

$$P_2^j=i\hat{k}_y\frac{1}{\Delta x_{j-1}+\Delta x_j}\left(\gamma\frac{\hat{V}_{th}^2}{1+i\hat{\nu}_l}\left(1-\frac{\frac{d\hat{n}_o}{d\hat{\ell}}}{n_o}\Delta x_{j-1}\right)-1\right) \tag{2.121}$$

$$P_3^j=-\gamma\frac{\hat{V}_{th}^2}{1+i\hat{\nu}_l}\frac{1}{\frac{1}{2}(\Delta x_{j-2}+\Delta x_{j-1})(\Delta x_j+\Delta x_{j+1})}+1-\frac{\hat{\omega}_p^2}{1+i\hat{\nu}_c}-\hat{k}_y^2 \tag{2.122}$$

$$P_4^j=-i\hat{k}_y\frac{1}{\Delta x_{j-1}+\Delta x_j}\left(\gamma\frac{\hat{V}_{th}^2}{1+i\hat{\nu}_l}\left(1+\frac{\frac{d\hat{n}_o}{d\hat{\ell}}}{\hat{n}_o}\Delta x_j\right)-1\right) \tag{2.123}$$

$$P_5^j=\gamma\frac{\hat{V}_{th}^2}{1+i\hat{\nu}_l}\frac{1}{\Delta x_{j-2}+\Delta x_{j-1}+\Delta x_j+\Delta x_{j+1}+\Delta x_{j+2}}\left(\frac{1}{\frac{1}{2}(\Delta x_{j-2}+\Delta x_{j-1})}+\frac{\frac{d\hat{n}_o}{d\hat{\ell}}}{\hat{n}_o}\right) \tag{2.124}$$

$$P_6^j=0 \tag{2.125}$$

and for <u>even</u> values of j, the coefficient are:

$$P_1^j=\frac{1}{\frac{1}{2}(\Delta x_j+\Delta x_{j+1})(\Delta x_{j-2}+\Delta x_{j-1}+\Delta x_j+\Delta x_{j+1})} \tag{2.126}$$

$$P_2^j = i\hat{k}_y \frac{1}{\Delta x_{j-1}+\Delta x_j}\left(\gamma \frac{\hat{V}_{th}^2}{1+i\hat{\nu}_l}-1\right) \tag{2.127}$$

$$P_3^j = 1-\frac{\hat{\omega}_p^2}{1+i\hat{\nu}_c}-\hat{k}_y^2\gamma\frac{\hat{V}_{th}^2}{1+i\hat{\nu}_l}-\frac{1}{\frac{1}{2}(\Delta x_{j-2}+\Delta x_{j-1})(\Delta x_j+\Delta x_{j+1})} \tag{2.128}$$

$$P_4^j = -i\hat{k}_y \frac{1}{\Delta x_{j-1}+\Delta x_j}\left(\gamma \frac{\hat{V}_{th}^2}{1+i\hat{\nu}_l}-1\right) \tag{2.129}$$

$$P_5^j = \frac{1}{\frac{1}{2}(\Delta x_{j-2}+\Delta x_{j-1})(\Delta x_{j-2}+\Delta x_{j-1}+\Delta x_j+\Delta x_{j+1})} \tag{2.130}$$

$$P_6^j = 0 \tag{2.131}$$

Since Eq. (2.119) consists of J-4 equations and there are J unknown values of the E's, four more equations are needed to solve the system of equations. The first two are obtained from boundary conditions Eq. (2.55):

$$\begin{aligned} E_{J-1} &= 0 \\ E_J &= 0 \end{aligned} \tag{2.132}$$

The next two are found by applying boundary conditions Eq. (2.102) to the second grid point and Eq. (2.103) to the third grid point:

$$E_3 = M_1E_2 + M_2E_1 + M_3 \tag{2.133}$$

$$E_4=N_1E_3+N_2E_2+N_3 \tag{2.134}$$

where

$$M_1=-\frac{\hat{\varepsilon}_2(\Delta x_1+\Delta x_2)}{1+\hat{\varepsilon}_1\Delta x_1}$$

$$M_2=1-\hat{\varepsilon}_1\Delta x_2 \tag{2.135}$$

$$M_3=\frac{\hat{\varepsilon}_3(\Delta x_1+\Delta x_2)}{1+\hat{\varepsilon}_1\Delta x_1}$$

and

$$N_1=-\frac{\zeta_2(\Delta x_2+\Delta x_3)}{1+\zeta_1\Delta x_2}$$

$$N_2=1-\zeta_1\Delta x_3 \tag{2.136}$$

$$N_3=\frac{\zeta_3(\Delta x_2+\Delta x_3)}{1+\zeta_1\Delta x_2}$$

Equations (2.119), (2.132), (2.133) and (2.134) constitute a system of J equations with J unknowns. This system of equations has a pentadiagonal matrix structure as shown in figure 2.6 and can be solved by a general version of the Thomas algorithm for tridiagonal equations [18]. The method of solution is described as follows. First it is assumed that E_{j+1} can be expressed as:

$$E_{j+1}=\alpha_jE_j+\beta_jE_{j-1}+\gamma_j \tag{2.137}$$

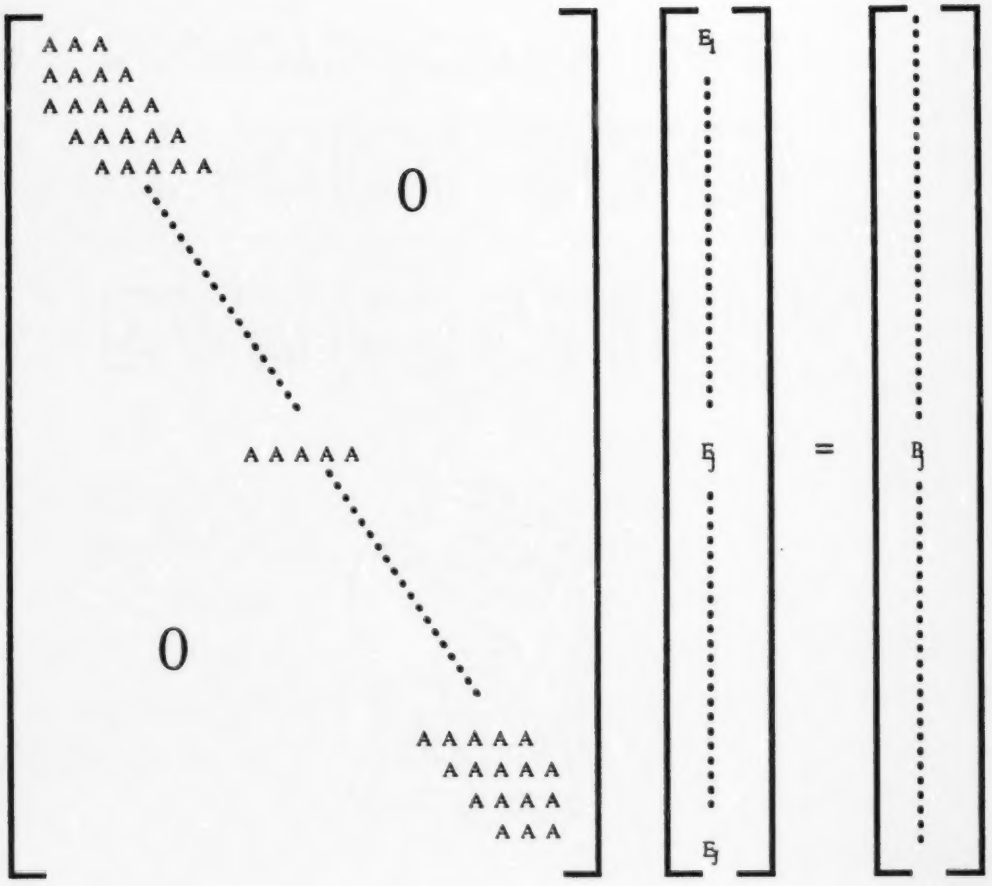

Figure 2.6: The Pentadiagonal Structure.

where α, β and γ are coefficients to be determined latter. This relation is then substituted into Eq. (2.119) in order to eliminate E_{j+2} and E_{j+1}:

$$P_1^j(\alpha_{j+1}E_{j+1}+\beta_{j+1}E_j+\gamma_{j+1})+P_2^j(\alpha_j E_j+\beta_j E_{j-1}+\gamma_j)+P_3^j E_j+P_4^j E_{j-1}+P_5^j E_{j-2}=P_6^j \qquad \textbf{(2.138)}$$

which can be written as:

$$E_j=\left[-\frac{P_1^j\beta_j\alpha_{j+1}+P_2^j\beta_j+P_4^j}{P_1^j(\alpha_j\alpha_{j+1}+\beta_{j+1})+\alpha_j\beta_j+P_3^j}\right]+\left[-\frac{P_5^j}{P_1^j(\alpha_j\alpha_{j+1}+\beta_{j+1})+\alpha_j P_2^j+P_3^j}\right]+\left[\frac{P_6^j-\gamma_j P_2^j-P_1^j(\gamma_j\alpha_{j+1}+\gamma_{j+1})}{P_1^j(\alpha_j\alpha_{j+1}+\beta_{j+1})+\alpha_j P_2^j+P_3^j}\right] \qquad \textbf{(2.139)}$$

Hence by comparing the form of Eq. (2.139) to that of Eq. (2.137) it is seen that the coefficients α, β and γ obey the recursive relations:

$$\begin{aligned}\alpha_{j-1}&=f_a[\alpha_j,\beta_j,\gamma_j;\ \alpha_{j+1},\beta_{j+1},\gamma_{j+1}]\\ \beta_{j-1}&=f_b[\alpha_j,\beta_j,\gamma_j;\ \alpha_{j+1},\beta_{j+1},\gamma_{j+1}]\\ \gamma_{j-1}&=f_g[\alpha_j,\beta_j,\gamma_j;\ \alpha_{j+1},\beta_{j+1},\gamma_{j+1}]\end{aligned} \qquad \textbf{(2.140)}$$

where f_a, f_b and f_g are given by the expressions in the corresponding square brackets in Eq. (2.139). Therefore in order to determine the coefficients, two sets of starting values are needed. The first set of these starting coefficients can be obtained from the difference equation at j = J-2 which can be written as:

$$E_{J-2}=-\frac{P_4^{J-2}}{P_3^{J-2}}E_{J-3}-\frac{P_5^{J-2}}{P_3^{J-2}}E_{J-4}+\frac{P_6^{J-2}-P_2^{J-2}E_{j-1}-P_1^{J-2}E_J}{P_3^{J-2}} \tag{2.141}$$

Since E_{J-1} and E_{J-2} are assumed zero from the boundary conditions given by Eqs. (2.132), $(\alpha, \beta, \gamma)_{J-3}$ can be determined:

$$\begin{aligned}\alpha_{J-3}&=-\frac{P_4^{J-2}}{P_3^{J-2}}\\ \beta_{J-3}&=-\frac{P_5^{J-2}}{P_3^{J-2}}\\ \gamma_{J-3}&=\frac{P_6^{J-2}}{P_3^{J-2}}\end{aligned} \tag{2.142}$$

Similarly:

$$\begin{aligned}\alpha_{J-4}&=-\frac{P_4^{J-3}+P_2^{J-3}\beta_{J-3}}{P_3^{J-3}+P_2^{J-3}\alpha_{J-3}}\\ \beta_{J-4}&=-\frac{P_5^{J-3}}{P_3^{J-3}+P_2^{J-3}\alpha_{J-3}}\\ \gamma_{J-4}&=\frac{P_6^{J-3}-P_2^{J-3}\gamma_{J-3}}{P_3^{j-3}+P_2^{J-3}\alpha_{J-3}}\end{aligned} \tag{2.143}$$

which are determined by using the difference equation at j = J-3 and the boundary conditions given by Eq. (2.132). Now that $(\alpha, \beta, \gamma)_{J-2}$ and $(\alpha, \beta, \gamma)_{J-3}$ are found, the rest of the coefficients can be obtained form the recursive relations given by Eq. (2.140).

According to Eq. (2.137) a knowledge of E_1 and E_2 is required in order to solve

for E. At j = 3 and j = 4 Eq. (2.137) becomes:

$$E_3=\alpha_2 E_2+\beta_2 E_1+\gamma_2$$
$$E_4=\alpha_3 E_3+\beta_3 E_2+\gamma_3 \qquad \textbf{(2.144)}$$

Hence Eq. (2.144) and the boundary conditions (2.133) and (2.134) consist of four equations in four unknowns (E_1, E_2, E_3 and E_4). This system of equations can then be solved to give:

$$E_2=\frac{\beta_2(\alpha_3-N_1)(\gamma_2-M_3)-(\beta_2-M_2)[\gamma_3-N_3+\gamma_2(\alpha_3-N_1)]}{(\beta_2-M_2)[\alpha_2(\alpha_3-N_1)+\beta_3-N_2]-\beta_2(\alpha_3-N_1)(\alpha_2-M_1)} \qquad \textbf{(2.145)}$$

$$E_1=\frac{M_3-\gamma_2-(\alpha_2-M_1)E_2}{\beta_2-M_2} \qquad \textbf{(2.146)}$$

Consequently E_i can be determined from the right hand side of the grid to the left hand side using Eq. (2.137).

2.9 Structure of Program

The laser code is written in FORTRAN 77. It is constructed as a subroutine which can be called from a driving program such as a hydro-code. The laser code itself calls five main routines as illustrated in figure 2.7. The input to the laser code EMREAB are the incident laser wavelength and intensity, the number of grid points, the space coordinates, the electron density profile, the electron temperature profile, and the ionic charge number profile. The output from the laser code are the electric field, magnetic field and the absorption profiles. CNVIN and CNVOUT are respectively the input

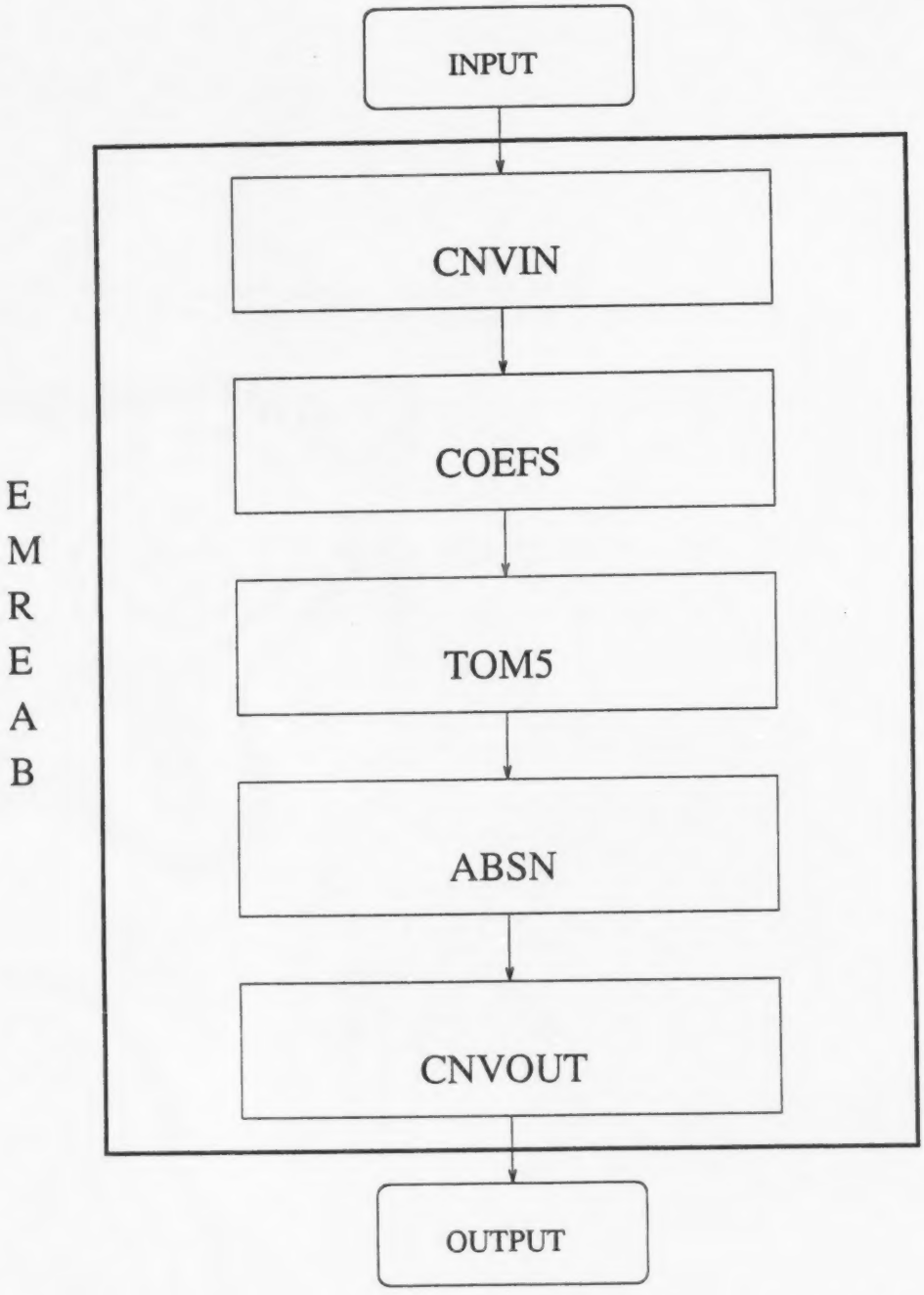

Figure 2.7: Structure of Laser Code.

conversion and output conversion subroutines. These routines facilitate the interfacing to a hydro-code with different coordinate and unit systems. COEFS calculates the coefficients P_i^j for the difference equations in (2.119). TOM5, which was taken from [19], solves the difference equations using the generalized Thomas algorithm. ABSN computes the absorption as a function of distance into the target. In ABSN, the code used to calculate the collisional frequency is taken from [20]. A listing of the laser code is given in Appendix B.

2.10 Summary

In this chapter, the development of the laser code has been discussed. The wave equations have been derived and the numerical method used to solve them has been described. The way of calculating the absorption has also been explained. Lastly, the structure of the laser code has been discussed.

In the next chapter the hydro-code to which EMREAB is interfaced will be described.

Chapter 3. The Hydro-Code

The hydrodynamic code MEDUSA used in the simulations was developed originally by Christiansen, Ashby and Roberts [20] and was intended for the study of plasma processes that can occur in laser fusion. The code has been extensively modified and improved by a number of researchers and graduate students of the laser-plasma group of the Department of Electrical Engineering at the University of Alberta. These improvements include a better model for describing the state of the plasma, the calculation of ionization from atomic physics, and the determination of x-ray emission and radiation transport.

This chapter does not attempt to give a detailed description of MEDUSA, but rather provides an overview of the fundamental equations, numerical structure and some of the modelling features that are relevant to the simulations intended for this study. Specifically the application of the code to the modelling of thermonuclear reactions, simulations with different species of ions and atoms, and simulations in cylindrical and spherical plasma geometries are omitted from the discussion below.

In this chapter, a general description of MEDUSA is given. This is followed by a discussion of the mathematical models and numerical scheme used in the code. Finally, the interfacing of MEDUSA to the laser code is described.

3.1 Introduction to MEDUSA

The plasma modelled by MEDUSA is described by four main dependent variables:

the mass density ρ, the fluid velocity u, the electron temperature T_e and the ion temperature T_i. Each of these variables is a function of time t and one spatial coordinate R. A two-fluid model is employed in which the plasma is assumed to consist of a charge-neutral mixture of electrons and ions with each species having its own thermodynamic system. The electron and ion systems are coupled by a common velocity due to charge-neutrality and by the exchange of energy due to collisions.

In order to evaluate the evolution of the plasma's hydrodynamic and thermodynamic responses as a function of time, MEDUSA solves numerically the electron and ion energy equations together with the Navier-Stokes equations. The energy equations are used to describe the thermodynamic behavior of the plasma while the Navier-Stokes equations are used to obtain the hydrodynamic response of the plasma. A one dimensional Lagrangian mesh and a five-level time integration scheme are used for the numerical calculations. In the Lagrangian mesh the plasma is decomposed into a number of fluid elements or cells with the mass in each cell kept constant throughout the course of the simulation. The cell boundaries are allowed to move at a rate governed by the Navier-Stokes equations and thus change the density of the cell. The thermodynamic quantities are computed at each cell by solving the energy equations. It should be noted that all quantities in MEDUSA are expressed in SI units.

3.2 Mathematical Model

The internal energies per unit mass for the electron fluid and ion fluid are given by:

$$U_e=\frac{p_eV}{\gamma_e-1} \quad J/kg$$
$$U_i=\frac{p_iV}{\gamma_i-1} \quad J/kg \tag{3.1}$$

where p_e and p_i are, respectively, the electron and ion pressures, γ_e and γ_i are, respectively, the electron and ion ratios of specific heats, and V is the specific volume given by:

$$V=\frac{1}{\rho} \quad m^3/kg \tag{3.2}$$

The mass density is calculated as:

$$\rho=n_iMm_H \quad kg/m^3 \tag{3.3}$$

where n_i is the ion number density, M the atomic mass number, and m_H the proton mass. In Eq. (3.3) the electron mass as well as the difference between neutron and proton masses are neglected. It is seen from Eq. (3.3) that once the mass density has been found, the ion number density can be determined. The electron number density, on the other hand, can be determined from the relation:

$$n_e=<Z>n_i \tag{3.4}$$

where <Z> is the average ionization number.

The energy equations for the electron and ion fluids can be written as:

$$\frac{dU_e}{dt}=-p_e\frac{dV}{dt}+S_e \quad W/kg$$
$$\frac{dU_i}{dt}=-p_i\frac{dV}{dt}+S_i \quad W/kg \tag{3.5}$$

which state that the rate at which energy enters into each system is equal to the work done by the pressure force and an energy source term S. The source terms $S_{e,i}$ are given by:

$$S_e=H_e+K+J+X \quad W/kg$$
$$S_i=H_i-K+Q \quad W/kg \tag{3.6}$$

Here $H_{e,i}$ represent the heat flow due to thermal conduction, K denotes the rate of exchange of energy between ions and electrons, J is the rate of bremsstrahlung emission, X is the rate of laser light absorption, and Q is the rate of viscous shock heating. The forms of $H_{e,i}$, K and Q can be found in [20]; a discussion of J is given in [21]; and X will be addressed later in this chapter. Note, however, that all these source terms are functions of the electron and ion number densities (and hence the mass density), electron and ion temperatures and the ionization number.

Using equations of state of the form:

$$p_e=p_e[\rho,T_e]$$
$$p_i=p_i[\rho,T_i] \tag{3.7}$$

the internal energies as given by Eq. (3.1) become functions of ρ and $T_{e,i}$ and the energy equations can then be rewritten as:

$$C_{ve}\frac{dT_e}{dt}+B_{Te}\frac{d\rho}{dt}+p_e\frac{dV}{dt}=S_e \quad W/kg$$
$$C_{vi}\frac{dT_i}{dt}+B_{Ti}\frac{d\rho}{dt}+p_i\frac{dV}{dt}=S_i \quad W/kg \tag{3.8}$$

where

$$C_{ve}\equiv\left(\frac{\partial U_e}{\partial T_e}\right)_\rho \;;\quad B_{Te}\equiv\left(\frac{\partial U_e}{\partial \rho}\right)_{T_e}$$
$$C_{vi}\equiv\left(\frac{\partial U_i}{\partial T_i}\right)_\rho \;;\quad B_{Ti}\equiv\left(\frac{\partial U_i}{\partial \rho}\right)_{T_i} \tag{3.9}$$

Equations (3.8) are solved by MEDUSA to determine the time evolution of the thermodynamic variables.

3.2.1 Equation of Motion

The hydrodynamics of the plasma is determined by the Navier-Stokes equation:

$$\rho\frac{du}{dt}=-\nabla p-\nabla q \tag{3.10}$$

where p is the hydrodynamic pressure defined as:

$$p \equiv p_e + p_i \tag{3.11}$$

and u is the common fluid velocity defining the motion of the Lagrangian coordinates R:

$$\frac{dR}{dt} = u[R,t] \tag{3.12}$$

The term q is an artificial viscous pressure and is discussed in [20].

3.2.2 Equation of State and Calculation of Ionization

The equation of state used in the hydro-code was developed by the laser-plasma group of the Department of Electrical Engineering at the University of Alberta. A brief discussion of the equations of state can be found in [22].

The average ionization number <Z> is calculated from the equation of state table using a best fit formula [23]:

$$\langle Z \rangle = \frac{m_i P_e}{\rho K_B T_e}\left(1 + 0.88388\alpha + 0.11310\alpha^2\right)^{-1/5} \tag{3.13}$$

where:

$$\alpha = \frac{1}{2}\left(\frac{2\pi m_e}{h^2}\right)^{-3/2} p_e \left(K_B T_e\right)^{-1/5} \tag{3.14}$$

3.2.3 Initial Conditions and Boundary Conditions

The initial conditions for solving the energy equations and the Navier-Stokes equations are such that the material target is initially a solid target with uniform solid density and temperature (300 K). The fluid velocity is therefore zero and the initial pressure can be calculated from the equation of state.

Since the energy equations contain a term $d^2T_{e,j}/dx^2$ in $H_{e,j}$ [20], two boundary conditions are required to solve them. These boundary conditions are such that there is zero thermal flux at both boundaries and the pressure at these two boundaries is zero [20,24].

3.3 Numerical Scheme

The Lagrangian mesh used by MEDUSA is shown in figure 3.1. The subscripts j and *l* are used to denote, respectively, quantities which are evaluated at the cell boundaries and quantities which are evaluated at the cell centers. Except for the fluid velocity u, which is calculated at the cell boundaries, all other quantities are determined at the cell centers. The elemental mass dM_l in each cell has units of mass per unit area (kg/m^2) and is held constant throughout the simulation.

The five level time integration scheme is shown in figure 3.2. Eqs. (3.8) are differenced accordingly as:

$$(c_v)_l^{n-1/2}\frac{T_l^n-T_l^{n-1}}{\Delta t^{n-1/2}}+(B_T)_l^{n-1/2}\frac{\rho_l^n-\rho_l^{n-1}}{\Delta t^{n-1/2}}+p_l^{n-1/2}\frac{V_l^n-V_l^{n-1}}{\Delta t^{n-1/2}}=S_l^{n-1/2} \qquad \textbf{(3.15)}$$

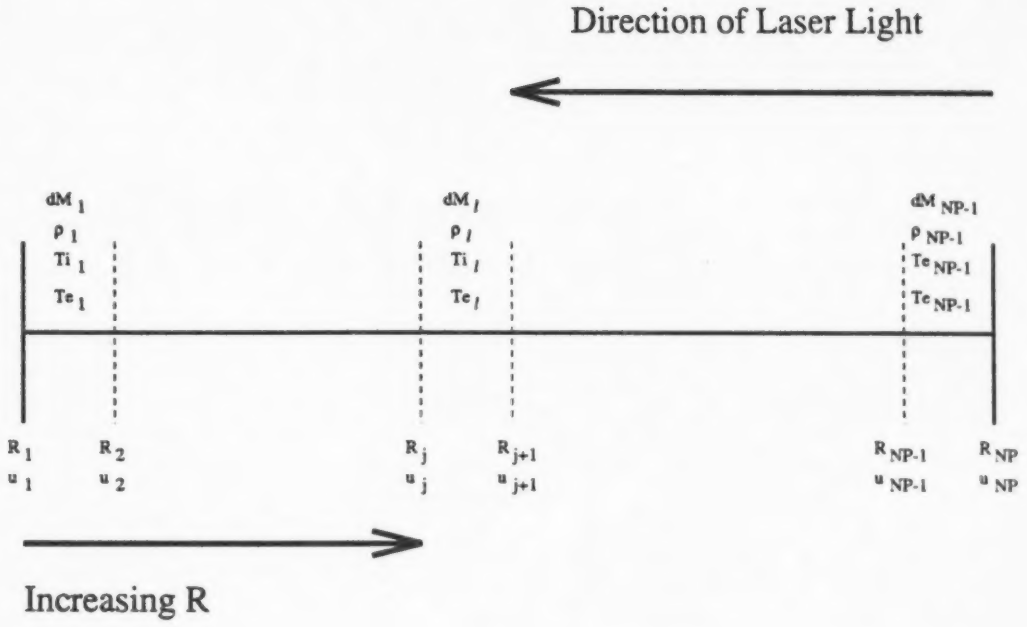

Figure 3.1: MEDUSA's Lagrangian Grid.

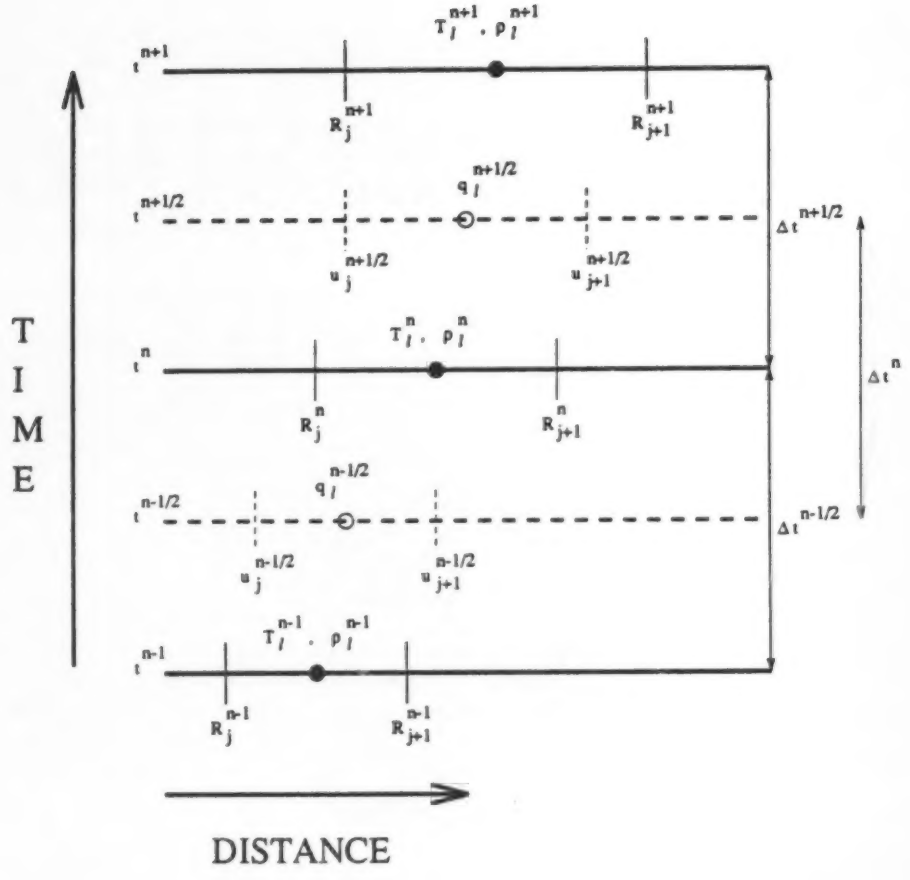

Figure 3.2: The Five Time Level Scheme.

where the subscripts e and i, used to represent electron and ion quantities, are omitted for brevity. In Eq. (3.15), only the artificial viscous pressure q, which is contained in the viscous shock heating term Q, is evaluated directly from time level n-1/2. All other quantities at this level are computed as the average of the corresponding quantities at the n and n-1 levels. For example:

$$(c_v)_l^{n-1/2}=\frac{1}{2}\left((c_v)_l^n+(c_v)_l^{n-1}\right) \tag{3.16}$$

Grouping the coefficients of T^n_{l-1}, T^n_l and T^n_{l+1} which arise from the heat flow source term H, Eq. (3.15) can be rewritten as:

$$A_l^n T_{l-1}^n+B_l^n T_l^n+C_l^n T_{l+1}^n=D_l^n+G_l^{n-1} \tag{3.17}$$

where the coefficients A, B, C, D are functions of T_l and ρ_l at the n time level and ρ_l at the n-1 time level. G contains T_l, T_{l-1}, T_{l+1} and ρ_l at the n-1 level.

The Navier-Stokes equation (3.10) is differenced as:

$$u_j^{n+1/2}-u_j^{n-1/2}=-R_j^n\frac{p_l^n-p_{l-1}^n+q_l^n-q_{l-1}^n}{dM_j}\Delta t^n \tag{3.18}$$

where the hydrodynamic pressure is calculated as:

$$p_l^n=(p_i+p_e)_l^n \tag{3.19}$$

and the elemental mass at the cell boundary is computed as:

$$dM_j=\frac{1}{2}\left(dM_{l-1}+dM_l\right) \tag{3.20}$$

Also Eq. (3.12) is differenced as:

$$R_j^{n+1}=R_j^{n}+u_j^{n+1/2}\Delta t^{n+1/2} \tag{3.21}$$

3.3.1 Method of Solution

The differenced energy equation (3.15) and the Navier-Stokes equation (3.18) are solved as follows. First, R_j and T_l are assumed to be known at t^{n-1} and u_j is assumed to be known at $t^{n-1/2}$. Then the mass density at t^{n-1} can be calculated as:

$$\rho_l^{n-1}=\frac{dM_l}{R_{j+1}^{n-1}-R_j^{n-1}} \tag{3.22}$$

Also R_j at t^n can be computed using Eq. (3.21) and hence ρ_l^n can be obtained. Since T_l^{n-1}, ρ_l^{n-1} and ρ_l^n are known quantities, Eq. (3.17) becomes a set of nonlinear equations in temperature at t^n. With boundary conditions as discussed in section 3.2.2, Eq. (3.17) can be solved iteratively using the Gauss elimination method. Once T_l^n is found p_e and p_i can be determined from the equations of state (3.7). Finally the fluid velocity at $t^{n+1/2}$ can be obtained from Eq. (3.18) and the cell boundary R_j^n from Eq. (3.21). With T_l^n, R_j^n, R_j^{n+1} and $u_j^{n+1/2}$ known, evaluation of the thermodynamic and hydrodynamic variables at the next time level t^{n+1} can be continued. Note that at $t = 0$, the temperature, cell boundaries

and fluid velocity are given by the initial conditions.

3.4 Interfacing between MEDUSA and EMREAB

MEDUSA and EMREAB are coupled through the laser energy source term X in the electron energy equation (3.1). In the simulations, X is calculated by EMREAB (as discussed in chapter 2) using the electron density, electron temperature and ionization profiles provided by MEDUSA. The ionic charge number Z as used in the laser code is replaced by the average ionization number <Z> as computed by the hydro-code. However since MEDUSA and EMREAB use different coordinate and unit systems, unit and profile conversions are needed when combining these two computer codes. The differences between MEDUSA's and EMREAB's coordinate systems are discussed below and a description of the conversion techniques will follow.

3.4.1 MEDUSA's and EMREAB's Coordinate Systems

Although the geometry of the target material -- a planar slab geometry -- is the same in MEDUSA and EMREAB, these two codes use different coordinate systems and grid structures to describe it. The differences between MEDUSA's and EMREAB's coordinate systems can be seen by comparing the MEDUSA grid shown in figure 3.1 with the EMREAB grid shown in figure 2.2. While the MEDUSA coordinate R is increasing from the left boundary (the solid-vacuum boundary) to the right boundary (or the plasma-vacuum boundary), the EMREAB coordinate x is increasing from the right boundary to the left. Also, whereas variables such as the electron density and temperature are

determined at the cell centers in MEDUSA, they are required at the cell boundaries in EMREAB to calculate the electric field . Furthermore, although the target lengths, $|R_{NP}-R_1|$ and $|x_J-x_1|$, must be equal, the grid spacing in EMREAB can be much finer than in MEDUSA, i.e. N >> J. This is because EMREAB is used to resolve the electric field inside the plasma. The electric field scale length, which is comparable to the local electromagnetic wavelength, can be much smaller than the hydrodynamic scale length modelled by MEDUSA.

3.4.2 Input Conversion

As discussed in chapter 2, the main inputs to EMREAB from MEDUSA are the electron number density, electron temperature and ionization number profiles. The transformation of these profiles to the EMREAB profiles is depicted in figure 3.3. First, a MEDUSA profile H, which can be the electron density, the electron temperature of the ionization number, is transformed to H^* according to:

$$\begin{aligned} R_j^* &= c_1\left(R_{NP}-R_{NP-j+1}\right) \\ H_j^* &= c_2\left(H_{NP-i}\right) \end{aligned} \qquad \textbf{(3.23)}$$

where c_1 and c_2 are SI to Gaussian unit conversion constants. This transformation simply redefines the origin of the MEDUSA coordinate system. Next the coordinate corresponding to H^* is found by:

$$R_i^{**} = \frac{1}{2}\left(R_i^* + R_{i+1}^*\right) \qquad \textbf{(3.24)}$$

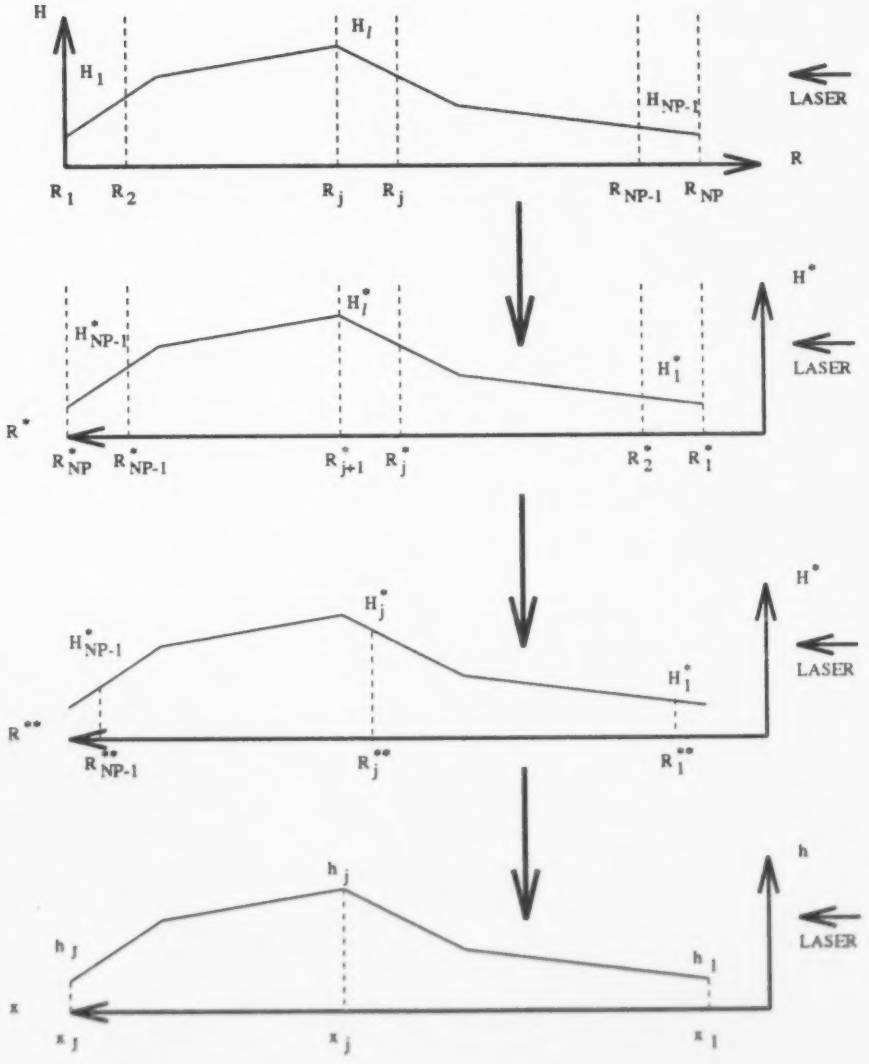

Figure 3.3: Input Profile Transformation.

Here, the coordinates corresponding to the cell centers are calculated. Then a EMREAB grid x is created such that $x_1 = R_1^* = 0$ and $R_{NP}^* = x_J$. To make the EMREAB grid finer J is chosen to be much greater the NP. Finally H^* is mapped into an EMREAB profile, h, by linear interpolation.

3.4.3 Output Conversion

The output from EMREAB to MEDUSA is the absorption profile which can be computed from the normalized energy flux profile. The conversion is illustrated in figure 3.4. First $\langle \hat{S}_x \rangle$ is converted into $\langle \hat{S}_x \rangle^*$ by linear interpolation. Then the MEDUSA energy flux profile $\langle S_x \rangle$ is obtained by:

$$\langle S_x \rangle_i = I_o \langle \hat{S}_x \rangle^*_{NP-i} \tag{3.25}$$

where I_o is the incident laser intensity. The absorption profile expressed in power per unit mass (W/kg) can then be calculated as:

$$X_i = \frac{\langle S_x \rangle_{i+1} - \langle S_x \rangle_i}{dM_i} \tag{3.26}$$

3.5 Summary

In this chapter, an overview of the hydro-code MEDUSA has been provided. The energy equations and the Navier-Stokes equations, which govern, respectively, the thermodynamic behavior and hydrodynamic response of the plasma, have been described.

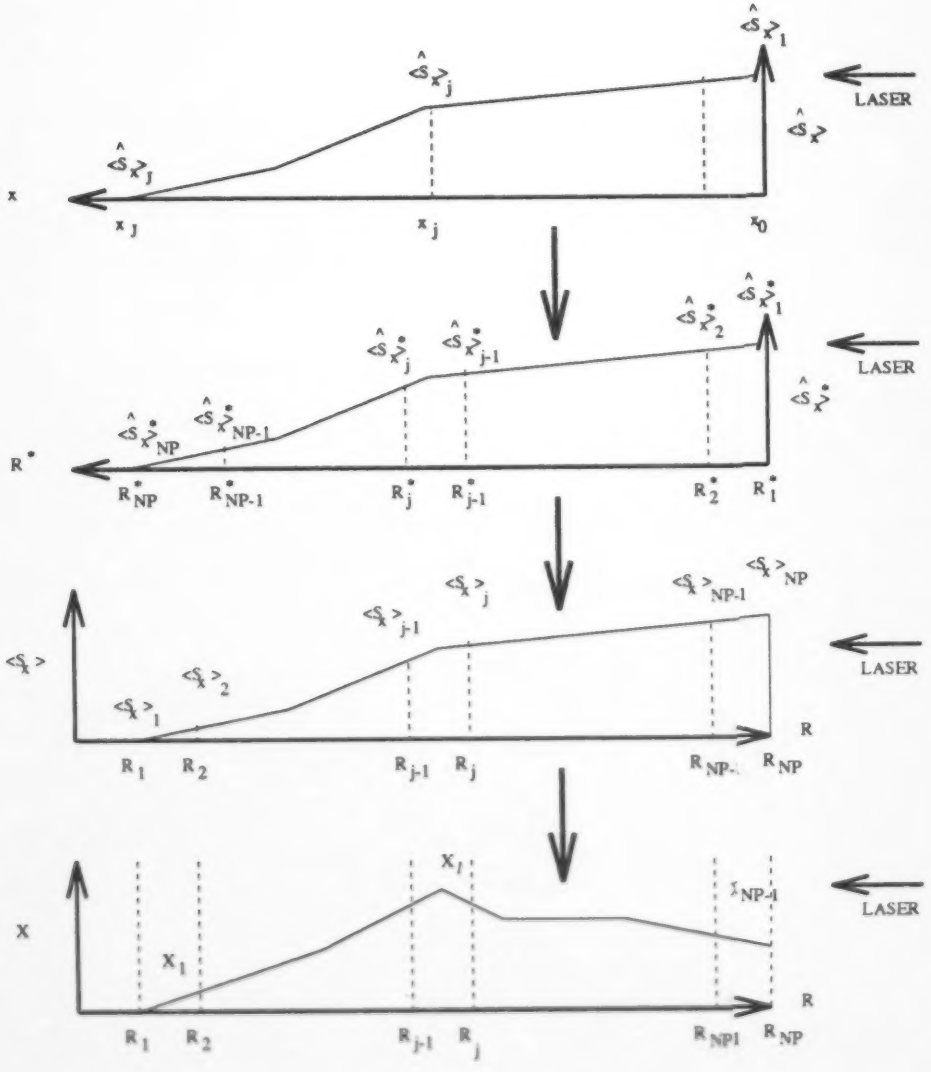

Figure 3.4: Output Profile Transformation.

The numerical scheme has been discussed. Lastly, the interfacing of the laser code to MEDUSA has been addressed.

In the next chapter the simulation results will be presented.

Chapter 4. Simulation Results

The simulation results presented in this chapter are divided into two main parts. The first part consists of results obtained from the simulations for fixed or time independent plasma density, temperature and ionization profiles. The hydrodynamic response to the absorption is not considered. Typical electric field and absorption profiles as computed by EMREAB are presented. The calculated total absorption fraction of the incident laser light is compared to known analytical as well as numerical results. The second part of this chapter consists of results from the simulations with time dependent plasma profiles. The response of the plasma's hydrodynamics is considered. Typical time evolution of the density, temperature and absorption profiles are presented. The calculated time-integrated absorption of the laser light is compared with experimental results. Also, the temperature at maximum absorption as a function of time is compared to theoretical predictions. It should be noted that all the graphical results are printed on the pages at the end of this chapter.

4.1 Simulations with Fixed Profiles

In these simulations, only the laser code is used. The hydrodynamic response of the plasma is not considered. The temperature and ionization are assumed to be constant throughout the plasma. The electron density is assume to depend either linearly or exponentially with distance and has a form:

$$n_{o(linear)}=n_c(R_o-R)/L; \quad R\le R_o$$
$$=0; \quad R>R_o \tag{4.1}$$

or

$$n_{o(exponential)}=n_c e^{-R/L} \tag{4.2}$$

where R_o is the depth of the plasma and L is the scale-length of the plasma. Also the density is set to be a constant once a maximum density n_{max} is reached. Depending on the size of L the results shown in this section are further subdivided into two categories. When L is larger than the incident laser wavelength, the laser-plasma interaction is considered long scale-length whereas when L is less than the incident laser wavelength, the interaction is considered short scale-length.

For both long and short scale-length results, the numerical mesh is constructed as follows. First the cell size at the critical density is chosen to be a fraction of scale-length:

$$\Delta R_c=d_o L \tag{4.3}$$

Then from the critical density to the low density region the cell size is increased at a geometrical rate:

$$\Delta R_{j+1}=d_1 \Delta R_j \tag{4.4}$$

where d_1 is a constant. From the critical density to the high density region the cell size is also increased at a geometrical rate:

$$\Delta R_{j-1}=d_2\Delta R_j \tag{4.5}$$

where d_2 is also a constant and can have a value different from d_1. The upper bound for the low density grid spacing is that it should be less than a fraction of the incident laser wavelength:

$$\Delta R_j \leq d_3\lambda_o \tag{4.6}$$

so that the electric field whose spatial variation in this region is of the order of the incident wavelength scale can be resolved. In the high density region, however, the electric field is evanescent and varies more gently so that an upper bound for the grid spacing is not critical. There are two reasons for using such a mesh. The first is that maximum absorption is assumed to occur near the critical density. Therefore a finer grid is needed in this region to give a better resolution of the absorption profile and hence a more accurate result for the total absorption. The second reason is that by choosing larger cell sizes at the right and left boundaries where absorption is not crucial, the number of grid points is reduced and computing time can therefore be saved.

In the following two sub-sections, the calculated electric field and absorption are presented in normalized units. It is because the wave equations (2.53) and (2.54) are linear differential equations in **E**. Therefore the electric field inside the plasma is proportional to the incident laser's electric field $\mathbf{A}_v$ at the plasma-vacuum boundary. The

absorption inside the plasma, which is proportional to $|E|^2$, is therefore proportional to the incident laser intensity which is proportional $|A_i|^2$. The mesh parameters used are: $d_o = 0.01$, $d_1 = 1.001$, $d_2 = 1.01$ and $d_3 = 0.01$.

4.1.1 Long Scale-Length Results

Figure 4.1 shows the normalized electric field and absorption profiles calculated for a linear density profile with a scale-length equal to twice the incident wavelength, a maximum density equal to twice the critical density, a temperature of 200 eV and an ionization level of 10. The laser wavelength is 1.06 μm and the angle of incidence is zero. The total absorption fraction as defined by Eq. (2.105) is found to be 0.52. Figure 4.2 shows the electric field and absorption profiles calculated for an exponential density profile using the same scale-length, temperature, ionization level, incident wavelength and angle of incidence. The maximum density is set to 200 n_c. The total absorption for the exponential density profile is found to be 0.61. In both cases the x-component of the electric field is zero. This can be explained as follows. Since the incident laser is impinging onto the plasma at zero angle of incidence, the E_x field at the right boundary is zero. Since E_x is also assumed to be zero at the left boundary, the only solution to the homogenous wave equation with these homogeneous boundary conditions is the trivial solution. The second observation to be made from these two figures is that the maximum absorption occurs very close to the critical density. The total absorption fraction for the exponential density profile (0.61) is slightly larger than that for the linear density profile. This is because the exponential profile contains a larger amount of low

density absorbing plasma. Consequently more laser energy is absorbed. Figure 4.3 shows the electric field corresponding to the exponential profile in figure 4.2. The temperature, ionization and laser wavelength are the same as in previous cases. However, the laser is impinging on the plasma at an angle of incidence of 20°. The E_x field is now non-vanishing and has a relatively large peak near the critical density. The absorption profile also has a large peak near the critical density. The total absorption fraction for this case is 0.76 which is larger than for the normal laser incidence case using the same exponential profile. The reason for a larger absorption fraction is due to resonant absorption (for example, see [13,17]). In resonant absorption, the incident laser light is incident on the plasma at an angle. A plasma wave is generated at the critical density by the finite local E_x field oscillating at the local plasma frequency. A significant portion of the laser energy can be converted to plasma wave energy. As the plasma wave is propagates towards the low density region, its energy is absorbed by the plasma due to collisional and collisionless mechanisms. Depending on the conversion efficiency, the absorption fraction for the oblique laser incidence can be larger than for normal laser incidence.

The absorption fraction as a function of incident angle is plotted in figure 4.4. Here, the density is linear with $L = 2\ \lambda_o$, a temperature of 26 keV and an ionization level of 1. The incident laser wavelength is 1.06 μm. For comparison, the results calculated by the laser code EMREAB are plotted together with the numerical results computed by Forslund et al [17] who solved a similar wave equation and used the same plasma parameters. It is seen that the results produced by EMREAB agree quit well with those

obtained by Forslund. From figure 4.4, it is seen that for such a high temperature the absorption at normal laser incidence is essentially zero and the maximum absorption occurs at an angle of incidence of about 20°.

For normal laser incidence, analytical expressions for the long density scale-length absorption fraction are known for both the linear and exponential profiles [26]:

$$\alpha_{linear}=1-\exp\left[-\frac{64}{15}\pi\frac{\nu_c^*}{\omega}\frac{L}{\lambda_o}\right] \tag{4.7}$$

and

$$\alpha_{exponential}=1-\exp\left[-\frac{16}{3}\pi\frac{\nu_c^*}{\omega}\frac{L}{\lambda_o}\right] \tag{4.8}$$

where ν_c^* is the collisional frequency at the critical density. The numerically calculated absorption fraction as a function of density scale-length L is shown in figure 4.5 together with that computed using Eqs. (4.7) and (4.8). The temperature is 200 eV, the ionization level is 10 and the laser wavelength is 1.06 μm. It is seen that the simulation results agree very well with the analytical results.

4.1.2 Short Scale-Length Results

Figures 4.6 to 4.8 show the electric field and absorption profiles for the same temperature (T_e = 200 eV), ionization level ($\langle Z \rangle$ = 10) and incident wavelength (λ_o = 1.06 μm) as in figures 4.1 to 4.3. However the density scale-length is now one

tenth of the incident laser wavelength ($L = 0.1\ \lambda_o$) and a maximum density of 100 n_c is imposed. Figures 4.6 and 4.8 are for a linear density profile while figure 4.7 is for an exponential profile. The incident laser angle in figures 4.6 and 4.7 is zero and the angle of incidence in figure 4.8 is 20°. Comparing figure 4.6 with figure 4.1, it is seen that the E_y field is evanescent beginning at the low density boundary and the harmonic wave nature of the electric field can not be noticed. The total absorption fraction is now 0.07 which is much less than that found in figure 4.1. The peak absorption, however, still occurs near the critical density. In figure 4.7, the oscillations of the electric field can still be noticed because of the long low density edge of the exponential profile which damps the propagating wave more gradually. The total absorption fraction here is also 0.07 which is the same as that for the short scale-length linear density case but much less than the corresponding long scale-length case. In figure 4.8, the plasma wave feature can be seen in the E_x field whose spatial variation has a scale length much smaller than the incident wavelength. This can be explained by examining the dispersion relation given by Eq. (2.38) for the plasma wave which predicts a shorter wavelength for the plasma wave than for the incident wave. Although the maximum absorption should still occur near the critical density, the minimum absorption now has a negative value. It is thought that the absorption pattern observed here is due to the interference of the plasma wave and the electromagnetic waves inside the plasma. The wave-wave interaction may be able to locally extract energy from the plasma. A more detailed physical interpretation will be examined in later investigations. However the total absorption calculated for this case is positive and has a value of 0.29. This means that, on average, the incident laser light

loses energy to the plasma. This is physical because the plasma considered here is a passive medium and cannot amplify the incoming laser light.

Figure 4.9 shows the absorption fraction calculated as a function of angle of incidence. The solid curve represents the calculation for a linear density plasma with a scale-length of $0.5 \cdot 10^{-6}\ \lambda_o$, where $\lambda_o = 1.06\ \mu m$. The temperature, ionization level and incident wavelength are 200 eV, 10 and 1.06 μm, respectively. The maximum density is chosen to be 200 n_c. The open circles represent the absorption fraction computed by using Fresnel's formula for a steplike density profile (L = 0):

$$\alpha_f = \left| \frac{\tan(\theta - \theta_c)}{\tan(\theta + \theta_c)} \right| \qquad (4.9)$$

where θ is the incident laser angle and θ_c is the complex propagation angle inside the plasma given by:

$$\theta_c = \arcsin\left[\frac{\sin\theta}{\left(1 - \frac{n_{eo}/n_c}{1 + i\nu_c/\omega} \right)^{1/2}} \right] \qquad (4.10)$$

where n_{eo} is the steplike density of the plasma. Here n_{eo} is also chosen to be 200 n_c. The temperature is 200 eV and the ionization level is 10. From figure 4.9, it is seen that the absorption calculated by the laser code agrees very well with the Fresnel's results for θ = 0° up to θ = 30°. The maximum discrepancy occurs at the maximum absorption and has a value of about 14 %. The differences do not diminish as L is further reduced in the laser code. This may be due to the fact that the Fresnel formula does not take into

account the effects of plasma wave generation at oblique incidence angles, which may become important near the optimum absorption angle (which is about 85° in this case). The absorption fraction for L = 0.1 λ_o with the same temperature, ionization and incident wavelength is also shown in figure 4.9 for comparison. It is seen that the change of scale-length does not alter the value of the maximum absorption dramatically. But the location of the maximum absorption is shifted to a smaller incidence angle.

4.2 Simulations with Time-Dependent Profiles

In the simulations to be discussed below, the plasma's hydrodynamic response due to the absorption of laser energy is accounted for. The target material is assumed to be a solid having an initial room temperature of 300° K. The laser intensity as a function of time is assumed to follow a Gaussian shaped profile:

$$I_o[t]=I_{max}e^{-\left(\frac{t-ab}{b}\right)^2} \tag{4.11}$$

where I_{max} is the maximum laser intensity, b is the half-width at $1/e^2$ of I_{max} and a is the number of b time intervals before maximum intensity. For a laser pulse with FWHM (Full Width at Half Maximum) equal to τ, a is computed as:

$$a=\frac{\tau}{2\sqrt{\ln(2)}} \tag{4.12}$$

2 of/de 2

PM-1 3½"x4" PHOTOGRAPHIC MICROCOPY TARGET
NBS 1010a ANSI/ISO #2 EQUIVALENT

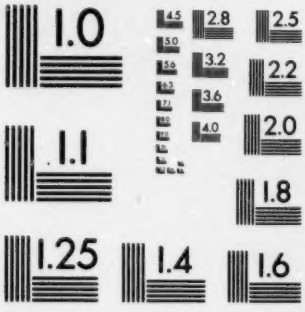

PRECISION[SM] RESOLUTION TARGETS

PIONEERS IN METHYLENE BLUE TESTING SINCE 1974

Micro-D

15000 COUNTY ROAD 5, BURNSVILLE, MN 55337, USA
TEL 612 435 7697 FAX 612 435 7697 TLX 910 563 3448

The time integrated absorption fraction is defined as:

$$\alpha_T = \frac{\int_{t=0}^{t=T_f} \alpha[t] I_o[t] dt}{\int_{t=0}^{t=T_f} I_o[t] dt} \qquad (4.13)$$

where α is the absorption fraction calculated at each time step and T_f is the time at which the laser light is switched off.

Since the target is assumed to be a solid initially, the electron density at the laser light boundary is much higher than the critical density. Hence the boundary conditions (section 2.4) derived for the wave equation which assume a low density and zero plasma gradient boundary are no longer valid. Therefore the laser code cannot be used to calculate the absorption. One simple way of modelling this stage of the interaction is to assume that all of the incident laser energy is absorbed by a thin solid layer at the surface of the target. In the simulations, this is done by depositing all of the laser energy into the first hydro-cell at the laser-target boundary. As the cell expands, its density drops. Once the electron density of this cell decreases below the critical density, the laser code is then switched on to solve the wave equation and calculate the absorption.

The hydro and laser meshes are constructed as follows. For the hydro-mesh, the cell at the laser-plasma boundary is chosen to be sufficiently small so that its density would drop below the critical density at the earliest stage of the simulation. Usually the cell size is chosen to be a fraction (typically 0.01) of the incident wavelength. The size of subsequent cells is then increased at a geometrical rate from the laser-plasma boundary to the solid boundary to save the number of simulation cells and hence reduce computing

time. For the laser mesh, the cell spacing is determined using the procedure discussed in section 4.1 except that the scale-length L is now defined as:

$$eL \equiv \left(\frac{1}{n_c} \frac{dn_o}{dR} \right)^{-1} \tag{4.14}$$

which is equivalent to the scale-length discussed before for linear or exponential profiles.

4.2.1 Typical Results

Figure 4.10 shows the time evolution of the electron density profile n_o, average ionization number profile <Z>, electron temperature profile T_e and absorption profile $<W_s>$ at three different times, for a laser pulse with $I_{max} = 10^{14}$ W/cm^2, $\lambda_o = 0.25$ μm and FWHM = 250 fs. These times correspond to the time when the laser code is just switched on (t = 0.05 ps), the time of maximum laser intensity (t = 0.3 ps) and the time just before the laser is turned off (t = 0.59 ps). The target material is aluminum. From the graph, the temperature and ionization profiles at the peak laser power are nearly constant in the region where most of the laser energy is absorbed. In this region, the temperature is about 30 eV and the ionization is about 4.5. The maximum electron density is about 15 times the critical density. The density scale-length as defined by Eq. (4.14) is found to be 0.011 λ. The input laser intensity, the absorbed laser intensity as well as the time-dependent absorption fraction (Eq. 2.105) are plotted in figure 4.11. The time-dependent absorption fraction being equal to unity at the beginning of the simulation is due to the assumption that the laser energy is totally absorbed in the cold

target stage. One interesting result observed from the graph is that the time-integrated total absorption fraction α_T which is 0.28 is nearly the same as the time-dependent absorption α at the peak laser intensity. This result is also observed for other angles of laser incidence. For $\theta = 45°$, with the same laser parameters and target material, the time evolution of the n_o, $<Z>$, T_e and $<W_s>$ profiles is plotted in figure 4.12. Although a significant amount of absorption also occurs in the region where temperature and ionization are nearly constant, some laser energy is absorbed in a lower temperature and ionization region. The temperature at the maximum absorption region now has a large value of 100 eV and the ionization level increases to about 9. The time-dependent absorption fraction is shown in figure 4.13. The time-integrated absorption fraction compares well to the time-dependent absorption at the peak of the laser pulse.

4.2.2 Angular Dependence of Absorption and Plasma Parameters

The calculated time-integrated total absorption of the incident laser light as a function of angle of incidence is shown in figure 4.14 (the solid line). Also shown are the experimental data obtained by Fedosejevs et at [6]. The laser parameters ($I_{max} = 10^{14}$ W/cm^2, FWHM = 250 fs and $\lambda_o = 0.25$ μm) are the same as those used in sub-section 4.2.1 which were chosen to model the experimental laser pulse. The target is aluminum. From figure 4.14, it is seen that the simulation results agree qualitatively with the experimental results. Both the experimental and calculated absorption fractions increase to a maximum from small angles and fall off at large angles. However, the calculated maximum angle of absorption is about 40° which is quite different from the

measured value of about 54°. The absorption determined from the simulations is also significantly lower than the experimental result, particularly at larger angles of incidence. The discrepancy remains to be investigated.

Since the simulation results agree qualitatively with experimental results, it is logical to infer the sensitivity of the plasma parameters to the angle of laser incidence. Table 4.1 presents the angular dependance of the maximum electron density (n_{om}), the ionization number and temperature at maximum local laser absorption ($\langle Z \rangle_m$ and T_{em}, respectively), and the density scale-length as defined by Eq. (4.14). From the data, it is seen that the dependence of these plasma parameters on the incident angles follows approximately the same trend as the time-integrated absorption fraction. They all rise to a maximum value at or near the maximum absorption angle and then decrease again. From normal laser incidence to the optimum absorption angle, the change of electron temperature is the most profound. The temperature at the optimum angle is about four times higher than at zero angle of incidence. The density scale-length and the ionization level show a lesser dependence on incident angle. The maximum electron density exhibits the weakest dependence.

For comparison, results are also obtained for $I_{max} = 2.5 \cdot 10^{15}$ W/cm^2 for the same pulse duration, laser wavelength and target material as before. Figure 4.15 shows the time-integrated absorption as a function of angles of incidence together with experimental results obtained from [6]. Table 4.2 tabulates the plasma parameters. In figure 4.15 the difference between simulation and experimental results can clearly be seen. The discrepancy at smaller incident angles is, however, larger than before. This is likely due

Table 4.1: Calculated Plasma Parameters for $I_{max} = 10^{14}$ W/cm^2

θ	L/λ_o	T_{em}	$\langle Z \rangle_m$	n_{om}/n_c	α_T
0	0.011	28.0	4.02	14.1	0.28
10	0.011	28.2	4.05	14.5	0.29
20	0.013	28.2	4.05	14.5	0.32
30	0.021	76.1	8.19	15.3	0.38
40	0.029	105.1	9.53	16.5	0.43
50	0.019	111.3	9.45	16.6	0.40
60	0.018	82.2	8.59	13.7	0.25
70	0.014	37.4	5.10	9.8	0.09
80	0.009	11.4	2.12	10.0	0.02

Table 4.1: Calculated Plasma Parameters for $I_{max} = 2.5 \cdot 10^{15}$ W/cm^2

θ	L/λ_o	T_{em}	$\langle Z \rangle_m$	n_{om}/n_c	α_T
0	0.05	213	10.5	39.5	0.16
10	0.07	408	11.2	41.0	0.17
20	0.10	958	12.6	46.2	0.37
30	0.12	1488	12.8	50.9	0.52
40	0.16	1607	12.9	51.2	0.54
50	0.15	1402	12.8	52.0	0.40
60	0.11	1013	12.6	50.8	0.26
70	0.09	582	11.8	45.2	0.15
80	0.04	109	9.4	15.0	0.02

to the laser prepulse which becomes more important when the intensity is increased. The plasma parameters obtained at this intensity show an angular dependence similar to the lower intensity case. Their values all reach a maximum at or near the optimum absorption angle. The variation of electron temperature is still the most noticeable and the change in the maximum density remains gentle. However the values of the parameters are significantly higher than in the lower intensity case. At optimum angle, the density scale-length is five times longer than before. The temperature is about thirteen times higher. The aluminum atoms which have an atomic charge of 13 are almost fully ionized. The electron density is now about three times higher than the previous case.

4.2.3 Comparison with Theoretical Predictions

Recently, W. Rozmus and V. Tikhonchuk [27] have developed a theory for obtaining scaling laws for plasma temperature, thickness of the heated region and other plasma parameters. The time evolution of the electron temperature has also been determined. In their theory, the plasma is assumed to have a steplike profile which does not change with time. The temperature and ionization are assumed to be constant throughout the plasma. The effects of inhibited heat fluxes and nonlocal thermal transport are considered. For a laser pulse having the pulse shape:

$$I_o[t]=I_{max}\sin^2\left[\frac{\pi t}{\tau_o}\right] \qquad (4.15)$$

and with $I_{max} = 10^{18}$ W/cm^2, $\tau_o = 230$ fs and $\lambda = 0.5$ μm, the temperature as a function of time is plotted in figure 16. The solid curve represents the temperature calculated from simulations and the dashed curve denotes the results predicted by theory. The scaling constants T. and t. are calculated from the theory by:

$$T_* = 16 Z^{-5/8} \lambda_o^{-1/2} I^{3/4} \quad keV \tag{4.16}$$

$$t_* = 90 Z^{-2} \lambda_o^{-3/4} I^{9/8} \quad ps \tag{4.17}$$

where I is in units of 10^{18} W/cm^2, and λ_o is in microns. These formulae are obtained by assuming a Coulomb logarithm of 5, a solid state density of $6 \cdot 10^{22}$ cm^{-3}. Using Z = <Z> obtained from the simulations and $\lambda_o = 0.5$ μm, T. and t. are calculated to be 5.4 keV and 2.3 ps, respectively. It is seen from figure 4.16 that the simulation results agree reasonably well with the theoretical results. The slight shift of the simulation curve to the right of the theoretical curve is likely due to the effects of plasma expansion which is not considered in the theory.

4.3 Summary

In this chapter, the simulation results have been presented. The results obtained with fixed plasma profiles have been compared with analytical as well as known numerical results. The time-dependent simulation results have also been tested against both experimental and theoretical results. The sensitivity of the plasma parameters to the angles of incidence and to the laser intensity has also been discussed.

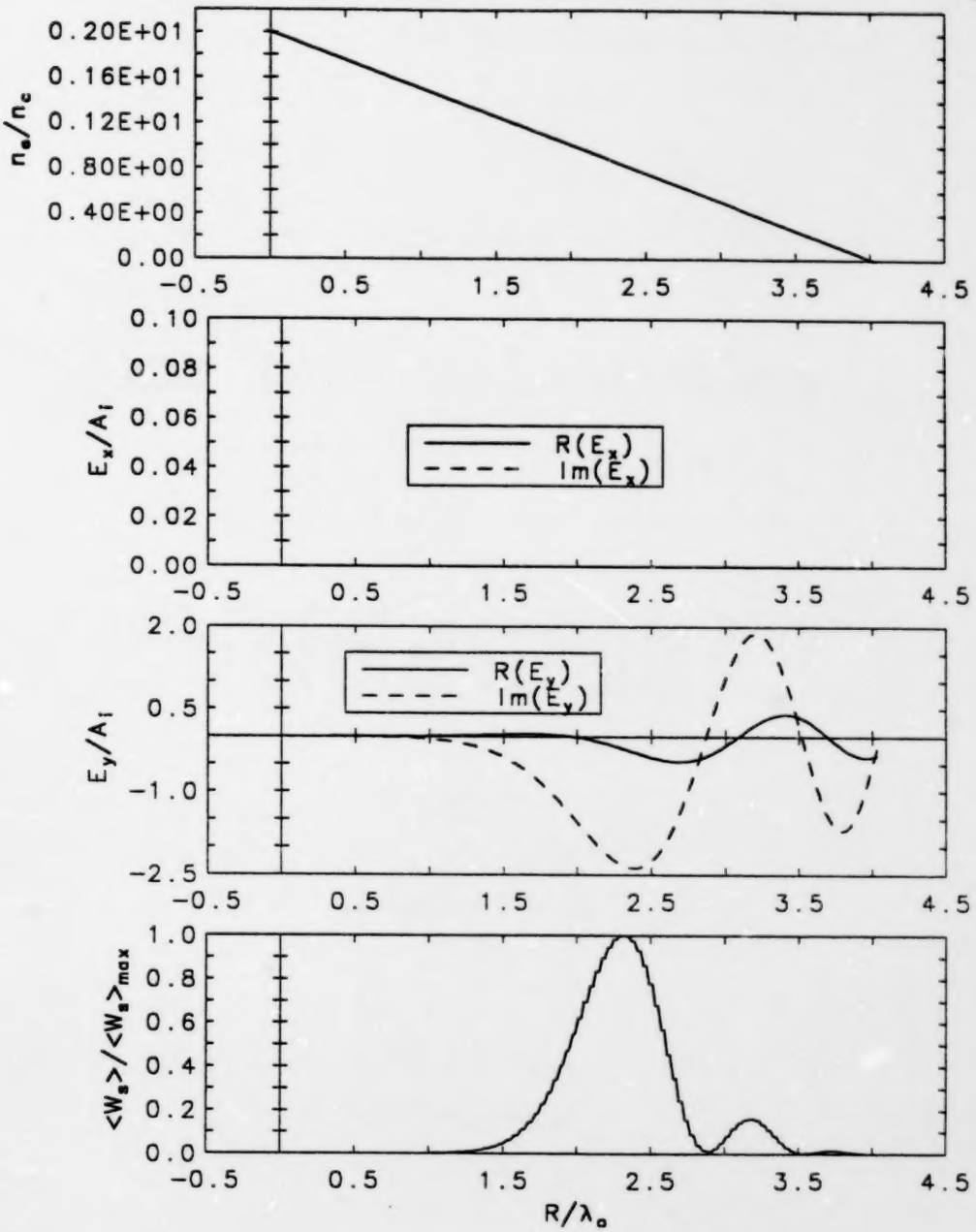

Figure 4.1: Electric field and absorption profiles calculated for a long scale-length linear density profile at zero angle of incidence.

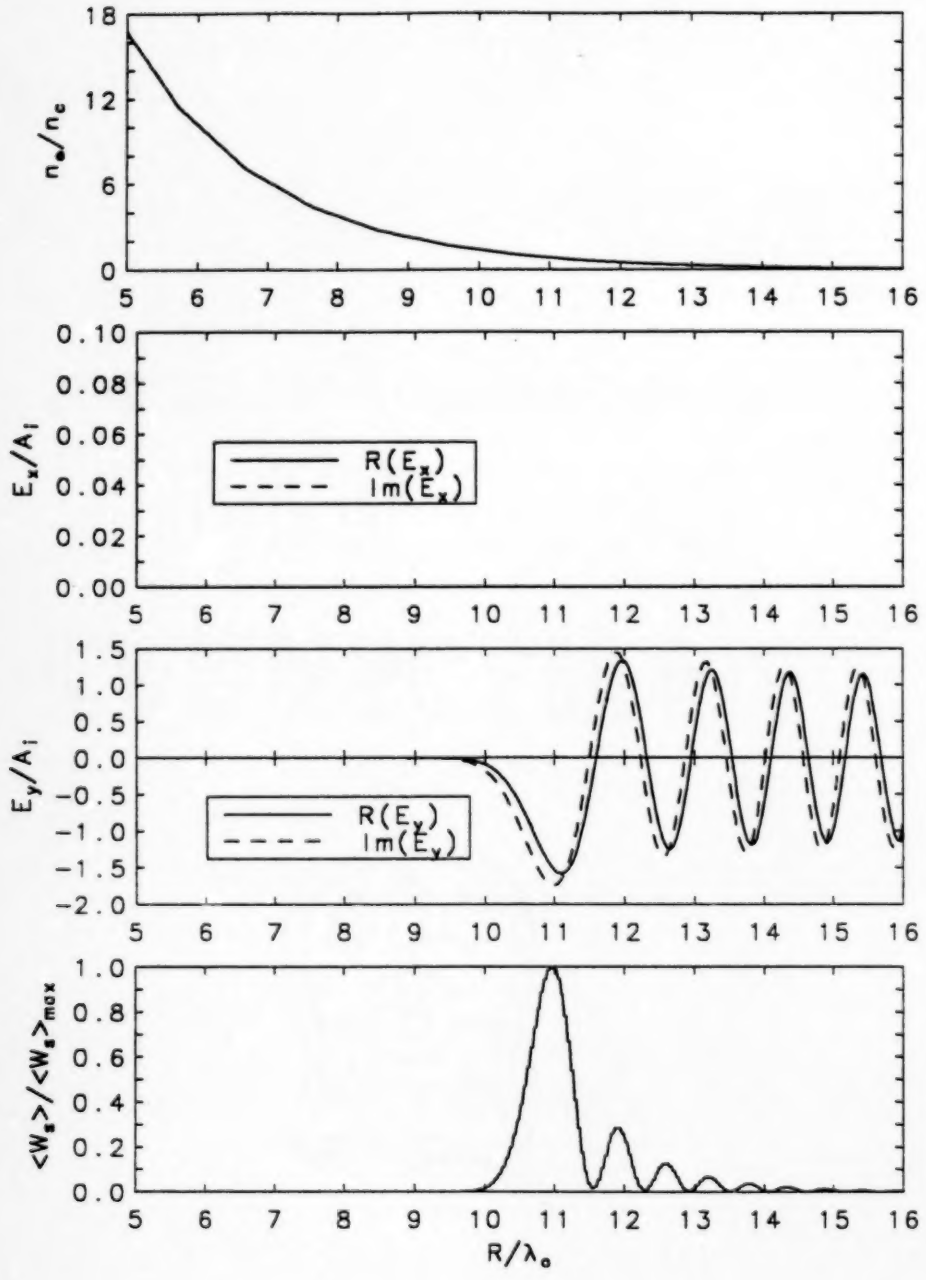

Figure 4.2: Electric field and absorption profiles calculated for a long scale-length exponential density profile at zero angle of incidence.

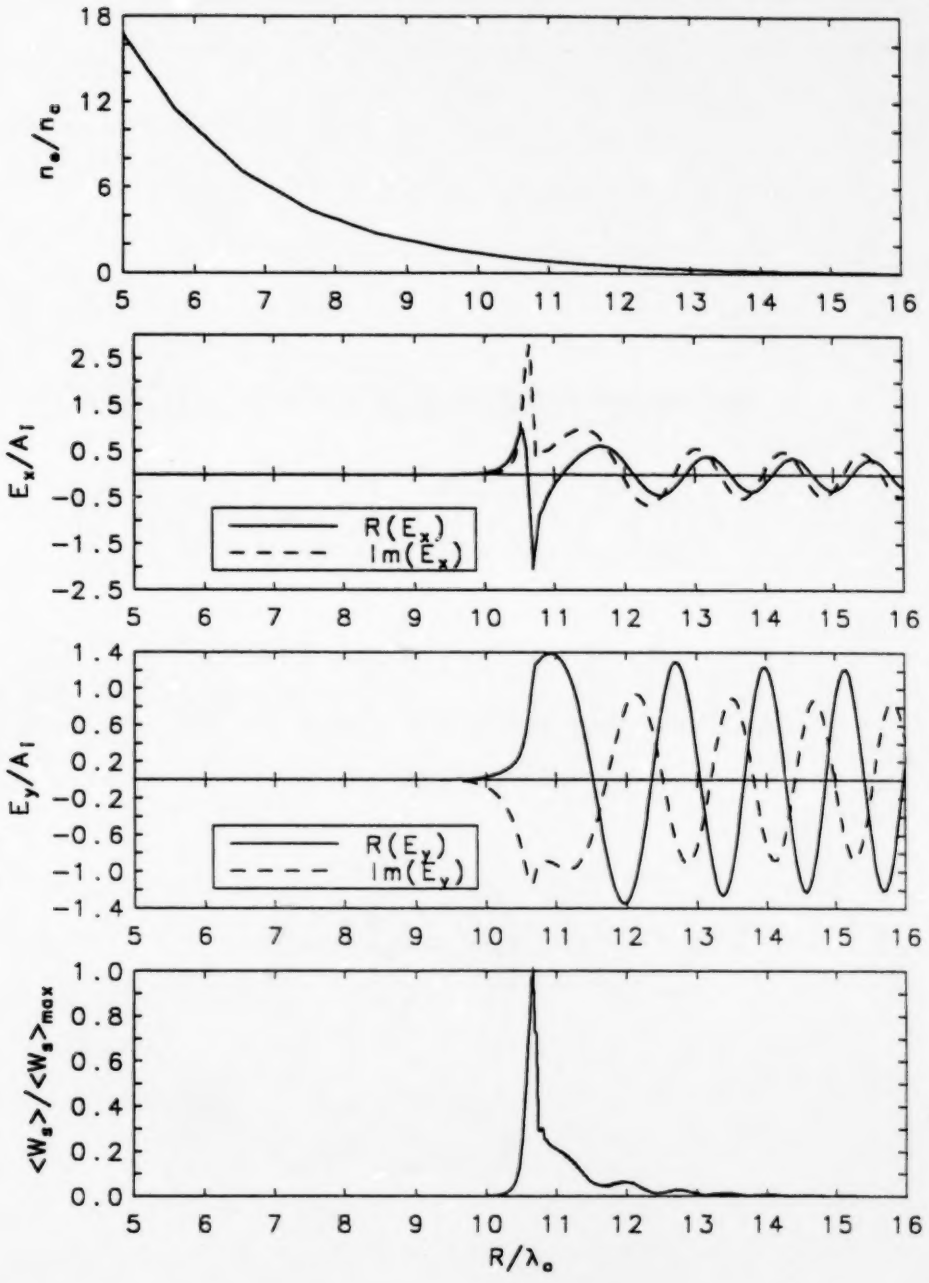

Figure 4.3: Electric field and absorption profiles calculated for a long scale-length exponential density profile at angle of incidence = 20°.

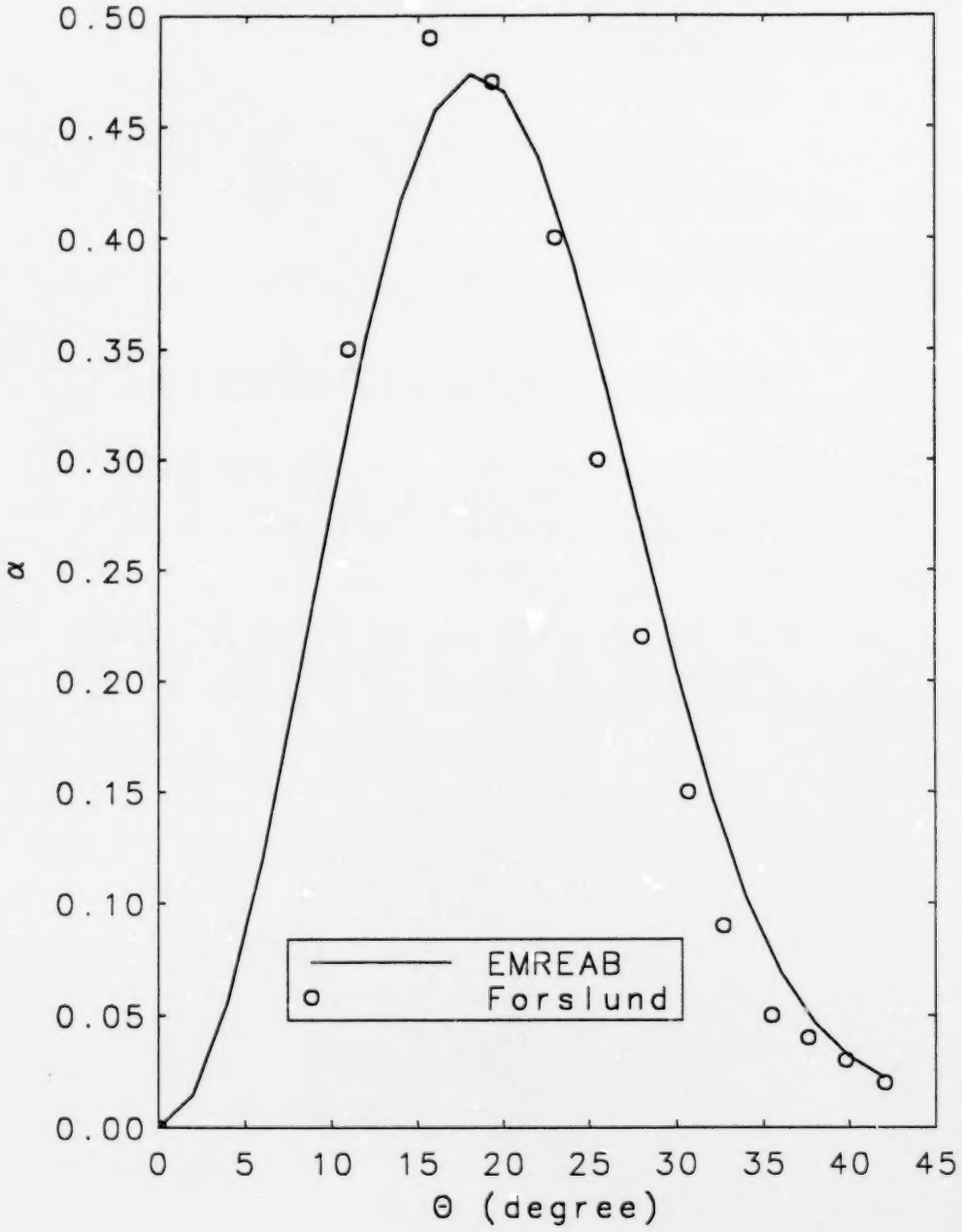

Figure 4.4: Angular dependence of total absorption fraction for a long scale-length linear density profile.

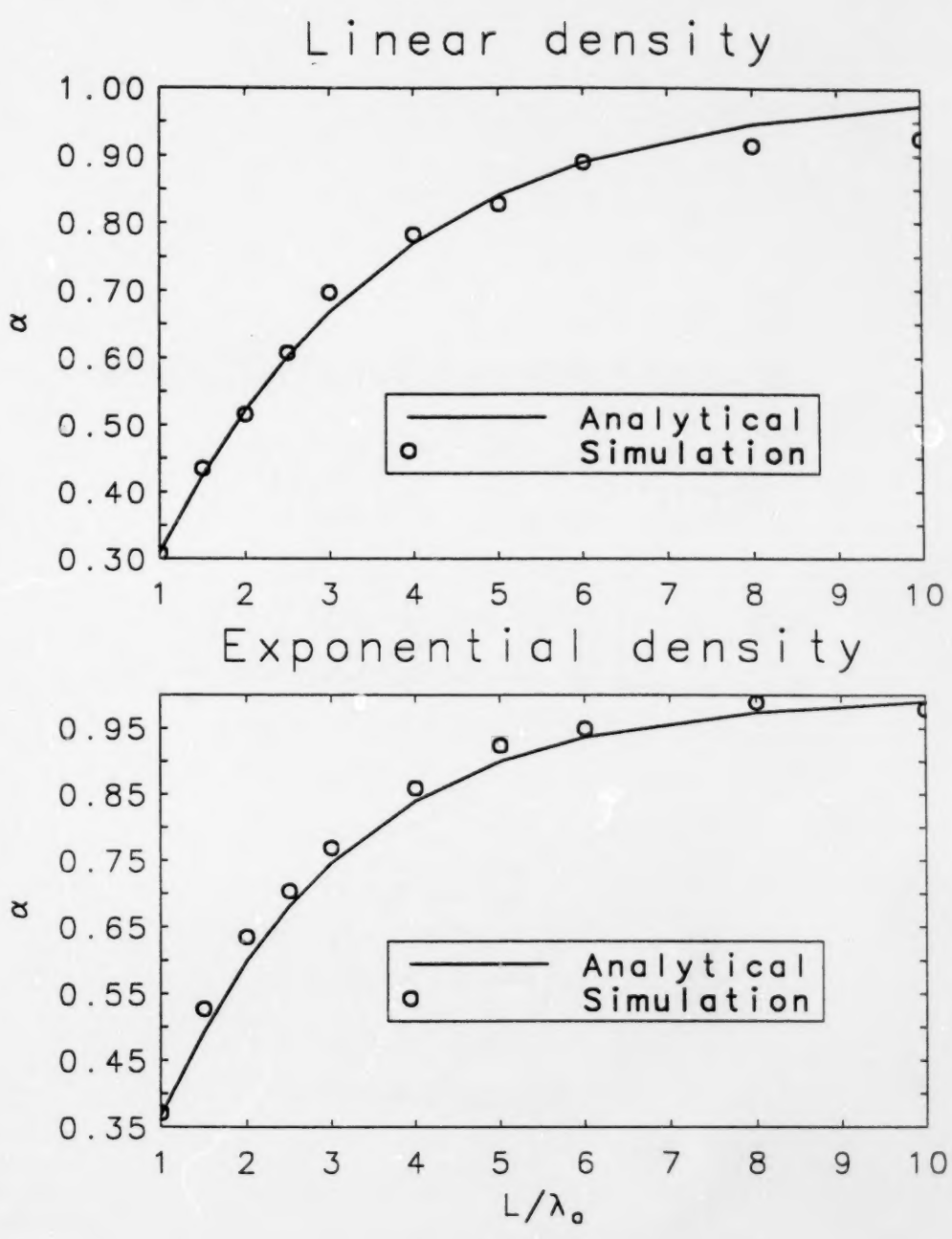

Figure 4.5: Dependence of total absorption fraction on density scale-length.

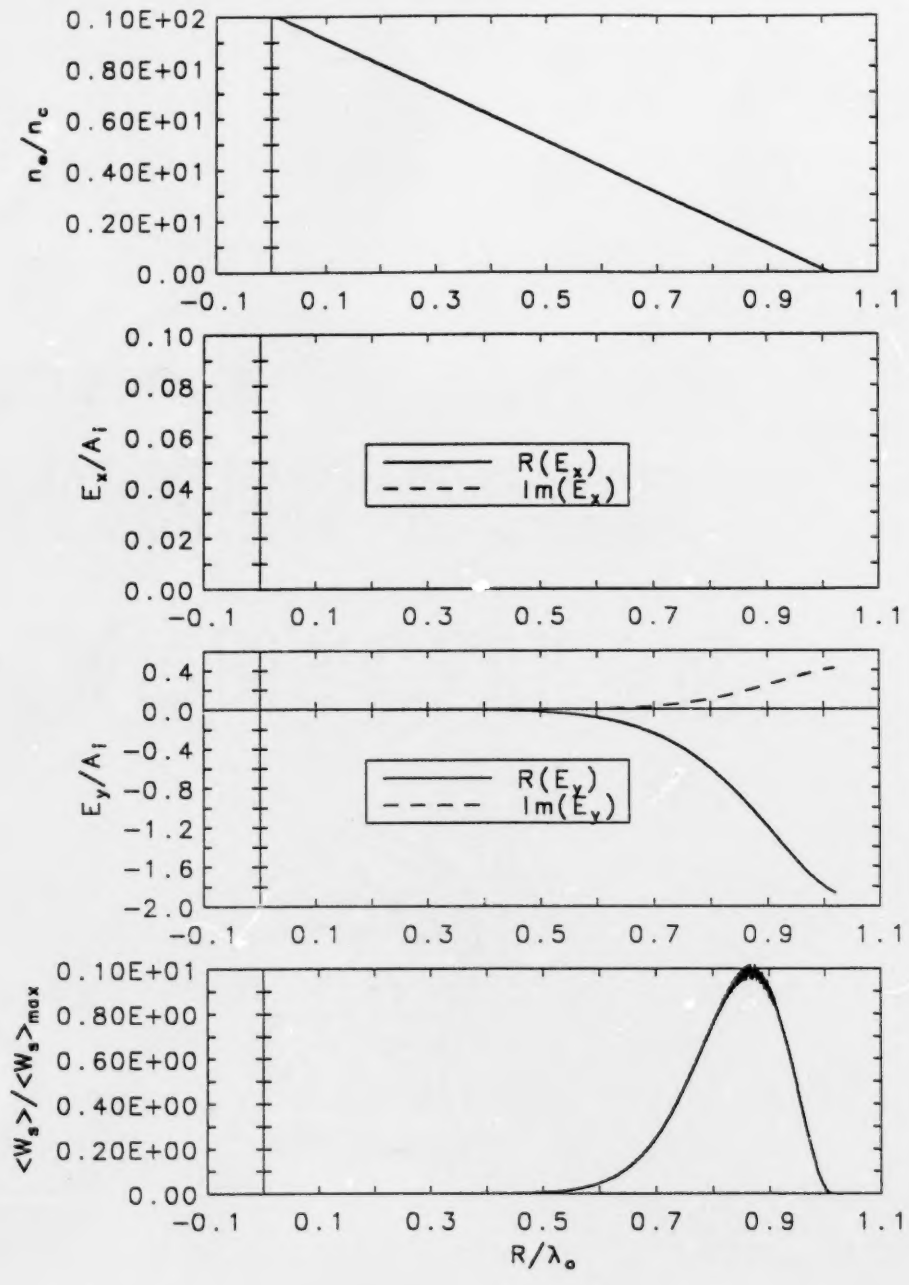

Figure 4.6: Electric field and absorption profiles calculated for a short scale-length linear density profile at zero angle of incidence.

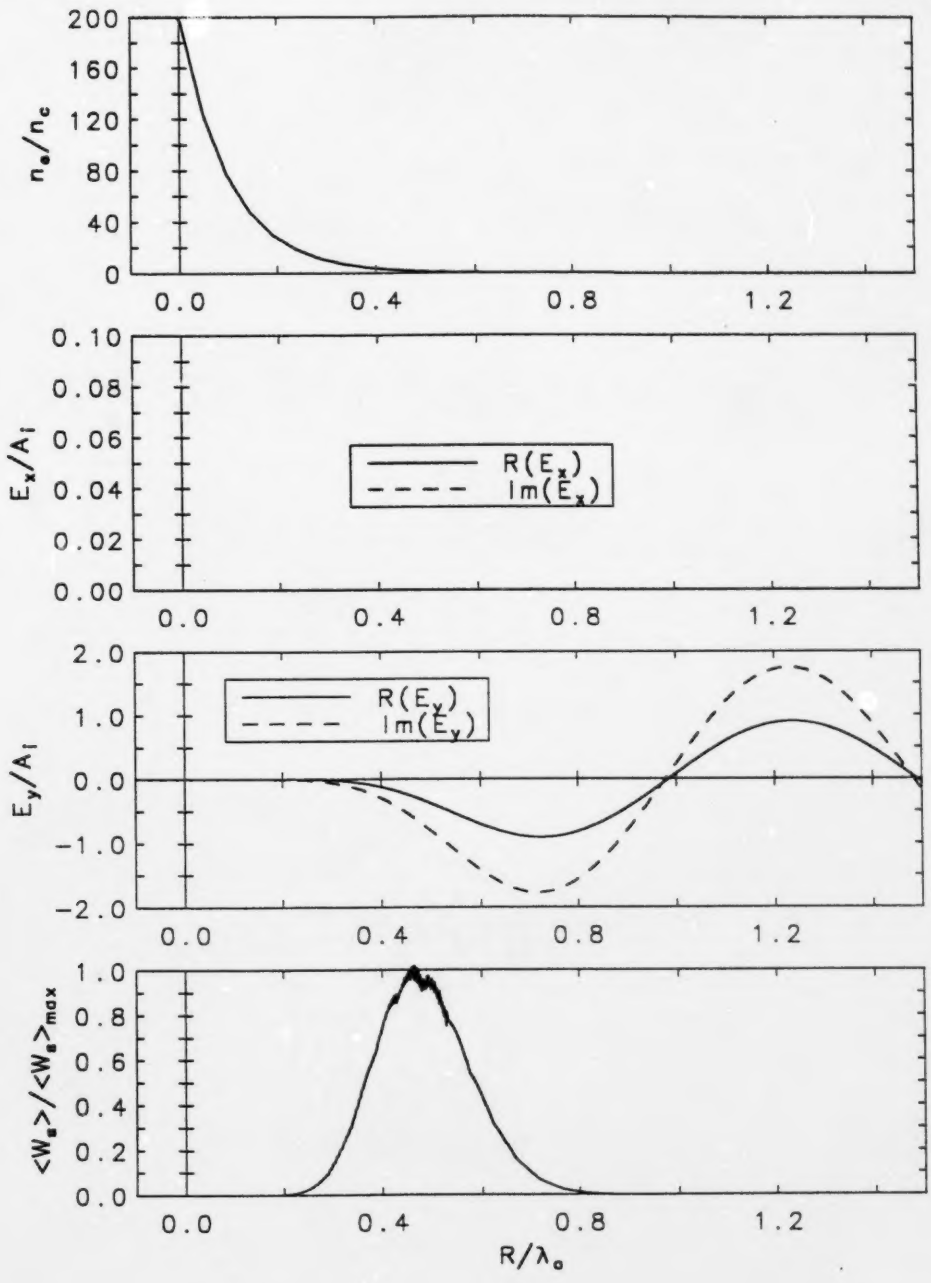

Figure 4.7: Electric field and absorption profiles calculated for a short scale-length exponential density profile at zero angle of incidence.

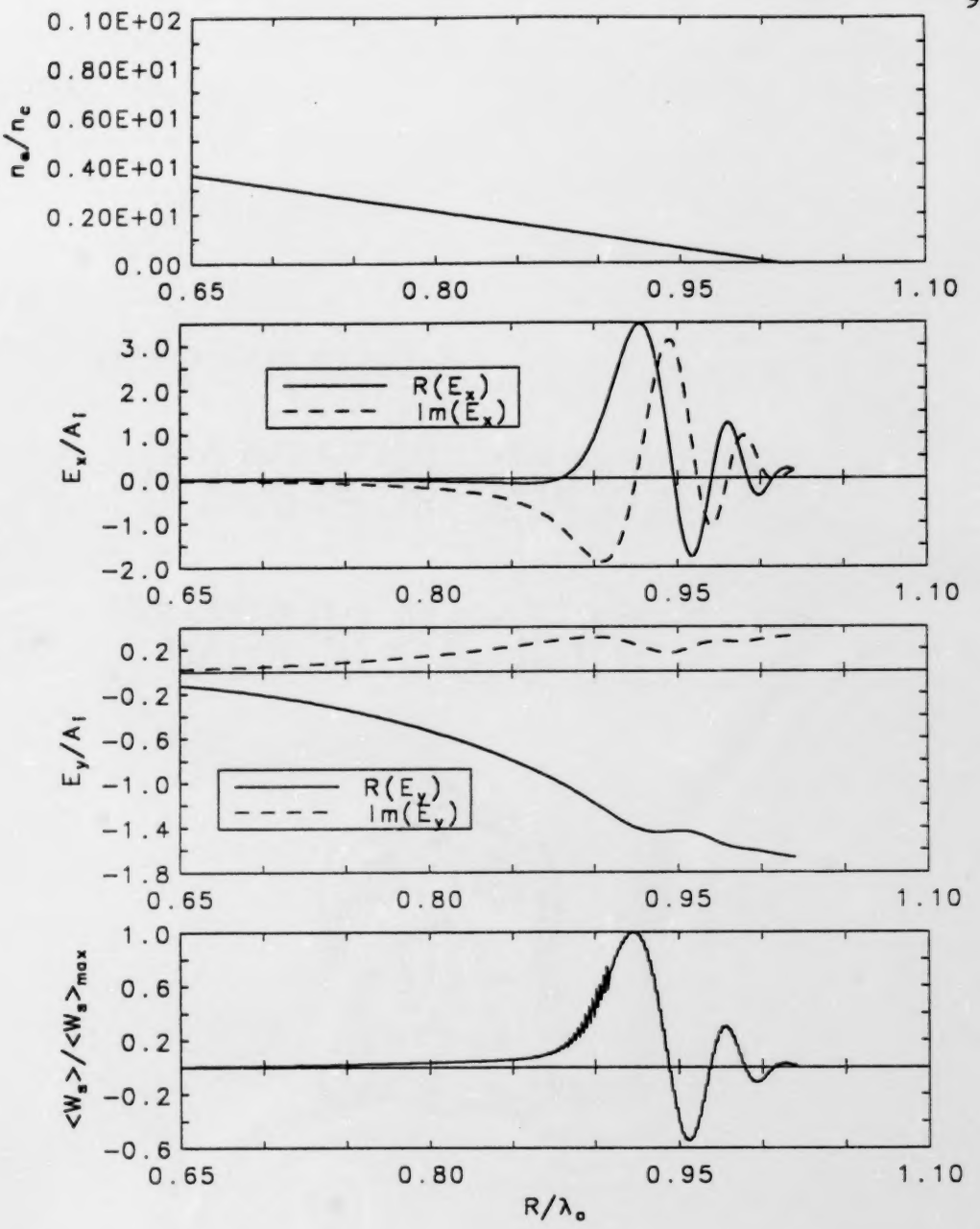

Figure 4.8: Electric field and absorption profiles calculated for a short scale-length linear density profile at angle of incidence = 20°.

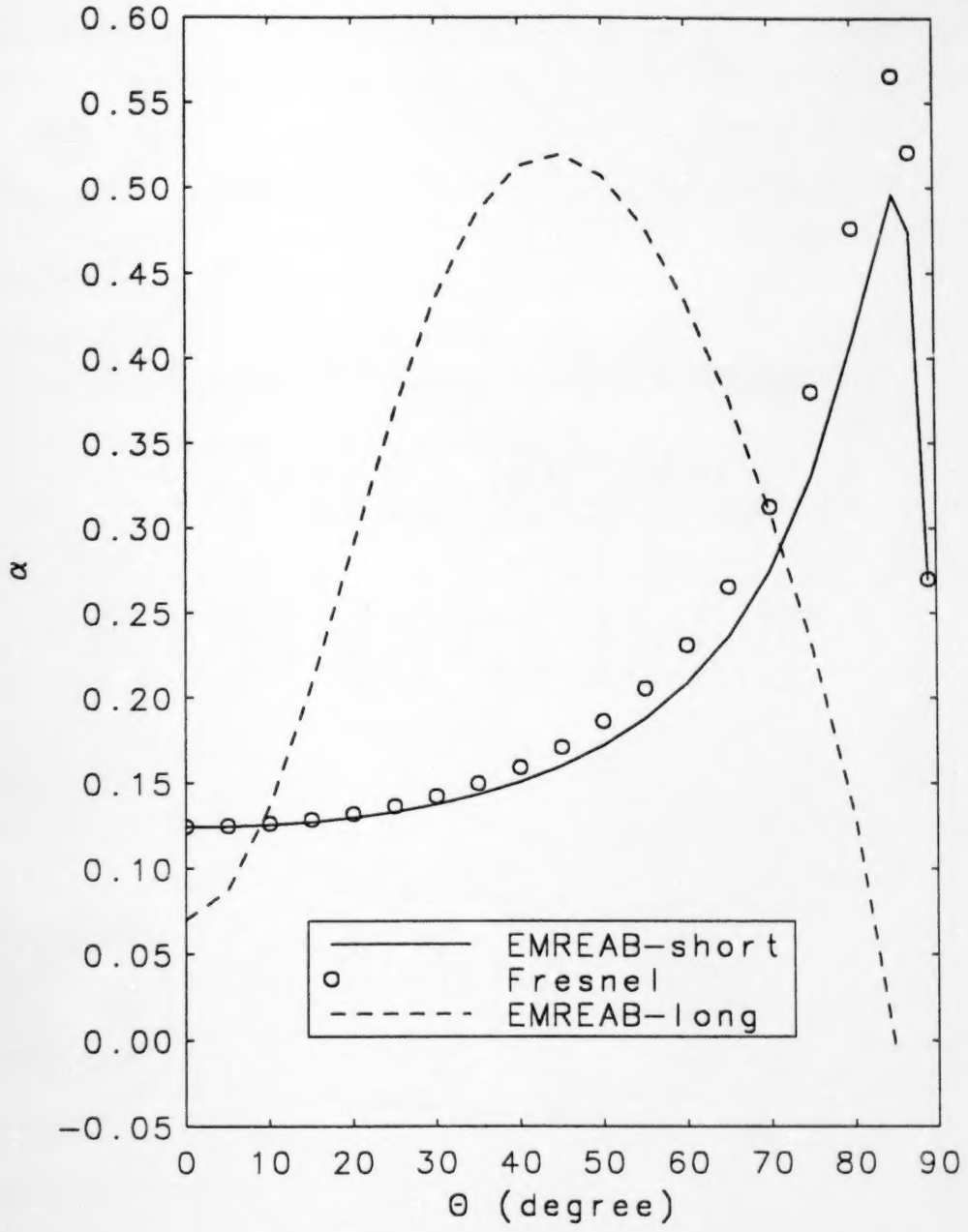

Figure 4.9: Angular dependence of total absorption fraction for a short scale-length linear density profile.

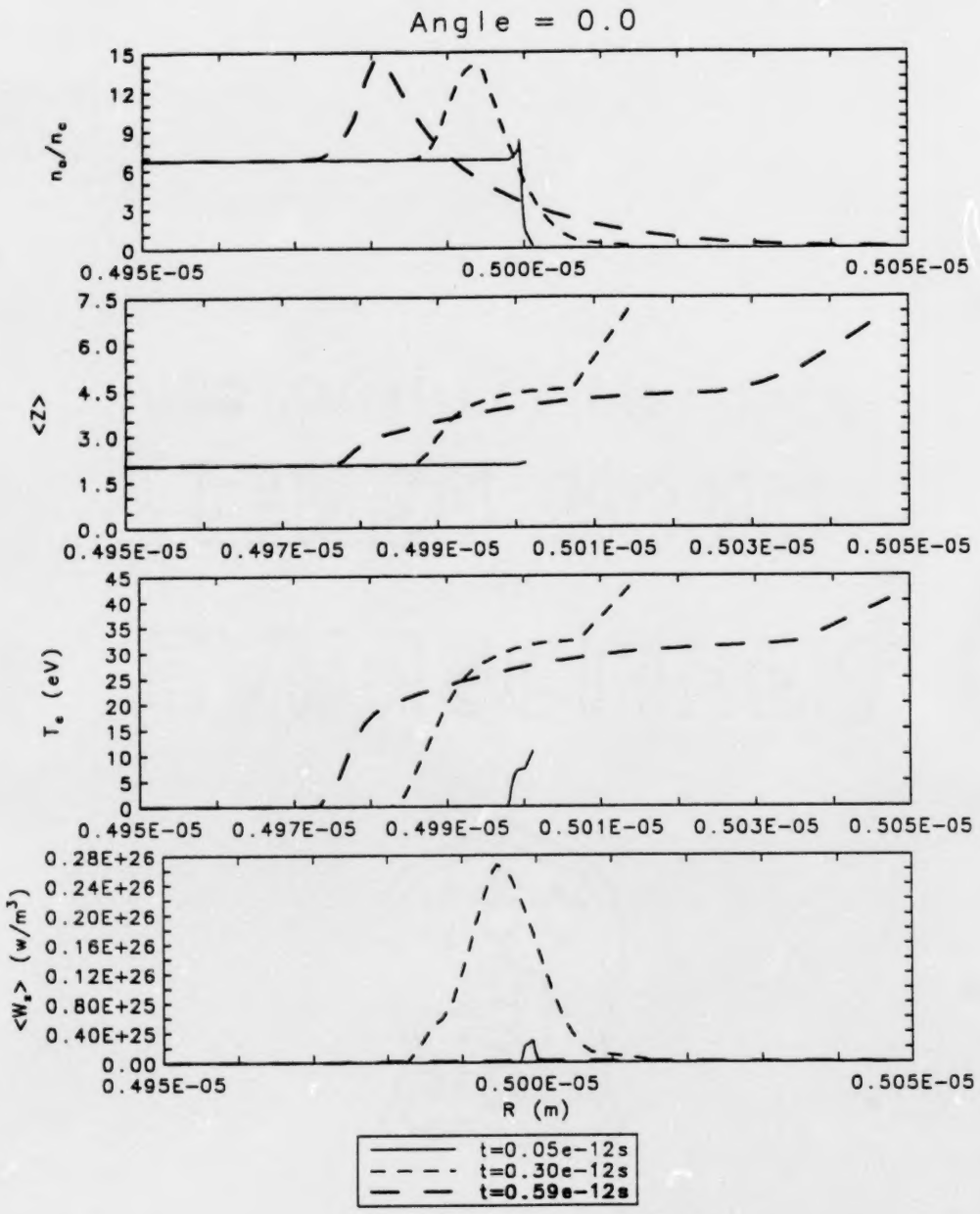

Figure 4.10: Time evolution of electron density, electron temperature, ionization level and absorption at zero angle of incidence.

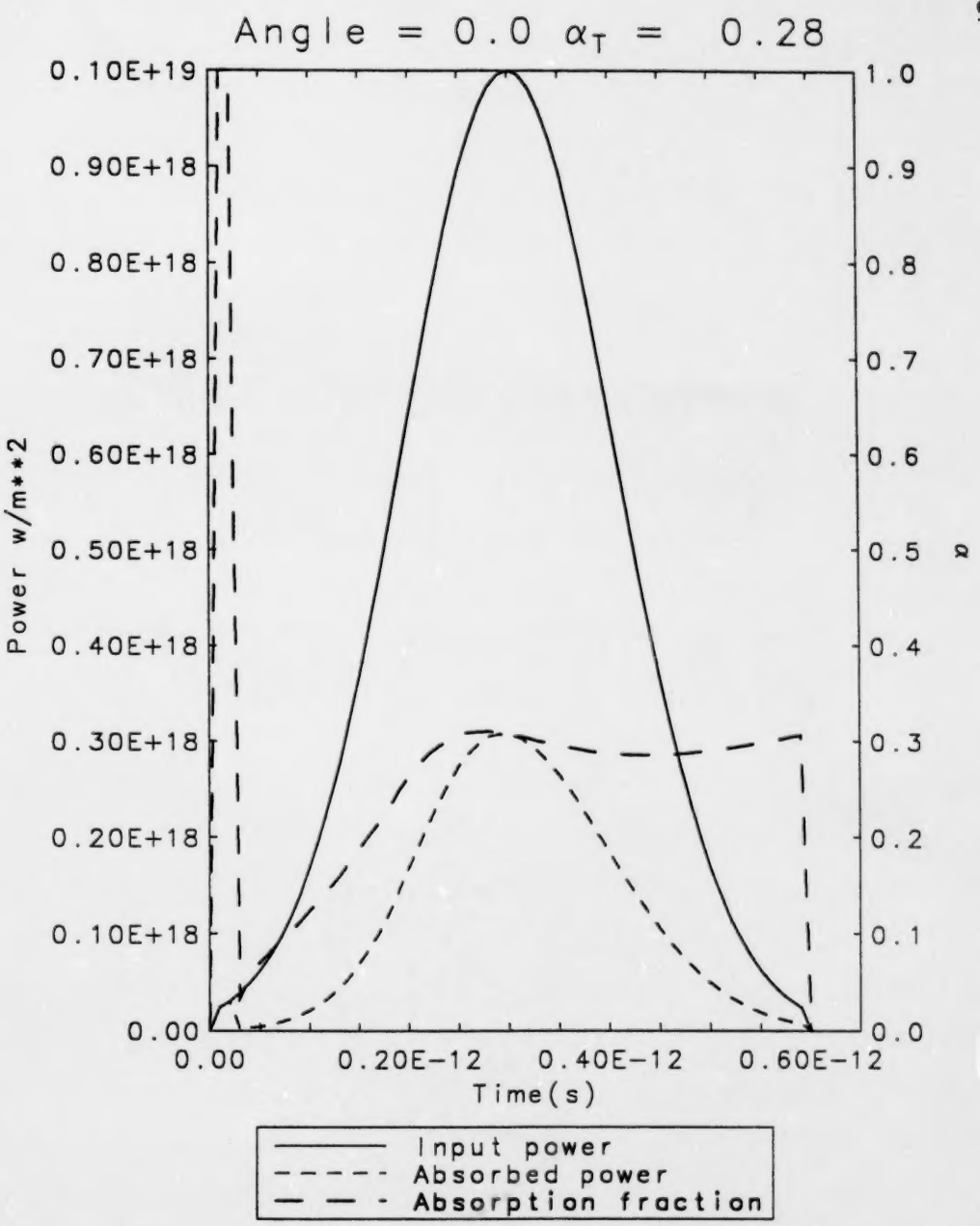

Figure 4.11: Time-dependent absorption fraction at zero angle of incidence.

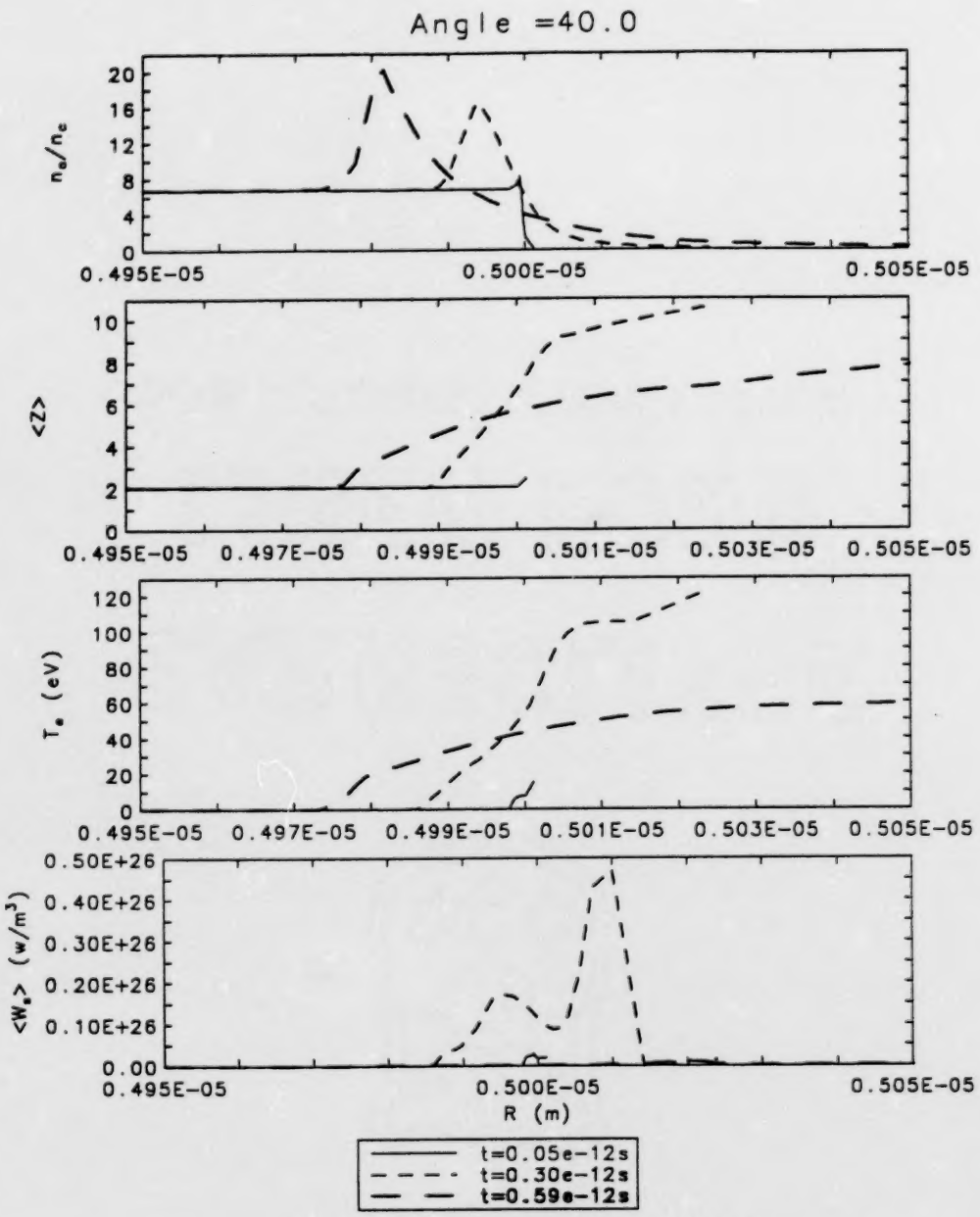

Figure 4.12: Time evolution of electron density, electron temperature, ionization level and absorption at angle of incidence = 40°.

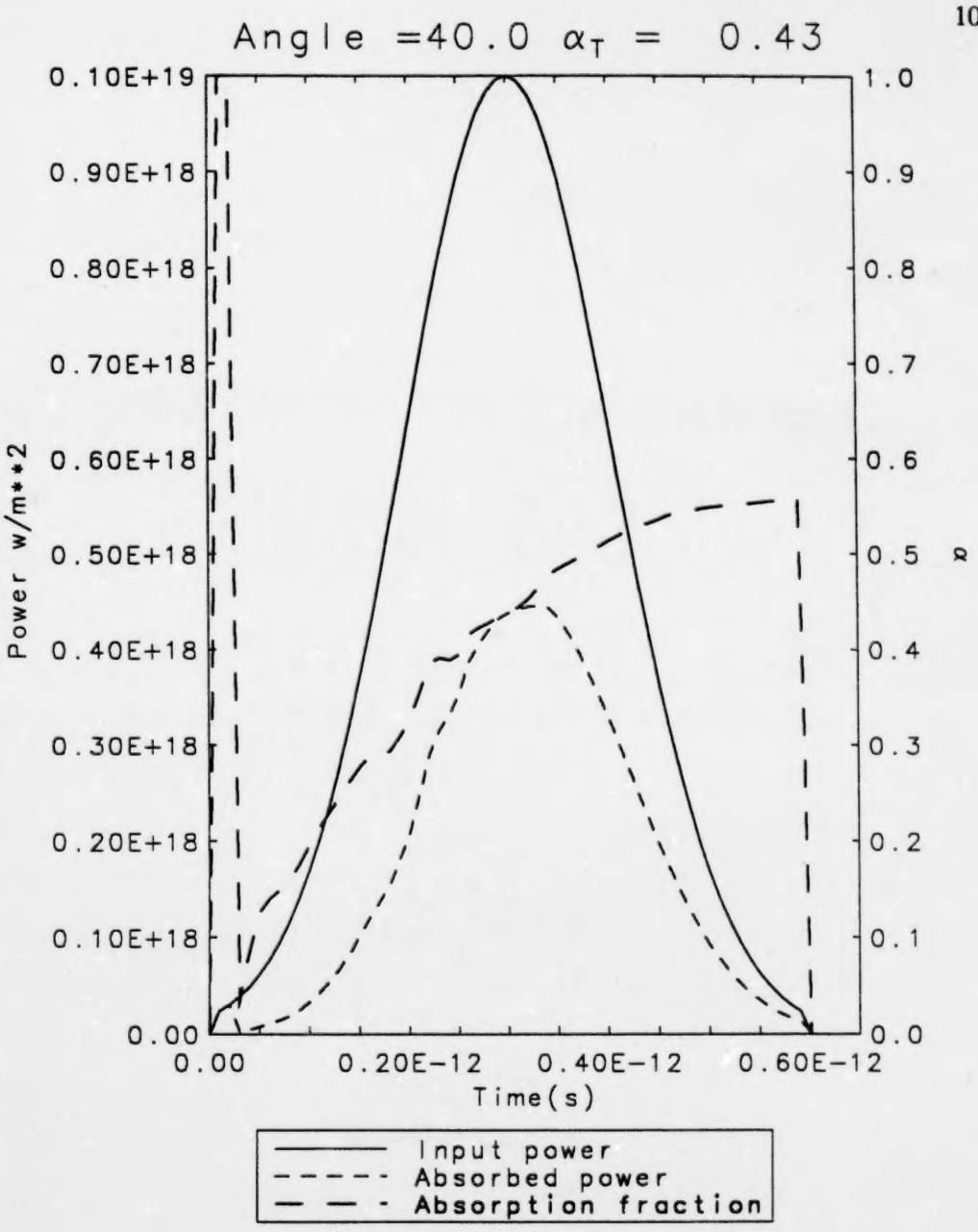

Figure 4.13: Time-dependent absorption fraction at angle of incidence = 40°.

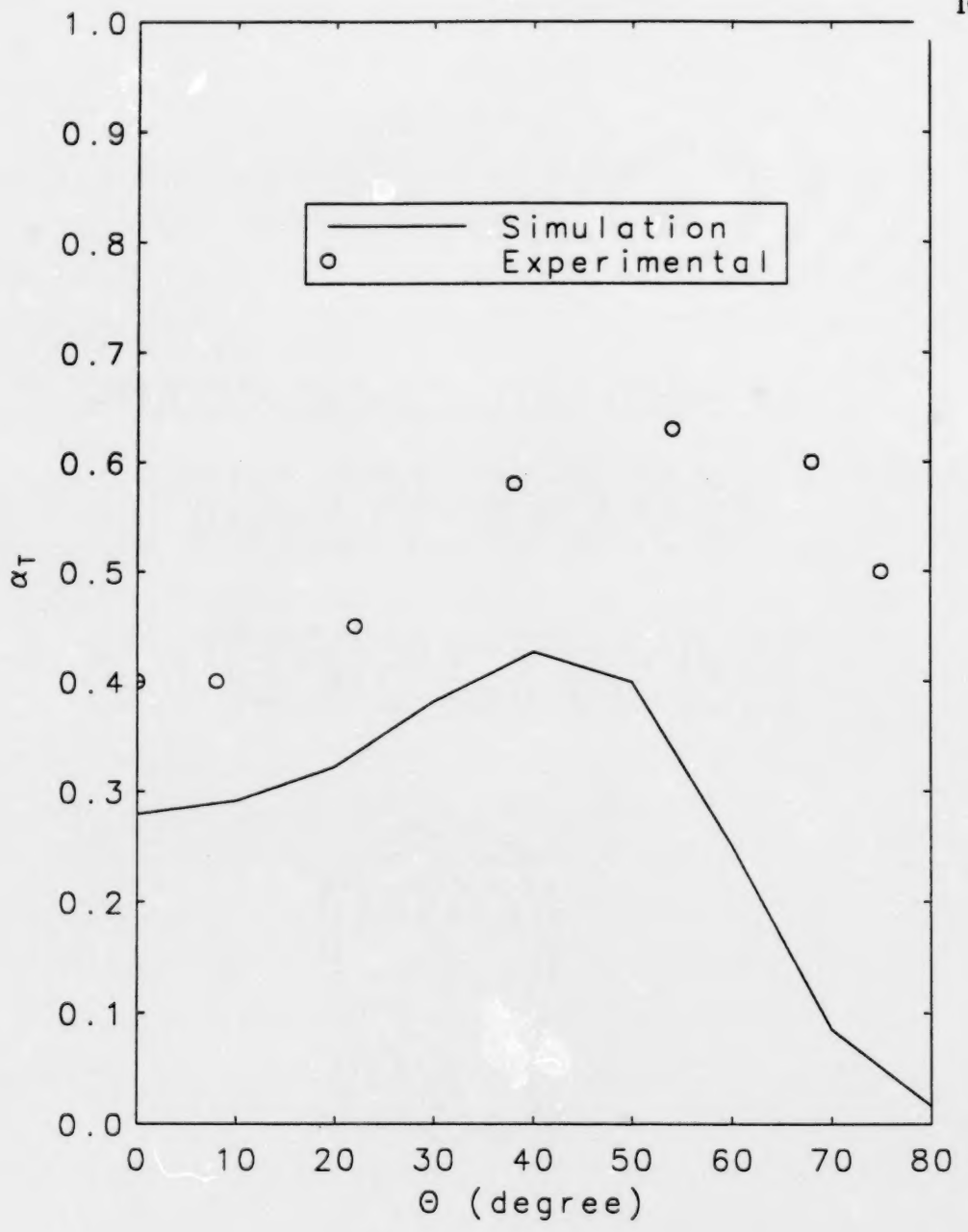

Figure 4.14: Angular dependence of time-integrated absorption fraction for $I_{max} = 10^{14}$ W/cm^2.

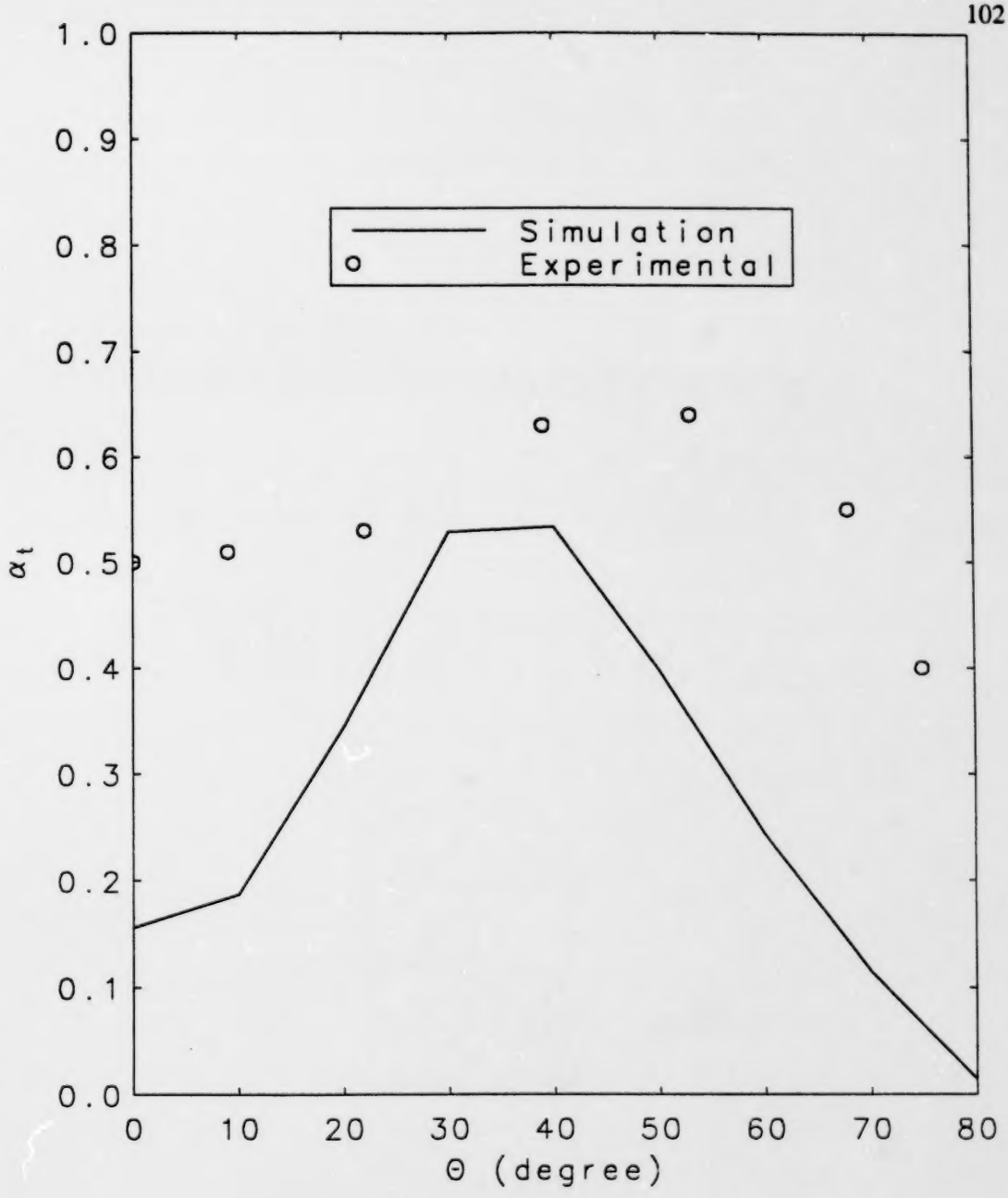

Figure 4.15: Angular dependence of time-integrated absorption fraction for $I_{max} = 2.5 \cdot 10^{15}$ W/cm^2.

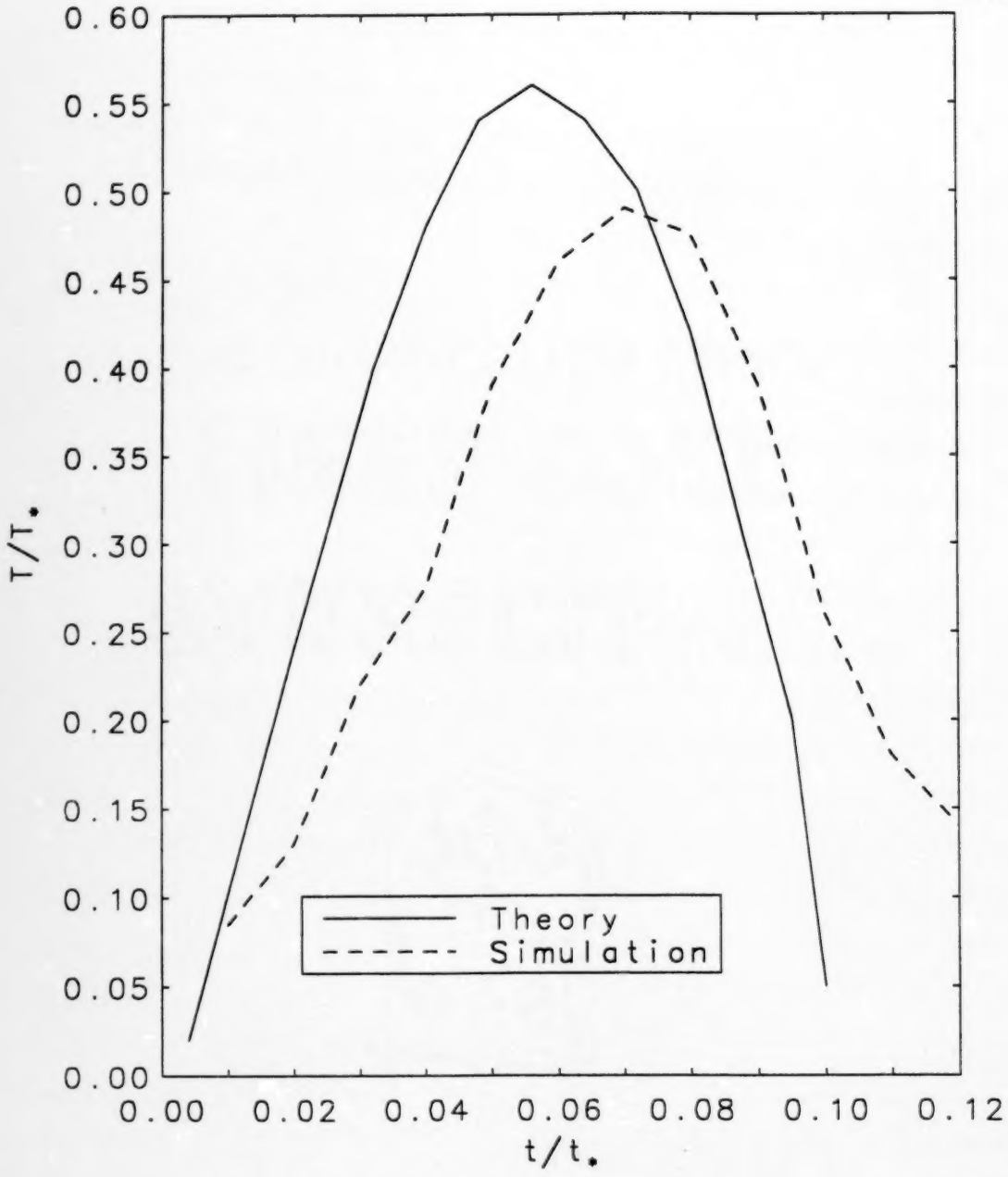

Figure 4.16: Electron temperature at maximum local absorption.

Chapter 5. Conclusion

5.1 Summary

A one dimensional simulation of the absorption of high intensity sub-picosecond laser light by steep gradient plasmas has been discussed. The computational scheme used consists of the incorporation of a laser code into a plasma hydrodynamic code. The laser code calculates the absorption of the laser light by numerically solving the electric wave equation for a one dimensional plasma. The numerical method involved employs a staggered mesh differencing scheme. The resulting difference equations constitute a petadiagonal matrix structure and are solved by the generalized Thomas algorithm. The absorption is calculated from the Poynting theorem which relates the energy flux to the electric field. The absorption determined by the laser code is used as a source term in the fluid energy equation which describes the thermodynamic behavior of the plasma. Together with the Navier-Stokes equations which govern the motion of the plasma, the nonlinear energy equation is numerically solved by the hydro-code MEDUSA. Numerically, a one dimensional Lagrangian mesh and a five time level integration scheme are used. A time stepping procedure is used where the absorption is calculated based on the plasma parameters calculated by the hydro-code.

Simulation results have been obtained for time independent and time dependent plasma profiles. For time independent profiles, the absorption calculated agrees quite well with both analytical and reported numerical results. For time dependent results, it has been found that the temperature and ionization are nearly constant in the region of highest

absorption. The time integrated absorption fraction has been found to match the time dependent absorption fraction at the peak of the laser pulse. The angular dependence of absorption has also been obtained. It agrees qualitatively with experiment results. The discrepancy for the high intensity case ($I_{max} = 2.5 \cdot 10^{15}$ W/cm^2) is thought to be caused by the laser prepulse which is not modelled in the simulations. The sensitivity of plasma density scale-length, electron temperature, ionization and maximum electron density to the angle of laser incidence have been inferred from the simulations. It has been found that the temperature has the strongest dependence. The simulated time evolution of the electron temperature at the maximum absorption region has been also compared with that predicted by theory. The results appear to agree quite well and the small difference is due to the theory's assumption that the plasma does not expand.

5.2 Future Enhancement of the Simulation

It is believed that the modelling of the laser-plasma interaction considered in this investigation can be improved by including the laser prepulse effects. This may reduce the gap between the absorption pattern obtained from simulations and that measured from experiment. The crude assumption that laser light is totally absorbed in the beginning of the simulation also deserves future consideration. A proper model for this stage could also result in better results for the overall absorption.

References

1. F.F. Chen, *Introduction to Plasma Physics and Controlled Fusion 2nd edition*, (Plenum Press, New York, 1984)

2. B.E. Keen, editor *Plasma Physics*, (The Institute of Physics, London and Bristol, 1974)

3. R.A. Cairns, editor *Laser-Plasma Interactions 2*, (Scottish Universities Summer School in Physics, 1983)

4. D.J. Rose and M. Clark, Jr., *Plasmas and Controlled Fusion*, (The M.I.T. Press, Cambridge, 1961)

5. W.W. Duley, *Laser Processing and Analysis of Materials*, (Plenum Press, New York, 1983)

6. R. Fedosejevs, R. Ottmann, R. Sigel, G. Kuhnle, S. Szatmari, and F.P. Schafer, *Absorption of subpicosecond ultraviolet laser pulses in high-density plasma*, Appl. Phys. B **50**, 79 (1990)

7. M. Chaker, J.C. Kieffer, J.P. Matte, H. Pepin, P. Audebert, P. Main, D. Strickland, P. Bado, and G. Mourou, *Interaction of a 1 ps laser pulse with solid matter*, Phys. Fluids B **3(1)**, 167 (1991)

8. J.C. Kieffer, J.P. Matt, S. Belair, M. Chaker, P. Audebert, H. Pepin, P. Main, D. Strickland, P. Bado, and G. Mourou, *Absorption of an ultrashort laser pulse in very steep plasma density gradients*, IEEE J. Quantum Electron. **25**. 2640 (1989)

9. G. Zorpette, *Rethinking X-ray Lithograph*, IEEE Spectrum, 33 (June, 1992)

10. D.L. Matthews and M.D. Rosen, *Soft-x-ray lasers*, Scientific American, 86 (December, 1988)

11. K.G. Budden, *The Propagation of Radio Waves*, (Cambridge University Press, 1985)

12. J.D. Jackson, *Classical Electrodynamics 2nd Edition*, (John Willey and Sons, 1975)

13. A.D. Piliya, *Wave conversion in a inhomogeneous plasma*, Sov. Phys. Tech. Phys. **11**, 609 (1966)

14. I.P. Shkarofsky, T.W. Johnston and M.P. Bachynski, *The Particle Kinetics of Plasmas*, (Addison-Wesley, Reading Mass., 1966)

15. R. Marchand and C.E. Capjack, *Polynomial fit to the coulomb logarithm for inverse bremsstrahlung*, Computer Physics Communications **38**, 357 (1985)

16. R. Cauble, F.J. Rogers and W. Rozmus, *An analytic expression for electrical resistivity in near-solid density, laser*-produced plasmas, SPIE **1229**, 211 (1990)

17. D.W. Forslund, J.M. Kindel, K. Lee, E.L. Lindman, and R. L. Morse, *Theory and simulation of resonant absorption in a hot plasma*, Phys. Rev. A **11**, 679 (1975)

18. D. Potter, *Computational Physics*, (John Willey & Sons, London, 1973)

19. R. Rankin, *the EMREFL code*, unpublished

20. R. Cauble, *the RHO code*, unpublished

21. J.P. Christiansen, D.E.T.F. Ashby, and K.V. Roberts, *MEDUSA, a one-dimensional laser fusion code*, Comput. Phys. Commun. **7**, 271 (1974)

22. C.E. Capjack, *Medusa equation of state*, Department of Electrical Engineering, University of Alberta, unpublished

23. D. Havazelet et al, *Onset of laser light filamentation in preformed plasmas*, Phys. Fluids **B 1(4)**, 893 (1989)

24. R.S. Craxton and R.L. McCrory, *Two-dimensional calculations of non-spherical laser fusion implosions*, Laboratory Report #99, the Laser-plasma group, Department of Electrical Engineering, University of Alberta

25. R.G. Evans, *MEDUSA: a 1D fluid code for the simulation of laser irradiated targets*, Laboratory Report #75, the Laser-plasma group, Department of Physics, University of British Columbia

26. V.L. Ginzburg, *The Propagation of Electromagnetic Waves in Plasmas*, (Pergamon, New York, 1970)

27. W. Rozmus and V. Tikhonchuk, *heating of solid targets by subpicosecond laser pulses*, Phys. Rev. A, accepted for publication, (1992)

Appendix A: The CRR Collisional Frequency

The CRR collisional frequency is given by:

$$\nu_{CCR}=M_{pp}-\frac{D-\omega^2}{G}(M_{pq}R_{rq}+M_{pr})+\frac{\omega^2}{G}(M_{qq}+M_{rr})(M_{pq}^2+M_{pr}^2) \tag{A.1}$$

and

$$\begin{aligned} D&=M_{rr}M_{qq}-M_{qr}^2 \\ G&=(D-\omega^2)^2+\omega^2(M_{qq}+M_{rr})^2 \\ R_{xy}&=M_{xx}M_{py}-M_{qr}M_{px} \end{aligned} \tag{A.2}$$

The elements of the momentum matrix **M** are given by:

$$\begin{aligned} M_{pp}&=\frac{A}{6\sqrt{2}Z}\Delta \\ M_{rr}&=A\left(\frac{3}{28}\Omega^{ee}+\frac{433}{1680\sqrt{2}Z}\Omega^{ei}\right) \\ M_{qq}&=A\left(\frac{1}{15}\Omega^{ee}+\frac{13}{60\sqrt{2}Z}\Omega^{ei}\right) \\ M_{qr}&=-\frac{A}{\sqrt{28}}\left(\frac{1}{5}\Omega^{ee}+\frac{23}{20\sqrt{2}Z}\Omega^{ei}\right) \\ M_{pq}&=-\frac{A}{8\sqrt{5}Z}\left(\Delta+\Omega^{ei}\right) \\ M_{pr}&=5\frac{A}{16\sqrt{35}Z}\left(\Delta+\Omega^{ei}\right) \end{aligned} \tag{A.3}$$

where

$$A=-\frac{n_e}{\pi\sqrt{\pi m_e K_B T_e}}$$

$$\Delta=\frac{(4\pi e^2 Z)^2}{K_B T_e}\frac{\ln[B_{ei}]}{2(1-B_{ei})}$$

$$\Omega^{ee}=\frac{-(4\pi e^2)^2}{K_B T_e}\left(\frac{-1}{2(1-B_{ee})}\ln[B_{ee}]+\frac{B}{2(1-B_{ei})}\frac{\Omega}{\lambda_{DI}^2}\right) \qquad \textbf{(A.4)}$$

$$\Omega^{ei}=\frac{4\pi e^2 Z)^2}{K_B T_e}\left(\frac{1}{2(1-B_{ei})}\ln[B_{ei}]+\frac{B}{2(1-B_{ei})}\frac{\Omega}{\lambda_{De}^2}\right)$$

and

$$B_{ei}=\frac{\lambda_{ei}^2}{\lambda_D^2}$$

$$B_{ee}=\frac{\lambda_{ee}^2}{\lambda_D^2} \qquad \textbf{(A.5)}$$

$$B=\lambda_{ee}^2-\lambda_{ei}^2$$

$$\Omega=\frac{1}{1-B_{ee}}\ln[B_{ee}]+\frac{\lambda_{ei}^2}{(1-B_{ee})\lambda_{ei}^2-(1-B_{ei})\lambda_{ee}^2}\ln\left[\frac{\lambda_{ei}^2}{\lambda_{ee}^2}\right]$$

where λ_{ee} and λ_{ei} are the thermal deBroglie wavelengths, $\lambda_D = (\lambda_{Di}^2 + \lambda_{De}^2)^{1/2}$ is the Debye length and v is given by:

$$v=\frac{1}{\sqrt{2}}\frac{v_E}{v_{th}}=\frac{1}{\sqrt{2}}\frac{\frac{eE}{m_e\omega}}{\sqrt{\frac{K_BT_e}{m_e}}} \tag{A.6}$$

The functions F_{ab} are given by:

$$F_{pp}=\frac{1}{v^3}\left(\frac{\sqrt{\pi}}{2}\text{erf}[v]-ve^{-v^2}\right)$$

$$F_{rr}=\frac{1}{2v^3}\left((3602+2242v^2-28v^4+1320v^6-240v^8)ve_{-v^2}-(3602-448v^2)\frac{\sqrt{\pi}}{2}\text{erf}[v]\right)$$

$$F_{qq}=\frac{1}{2v^3}\left((82+8v^2)\frac{\sqrt{\pi}}{2}\text{erf}[v]-(82+54v^2+36v^4)ve^{-v^2}\right) \tag{A.7}$$

$$F_{qr}=\frac{1}{2v^3}\left(-360\frac{\sqrt{\pi}}{2}\text{erf}[v]+(360+286v^2+120v^6)ve^{-v^2}\right)$$

$$F_{pq}=\frac{1}{v^3}\left(-\frac{\sqrt{\pi}}{2}\text{erf}[v]+(1+v^2)ve^{-v^2}\right)$$

$$F_{pr}=e^{-v^2}(1-2v^2)$$

Appendix B: Listing of EMREAB

```
************************************************************************
      SUBROUTINE EMREAB(NP,NLD,R3,DM,NE,TE3,XL3,LAMDA1,PLAS1,NECRI1,
     +                  FZSQ3,FZ3,KY)
*
*     This routine aims to find the electric field in a
*     plasma having an arbitrary density gradient from zero up to and
*     beyond the critical density which has an em wave incident on it's
*     underdense boundary.  The program also attempts to determine the
*     absorption of the laser energy by the plasma.  The staggered
*     mesh difference scheme is used.
*
*     Version 25.
*-----------------------------------------------------------------*
*
*     NP - number of MEDUSA cells.
*     NLD - switch on Landau damping if equal to 1.
*     R3 - MEDUSA coordinates.
*     DM - mass in MEDUSA cells.
*     NE - MEDUSA electron density profile.
*     TE3 - MEDUSA electron temperature profile
*     XL3 - MEDUSA laser absorption profile.
*     LAMDA1 - laser wavelength in (m).
*     PLAS1 - incident intenisty in W/m**3.
*     NECRI1 - critical density in 1/m**3.
*     FZSQ3 - MEDUSA <Z**2>
*     FZ3 - MEDUSA <Z>
*     KY = the SIN() of the incident angle.

      REAL R3(151), DM(151), NE(151), TE3(151), XL3(151)
      REAL FZSQ3(151), FZ3(151)
      REAL LAMDA1, PLAS1, NECRI1

      REAL KY

      INTEGER J
      INTEGER NP
      INTEGER NLD

*-----------------------------------------------------------------*
*     Calculate absorption only when boundary density < critical
*     density.

      IF (NE(NP-1).LT.(0.8*NECRI1)) THEN

*.................................................................*
*      Transformed MEDUSA profiles to EMREAB profiles.

       CALL CNVIN(J,R3,NE,TE3,FZSQ3,FZ3,LAMDA1,NP,NECRI1)

*.................................................................*
*      Find the coefficients for the finite difference equations.

       CALL COEFS(J,KY,NLD)

*.................................................................*
*      Solve the finite difference equations.

       CALL TOMS(J, KY)

*.................................................................*

*      Calculate absorption.

       CALL ABSN(J,KY,NLD)

*.................................................................*

       CALL CNVOUT(J,NP,LAMDA1,XL3,DM,PLAS1,R3,NP)

*-----------------------------------------------------------------*
*     Dump all the power into the boundary cell when boundary density
*     > critical density
```

```
      ELSE

        DO 10 I = 1, NP-2
          XL3(I) = 0.0
10      CONTINUE

        XL3(NP-1) = PLAS1/DM(NP-1)

      ENDIF

*-----------------------------------------------------------------------*

      RETURN
      END

*****************************************************************
      SUBROUTINE CNVIN(J,R3,NE,TE3,FZSQ3,FZ3,
     +                 LAMDA1,NP,NECRI1)
*
*     This routine transforms the MEDUSA profiles to the
*     normalized EMREAB profiles.
*     This routine also calculates the EMREAB density
*     gradient profile.
*
*     X - EMREAB's coordinates.
*     DN - EMREAB's electron density profile.
*     DDN - EMREAB's electron density gradient profile.
*     DLX - EMREAB's grid spacing.
*     VESQR - the normalized thermal velocity.
*     AVEZZ - EMREAB's <Z>
*     DPC - the collisional damping term: 1/(1+i*NUC) where
*           NUC is the collisional damping frequency

      parameter(nmax=80000)

      REAL R3(151), NE(151), TE3(151)
      REAL FZSQ3(151), FZ3(151)
      REAL LAMDA1, NECRI1
      INTEGER NP

      REAL TR3(151), TTR3(151), TNE(151), TTE3(151), TVESQR(151)
      REAL TZZ(151), TTZZ(151)

      REAL TDLX
      REAL TWOPI, LAMBDA, DC
      REAL X(nmax), DN(nmax), DDN(nmax), DLX(nmax)
      REAL VESQR(nmax), DVESQR(nmax)
      REAL AVEZZ(nmax), DAVEZZ(nmax)
      COMPLEX DPC(nmax)
      REAL TX1(nmax), TX2(nmax)

      INTEGER NPM1, J

*.....................................................................*

      COMMON/COM1/ LAMBDA, DC, XS
      COMMON/COM2/ X, DN, DDN, DLX, AVEZZ, DPC, VESQR

*.....................................................................*
      REAL XO(nmax), WO(nmax), SWO(nmax)
      COMPLEX EXO(nmax), EYO(nmax), BZO(nmax), PN(nmax)
      REAL EFLUX(nmax), DNO(nmax)
      REAL NUCO(nmax), VESQRO(nmax)
      REAL ALPHAA,ALPHAB, ALPHAW, ALPHAS
      REAL SCALEX
      INTEGER JEM
      COMPLEX BR, DL
      REAL DD0,DD1,DD2,DLX1MX,DLX2MX

      common/comemb/ XO, EXO, EYO, WO, SWO, EFLUX, DNO, BZO, PN, NUCO,
     +               VESQRO,BR, DL, ALPHAA,ALPHAB, ALPHAW, ALPHAS,
     +               SCALEX, JEM, DD0, DD1, DD2,
     +               DLX1MX, DLX2MX
*.....................................................................*

      NPM1 = NP-1
```

```
*     LAMDA1 is in m.
*     LAMBDA is in cm.

      LAMBDA = LAMDA1*100.0
      TWOPI = 2.0*3.1415927

*     DC is the critical density (in (cm)**(-3)).

       DC = NECRI1/(100.0**3)

*     Compute Ave(Z*Z)/Ave(Z)

      DO 5 I = 1, NPM1
        TZZ(I) = FZSQ3(I)/FZ3(I)
    5 CONTINUE

*     Transform the grid.

      DO 10 I = 1, NPM1, 1
        TR3(I) = (R3(NP)-R3(NP-I+1))
        TNE(I) = NE(NP-I)
        TTE3(I) = TE3(NP-I)
        TTZZ(I) = TZZ(NP-I)
   10 CONTINUE
      TR3(NP) = (R3(NP)-R3(1))

*     Normalize density and coodinates.
*     Note: (Ve/c)**2 = (kTe/me)/c**2 * Te where Te is in K.
*     IXC is the point just above the critical density.

      DONE = 0.0
      DO 35 I = 1, NPM1, 1
       TNE(I) = TNE(I)/NECRI1
       TR3(I) = TR3(I)*TWOPI/LAMDA1
       TVESQR(I) = 1.684E-10*TTE3(I)
       IF ((TNE(I).GT.1.0).AND.(DONE.LT.0.5)) THEN
          IXC = I
          DONE = 1.0
       ENDIF
   35 CONTINUE
      TR3(NP) = TR3(NP)*TWOPI/LAMDA1

*     Find cell center coordinates.

      DO 70 I = 1, NPM1
         TTR3(I) = 0.5*(TR3(I)+TR3(I+1))
   70 CONTINUE

*     The critical density is located between
*     TR3L and TR3H

      TR3L = 0.5*(TTR3(IXC) + TTR3(IXC-1))
      TR3H = 0.5*(TTR3(IXC+1) + TTR3(IXC))

*     Find location of critical density.

      ZXC = TR3L + (1.0-TNE(IXC-1))*(TR3H-TR3L)
     +             /(TNE(IXC)-TNE(IXC-1))

*     Set the initial delta x to a fraction of the
*     density scale-length.

      DLXINI = DD0*( (TR3H-TR3L)/(TNE(IXC)-TNE(IXC-1)) )

*     Generating the new grid

*     From Nc to underdense region
*
*     TX1 is the coordinates from Nc to underdense boundary.
*     DXMX is the normalized upper bound for the grid
*     spacing in the underdense region.
*     The cell spacing TDLX is increased at a rate
*     TDLX = TDLX*DD1.

      DXMX = (DLX1MX*LAMBDA)*(TWOPI/LAMBDA)
      TDLX = DLXINI
      J1 = 1
```

```
      TX1(1) = ZXC
65    IF (TX1(J1).GE.TR3(1)) THEN
         IF (TX1(J1).GT.(ZXC-DLXINI/DD0)) THEN
            J1 = J1 + 1
            TX1(J1) = TX1(J1-1) - TDLX
         ELSE
            J1 = J1 + 1
            TX1(J1) = TX1(J1-1) - TDLX
            IF (TDLX.LT.DXMX) TDLX = TDLX*DD1
         ENDIF
         GOTO 65
      ENDIF

*     From Nc to overdense region.
*
*     TX2 is the coordinates from Nc to overdense boundary.
*     DXMX is the normalized upper bound for the grid
*     spacing in the overdense region.
*     The cell spacing TDLX is increased at a rate
*     TDLX = TDLX*DD2.

      DXMX = DLX2MX*( (TR3(NPM1)-TTR3(NP)) )
      TDLX = DLXINI
      J2 = 1
      TX2(1) = ZXC + DLXINI
67    IF (TX2(J2).LE.TTR3(NPM1)) THEN
         J2 = J2 + 1
         TX2(J2) = TX2(J2-1) + TDLX
         IF(TDLX.LT.DXMX) TDLX = TDLX*DD2
         GOTO 67
      ENDIF

*     Combine TX1 and TX2 to generate the overall grid X.

      DO I = 1, J1
         X(I) = TX1(J1-I+1)
      ENDDO

      DO I = J1+1, J1+J2
         X(I) = TX2(I-J1)
      ENDDO

      J = J1+j2

*     Make sure J is even.

*     If J is odd

      IF (INT(J/2)*2.NE.J) THEN

*      ...add an extra poins at the end.

       J = J + 1
       X(J) = X(J-1) + DLX2
      ENDIF

      DO I = 1, J-1
        DLX(I) = X(I+1)-X(I)
      ENDDO
        DLX(J) = 9999.9999


*     Obtain the new profiles by linear interpolation.

      CALL LINE(NPM1,TTR3,TVESQR,J,X,VESQR,DVESQR)
      CALL LINE(NPM1,TTR3,TNE,J,X,DN,DDN)
      CALL LINE(NPM1,TTR3,TTZZ,J,X,AVEZZ,DAVEZZ)

*     Make sure the transformed temperature does not
*     go below 300 K as a result of interpolation.
*     XS is where the temperature has droped from
*     600 K.

      IDONE = 0
      VES300 = 300.0*1.684E-10
      DO 75 I = 1, J
        IF (VESQR(I).LT.VES300) VESQR(I) = VES300
```

```
        IF ((VESQR(I).LT.2*VES300).AND.(IDONE.EQ.0)) THEN
          XS = X(I)
          IDONE = 1
        ENDIF
   75 CONTINUE

*     Find the collisional damping rate.

      DO 85 I = 1, J
          CALL DAMPC(X(I),DN(I),DPC(I),VESQR(I),AVEZZ(I))
   85 CONTINUE

      RETURN
      END

*************************************************************
      SUBROUTINE COEFS(J,KY,NLD)
*
*     This routine finds the coefficients for the finite
*     difference equations.
*
      parameter(nmax=80000)

      COMPLEX EPSIL1, EPSIL2, EPSIL3, P1, P2, P3, A(6), AA(nmax,6)
      COMPLEX CDENOM
      REAL RDENOM

      REAL WPSQR, WP1SQR, WP2SQR, WP3SQR, WP4SQR, DWPSQR
      REAL VESQR(nmax)

      REAL D1234, D12,D23, D34

      COMPLEX DPL

      REAL DLX(nmax), DX
      REAL X(nmax), DN(nmax), DDN(nmax)
      REAL AVEZZ(nmax)
      COMPLEX DPC(nmax)

      REAL KTX, KY, KT, KPX

      COMPLEX CKTX, CKPX

      INTEGER J, LILJ
      INTEGER NLD

*-------------------------------------------------------------------*

      COMMON/COM2/ X, DN, DDN, DLX, AVEZZ, DPC, VESQR

      COMMON/COMAA/ AA, A

*-------------------------------------------------------------------*
*     Determine the coefficients for the j=1 and j=2 grid points,
*     those that satisfy the boundary conditions (the amplitude of
*     the incoming wave is set to 1 and KT is set to 1).

*     Calculate the coefficients that will be used by the TOM5
*     subroutine and write them to array AA.

*     Begin with the coefficients for j=1 and 2.
*     Caution- these grid points are special: the following
*     coefficients are of a form different from the j=3 to J
*     coefficients and are used differently in TOM5.

*     Calculate the coefficients at x=deltax :

      WP2SQR = DN(2)
      DWPSQR = DDN(2)

*     Use Landau damping term depending on switch.

        DPL = DPC(1)
      IF (NLD.EQ.1) THEN
        CALL DAMPL(WP2SQR,DPL)
      ENDIF
```

```
      CKTX  = SQRT( 1. - WP2SQR*DPC(1) - KY*KY )

      CKPX = SQRT( (1.- WP2SQR*DPC(1))/(3.0*VESQR(2)*DPL) - KY*KY )

      KTX = REAL(CKTX)
      KPX = REAL(CKPX)
      KT = SQRT( KTX*KTX + KY*KY)


      RDENOM = KY*KY + KPX*KTX

      EPSIL1 = CMPLX(0.0,1.0)
     +          *( CKPX*KPX*KTX + CKTX*KY*KY) / RDENOM

      EPSIL2 = CMPLX(0.0,-1.0)
     +          *( KY*KPX*( CKPX - CKTX) ) / RDENOM

      EPSIL3 = CMPLX(0.0,2.0) * CEXP( (0.,1.)*KTX*DLX(1) )
     +          *KY/KT * (CKPX*KPX*KTX + CKTX*KY*KY) / RDENOM

      CDENOM = ( 1.0 + EPSIL1*DLX(1) ) /
     1         ( DLX(1) + DLX(2) )

      A(1) = CMPLX(1.0,0.0)
      A(2) = EPSIL2 / CDENOM
      A(3) =  EPSIL1 / CDENOM - 1.0
      A(4) = CMPLX(0.0,0.0)
      A(5) = CMPLX(0.0,0.0)
      A(6) = EPSIL3 / CDENOM

       JJJ = 1
       CALL PUTAA(JJJ)

*     Calculate the coefficients at x=2*deltax :

      WP3SQR = DN(3)
      DWPSQR = DDN(3)

        DPL = DPC(3)
      IF (NLD.EQ.1) THEN
         CALL DAMPL(WP3SQR,DPL)
      ENDIF

      CKTX  = SQRT( 1. - WP3SQR*DPC(3) - KY*KY )

      CKPX = SQRT( (1.- WP3SQR*DPC(3))/(3.0*VESQR(3)*DPL) - KY*KY )

      KTX = REAL(CKTX)
      KPX = REAL(CKPX)
      KT = SQRT( KTX*KTX + KY*KY)

      RDENOM = KY*KY + KPX*KTX

      P1 = CMPLX(0.0,1.0)
     +     *( CKPX*KY*KY + CKTX*KPX*KTX ) / RDENOM

      P2 = CMPLX(0.0,-1.0)
     +     *KY * KTX *(CKPX - CKTX) / RDENOM

      P3 = CMPLX(0.0,-2.0) * CEXP( (0.,1.)*KTX*( DLX(1)
     +                          + DLX(2) ) )
     +     *KTX/KT * ( CKPX*KY*KY + CKTX*KPX*KTX) / RDENOM

      CDENOM = ( 1.0 + P1*DLX(2) ) /
     1         ( DLX(2) + DLX(3) )

      A(1) = CMPLX(1.0,0.0)
      A(2) = P2 / CDENOM
      A(3) = P1 / CDENOM - 1.0
      A(4) = CMPLX(0.0,0.0)
      A(5) = CMPLX(0.0,0.0)
      A(6) = P3 / CDENOM

       JJJ = 2
       CALL PUTAA(JJJ)
*.....................................................................*
*     Continue with the coefficients for j=3 to J-2.
```

```
      WP4SQR = DN(4)
      DWPSQR = DDN(4)

      DO 10 LILJ = 3, J - 2

*        Note that only the odd DWPSQR points will be used for Ex.

         WPSQR = DN(LILJ)
         DWPSQR = DDN(LILJ)

*        Calculate damping terms DPL (Landau) and DPC
*        (collisional).  DPL = 1/(1 + i*NUL/W),
*        DPC = 1/(1 + i*NUC/W), where NUL and NUC are
*        the Landau and collisional damping rates, respectively.

         DPL = DPC(LILJ)
         IF (NLD.EQ.1) THEN
            CALL DAMPL(WPSQR,DPL)
         ENDIF

         D1234 = 1.0/( DLX(LILJ-2) + DLX(LILJ-1)
     1          + DLX(LILJ)  + DLX(LILJ+1) )
         D12 = 1.0/( DLX(LILJ-2) + DLX(LILJ-1) )
         D23 = 1.0/( DLX(LILJ-1) + DLX(LILJ) )
         D34 = 1.0/( DLX(LILJ) + DLX(LILJ+1) )

         IF (  INT(LILJ/2) * 2  .NE.  LILJ  ) THEN

*           j is odd (Ex values)

*           Make sure no division of 0 occurs.

            IF ( WPSQR .GT. 1E-10) THEN
               DX  =  DWPSQR / WPSQR
            ELSE
               DX = 0.0
            ENDIF

            DX = DX

            A(1) =  CMPLX(1.0,0.0) * VESQR(LILJ)* DPL * D1234
     1              * (6.0*D34 - DX)

            A(2) =  CMPLX(0.0,1.0) * KY * D23 *
     1             (VESQR(LILJ)*DPL*(3.0 - DX*DLX(LILJ-1))
     1        -1.0 )

            A(3) = -CMPLX(6.0,0.0) * VESQR(LILJ)* DPL
     1                    *D12*D34
     1             - KY**2*CMPLX(1.0,0.0)
     1             - CMPLX(WPSQR,0.0)*DPC(LILJ)
     1             + CMPLX(1.0,0.0)

            A(4) = -CMPLX(0.0,1.0)* KY * D23 *
     1              ( VESQR(LILJ)*DPL*(3.0 + DX*DLX(LILJ))
     1        -1.0 )

            A(5) =  CMPLX(1.0,0.0) * VESQR(LILJ)* DPL * D1234
     1              * (6.0*D12 + DX)

            A(6) =  CMPLX(0.0,0.0)

            JJJ = LILJ
            CALL PUTAA(JJJ)

         ELSE

*           j is even (Ey values)

            A(1) =  CMPLX(2.0,0.0) * D34 * D1234
            A(2) =  CMPLX(0.0,1.0) * KY * D23
     1              * (3.0*VESQR(LILJ)*DPL - 1.0)
            A(3) =  CMPLX(1.0,0.0)
     1              - CMPLX(2.0,0.0)*D12*D34
     1              - CMPLX(3.,0.)*VESQR(LILJ)
     1             * DPL * KY ** 2 - CMPLX(WPSQR,0.0)*DPC(LILJ)
            A(4) = -A(2)
```

```
            A(5) =  CMPLX(2.0,0.0) * D12 * D1234
            A(6)  = CMPLX(0.0,0.0)

            JJJ = LILJ
            CALL PUTAA(JJJ)

          ENDIF

   10   CONTINUE

*       Finish with the coefficients for j=J-1 and J.
*       These coefficients are not used, but are here just to
*       satisfy any questions about them.

        A(1) = CMPLX(0.0,0.0)
        A(2) = CMPLX(1.0,0.0)
        A(3) = CMPLX(0.0,0.0)
        A(4) = CMPLX(0.0,0.0)
        A(5) = CMPLX(0.0,0.0)
        A(6) = CMPLX(0.0,0.0)

        JJJ = J-1
        CALL PUTAA(JJJ)

        A(1) = CMPLX(1.0,0.0)
        A(2) = CMPLX(0.0,0.0)

        JJJ = J
        CALL PUTAA(JJJ)

        RETURN
        END

*************************************************************************
        SUBROUTINE TOM5(J, KY)
*
*
*       This routine performs a sweep backward to and then forward from
*       the entry boundary of the plasma to find E at all points
*       on the grid.

*       The coefficents of the finite difference equation are in
*       a (5+1)xJ matrix AA.  They represent the diagonal
*       terms of the actual pentadiagonal matrix.  They have been
*       evaluated at each of the J points on the grid.  They are
*       preceeded in the file by the boundary conditions' coefficients.

*       The E field at the boundary is the sum of the E field
*       due to the em wave and the electrostatic plasma wave.

*       The E field data are put into array EXY.

        parameter(nmax=80000)

        COMPLEX DENOM, RNUM, EJM10, EJ0

        COMPLEX A(6), AA(nmax,6), B(3), BB(nmax,3), C(3), D(3)

        COMPLEX UJ, UJM1, BR, BRY, BRX, CDENOM

        COMPLEX AL2, BT2, GM2, AL3, BT3, GM3

        COMPLEX M1, M2, M3, N1, N2, N3

        COMPLEX E2N, E2D, E2, E1, EJ, EJM1, EJM2

        REAL DLX(nmax)
        REAL X(nmax), DN(nmax), DDN(nmax)
        REAL AVEZZ(nmax)
        COMPLEX DPC(nmax), VESQR(nmax)

        REAL KY
        INTEGER I, J

        COMPLEX EXY(nmax)
*.......................................................................*
```

```
      COMMON/COM2/ X, DN, DDN, DLX, AVEZZ, DPC, VESQR
      COMMON/COMAA/ AA, A
      COMMON/COMBB/ BB, B
      COMMON/COMEXY/ EXY

*.....................................................................*

*     The coefficients data are in aray AA.
*     The final two sets of coefficients are determined
*     by the boundary conditions which we know: Ex=0
*     and Ey=0 deep in the plasma beyond the critical layer.

*     Set the E field at the end of the grid to zero.

      UJ   = CMPLX(0.0,0.0)
      UJM1 = CMPLX(0.0,0.0)

*     Do preliminary set-up before the sweep back.

      JJJ = J-2
      CALL GETAA(JJJ)

      B(1) = -A(4) / A(3)
      B(2) = -A(5) / A(3)
      B(3) = ( A(6) / A(3) ) - ( (A(2)*UJM1 + A(1)*UJ) / A(3) )

      KKK = 1
      CALL PUTBB(KKK)

      JJJ = J-3
      CALL GETAA(JJJ)

      AL3 = B(1)
      BT3 = B(2)
      GM3 = B(3)

      B(1)  = -(A(4) + A(2)*BT3) / (A(3) + A(2)*AL3)
      B(2)  = -A(5) / (A(3) + A(2)*AL3)
      DENOM = (A(3) + A(2)*AL3)
      RNUM  =  A(6) - A(1)*UJM1 - A(2)*GM3
      B(3)  =  RNUM/DENOM

      KKK = 2
      CALL PUTBB(KKK)

      KKK = 1
      CALL GETBB(KKK)
      C(1) = B(1)
      C(2) = B(2)
      C(3) = B(3)

      KKK = 2
      CALL GETBB(KKK)
      D(1) = B(1)
      D(2) = B(2)
      D(3) = B(3)

*.....................................................................*

*     Do the backward sweep.

      DO 10 I = J - 4, 3, -1

       JJJ = I
       CALL GETAA(JJJ)

       CDENOM = A(1) * (D(1)*C(1) + C(2)) + A(2) * D(1) + A(3)

       B(1) = -(A(1)*D(2)*C(1) + A(2)*D(2) + A(4)) / CDENOM

       B(2) = -A(5) / CDENOM

       B(3) = (A(6) - D(3)*A(2) - A(1)*(D(3)*C(1) + C(3))) / CDENOM

       KKK = KKK + 1
       CALL PUTBB(KKK)
```

```
      C(1) = D(1)
      C(2) = D(2)
      C(3) = D(3)

      D(1) = B(1)
      D(2) = B(2)
      D(3) = B(3)

   10 CONTINUE

*.....................................................................*
*     From boundary conditions at left, j=1, side of the grid,
*     calculate E1 and E2.

      AL2 = D(1)
      BT2 = D(2)
      GM2 = D(3)

      AL3 = C(1)
      BT3 = C(2)
      GM3 = C(3)

*     Get the coefficients for the entry boundary conditions.

      JJJ = 1
      CALL GETAA(JJJ)
      M1 = -A(2)
      M2 = -A(3)
      M3 =  A(6)

      JJJ = 2
      CALL GETAA(JJJ)
      N1 = -A(2)
      N2 = -A(3)
      N3 =  A(6)

      E2N =    BT2 * (AL3 - N1) * (GM2 - M3)
      E2N =    E2N - (   (BT2 - M2) * (GM3-N3)   )
      E2N =    E2N - (   (BT2 - M2) * GM2*(AL3-N1)   )
      E2D =   (BT2 - M2)*(   AL2*(AL3 - N1)   )
      E2D =    E2D + (   (BT2 - M2) * (BT3 - N2)   )
      E2D =    E2D - (   BT2 * (AL3-N1) * (AL2-M1)   )

      E2 = E2N / E2D

      E1 =    (M3 - GM2) / (BT2 - M2)
      E1 = E1 - (   (E2*(AL2 - M1)) / (BT2 -M2)   )

      NEX = 1
      NEY = 1

      I1 = 1
      EXY(I1) = E1
      I2 = 2
      EXY(I2) = E2

      EJM1 = E2
      EJM2 = E1
*.....................................................................*
*     Do forward sweep.

      KKK = KKK + 1

      DO 20 I = 3, J - 2

       KKK = KKK -1
       CALL GETBB(KKK)

       EJ = EJM1 * B(1) + EJM2 * B(2) + B(3)

       EJM2 = EJM1
       EJM1 = EJ

       EXY(I) = EJ

   20 CONTINUE
```

```
      EJM10 = CMPLX(0.0,0.0)
      EJ0   = CMPLX(0.0,0.0)

      EXY(J-1) = EJM10
      EXY(J) = EJ0

      RETURN
      END

************************************************************
      SUBROUTINE ABSN(J,KY,NLD)
*
*     This routine first calculates the normalized instantaneous
*     power dissipated by the plasma per unit volume and the
*     absorption fraction.
*
*     WO - absorption profiles by E*J method.
*     SWO - absorption profiles by ExB method.
*     ALPHAW - absorption fraction by E*J method.
*     ALPHAS - absorption fraction by ExB method.
*     BZO - magnetic field.
*     PN - perturbed density.

      parameter(nmax=80000)

      INTEGER J, L
      REAL DLX(nmax), D12, D23, D34, D1234
      REAL X(nmax),XO(nmax), DN(nmax), DDN(nmax), DNO(nmax)
      REAL AVEZZ(nmax)
      REAL ER, EI
      REAL WPSQR, DWPSQR
      COMPLEX E(5)
      COMPLEX EX, DEX, D2EX, EY, DEY, TD2EX
      COMPLEX NT, M, DPL
      REAL W, WSUM, WO(nmax), KX, KY, VESQR(nmax), TX
      COMPLEX EXC, EYC
      INTEGER NLD
      REAL S1, S2, SW, SWO(nmax), SINIT
      COMPLEX EXY(nmax),EXO(nmax),EYO(nmax), BZO(nmax), PN(nmax)
      COMPLEX B3T,B5T,P3T,P5T,W3T,W5T
      REAL EXR(3), EXI(3), EYR(3), EYI(3)
      REAL ALPHAA, ALPHAB,ALPHAW,ALPHAS
      REAL KT, KTX, KP, KPX
      COMPLEX CKTX, CKPX
      COMPLEX DL,BR
      REAL DLSQR
      COMPLEX DEXDX, DEYDX, EXT, EYT
      INTEGER NEX, NEY
      COMPLEX EE1, EE5, EE3
      REAL EFLUX(nmax)
      REAL LAMBDA, DC
      REAL NUCO(nmax)
      REAL VESQRO(nmax)
      INTEGER JEM
      REAL DD0,DD1,DD2,DLX1MX,DLX2MX
      COMPLEX DPC(nmax)

*.............................................................*

      COMMON/COM1/ LAMBDA, DC, XS
      COMMON/COM2/ X, DN, DDN, DLX, AVEZZ, DPC, VESQR
      COMMON/COMEXY/ EXY
      Common/comemb/ XO, EXO, EYO, WO, SWO, EFLUX, DNO, BZO, PN, NUCO,
     +               VESQRO, BR,DL, ALPHAA, ALPHAB, ALPHAW, ALPHAS,
     +               SCALEX,JEM, DD0, DD1, DD2,
     +               DLX1MX, DLX2MX
*.............................................................*

*     Calculate W, S, Bz, Pn at grid points 3 to J-2.
*     Note that at the entrance these quantities are computed by
*     extrapolating from the 3rd and 4th grid points.  And
*     at the end these quantities are set to 0.

      E(1) = EXY(1)
      E(2) = EXY(2)
      E(3) = EXY(3)
      E(4) = EXY(4)
```

```
      E(5) = EXY(5)

      DO 50 I = 3, J-2, 1

         ZZI = I

         D12 = DLX(I-2)+DLX(I-1)
         D23 = DLX(I-1)+DLX(I)
         D34 = DLX(I)+DLX(I+1)
         D1234 = D12 + D34

         IF ( INT(I/2)*2 .NE. I ) THEN

*        Calculate EX, EY and their derivatives at
*        odd grid points.

            EX = E(3)
            DEX = ( E(5) - E(1) )/D1234
            D2EX = ( E(5)*D12 + E(1)*D34 - E(3)*D1234 )/
     1           ( D12*D34*D1234*0.5 )
            DEY = ( E(4) - E(2) )/D23
            EY = E(2) + DEY*DLX(I-1)

         ELSE

*        Calculate EX, EY and their derivatives at
*        even grid points.

            EY = E(3)
            DEY = ( E(5) - E(1) )/D1234
            DEX = ( E(4) - E(2) )/D23
            EX = E(2) + DEX*DLX(I-1)

         ENDIF

         EXC = CONJG(EX)
         EYC = CONJG(EY)

*        Calculate the EM energy flux S.

         EFLUX(I) = -REAL( EYC*( KY*EX + CMPLX(0.0,1.0)*DEY ) )

*        Calculate the flux absorbed per cell.

         WPSQR = DN(I)
         DWPSQR = DDN(I)

*        Calculate damping terms

            DPL = DPC(I)
         IF (NLD.EQ.1) THEN
            CALL DAMPL(WPSQR,DPL)
         ENDIF

         IF (WPSQR.EQ.0.0) THEN
           WPSQR = 1.0
           DWPSQR = 0.0
         ENDIF

         DWPSQR = DWPSQR

*        Calculate W only at odd grid points.

         IF ( INT(I/2)*2 .NE. I ) THEN

           M = 3.0*( EXC*( D2EX + CMPLX(0.0,KY)*DEY )
     1           +EYC*( CMPLX(0.0,KY)*DEX - KY*KY*EY ) )
     1       - ( DEX + CMPLX(0.0,KY)*EY )*EXC*DWPSQR*1.0/WPSQR

           NT = CMPLX(0.0,1.0)*( WPSQR*DPC(I)*( EXC*EX + EYC*EY )
     1          - VESQR(I)*DPL*M )

           W = REAL(NT)

         ENDIF

         EXO(I) = EX
```

```
            EYO(I) = EY
            WO(I) = W

*       Compute Bz and perturbed density.

            BZO(I) = 2*3.14159/LAMBDA*(DEY-CMPLX(0.0,KY)*EX)
            PN(I) = -9.31956e-5*LAMBDA*(DEX+CMPLX(0.0,KY)*EY)

*           Read another E point.

            IF (I.NE.(J-2)) THEN
              DO 40 L = 1,4,1
                 E(L) = E(L+1)
   40         CONTINUE
              E(5) = EXY(I+3)
            ENDIF

      50 CONTINUE

*       Interpolate energy flux, E*J, Ex, Ey, Bz and Pn
*       at the first 2 grid points from the third
*       and forth grid points

            S5T = EFLUX(5)
            S3T = EFLUX(3)
            EFLUX(1) = S5T - (DLX(4)+DLX(3)+DLX(2)+DLX(1))
           +                 *(S5T-S3T)/(DLX(4)+DLX(3))
            EFLUX(2) = S5T - (DLX(4)+DLX(3)+DLX(2))
           +                 *(S5T-S3T)/(DLX(4)+DLX(3))
            SINIT = EFLUX(1)

            B5T = BZO(5)
            B3T = BZO(3)
            BZO(1) = B5T - (DLX(4)+DLX(3)+DLX(2)+DLX(1))
           +               *(S5T-S3T)/(DLX(4)+DLX(3))
            BZO(2) = B5T - (DLX(4)+DLX(3)+DLX(2))
           +               *(B5T-B3T)/(DLX(4)+DLX(3))

            P5T = PN(5)
            P3T = PN(3)
            PN(1) = T5T - (DLX(4)+DLX(3)+DLX(2)+DLX(1))
           +              *(P5T-P3T)/(DLX(4)+DLX(3))
            PN(2) = T5T - (DLX(4)+DLX(3)+DLX(2))
           +              *(P5T-P3T)/(DLX(4)+DLX(3))
            W5T = WO(5)
            W3T = WO(3)
            WO(1) = W5T - (DLX(4)+DLX(3)+DLX(2)+DLX(1))
           +              *(W5T-W3T)/(DLX(4)+DLX(3))

            EXO(1) = EXY(1)
            EYO(2) = EXY(2)
            EYO(1) = EYO(2) - DLX(1)*(EYO(3)-EYO(2))/DLX(2)
            EXO(2) = EXO(1) + DLX(1)*(EXO(3)-EXO(1))/(DLX(2)+DLX(1))

*       At the end of the grid, there is no E field and therefore
*       no flux.

            EXO(J-1) = 0.0
            EYO(J-1) = 0.0
            WO(J-1) = 0.0
            SWO(J-1) = 0.0
            EFLUX(J-1) = 0.0
            BZO(J-1) = 0.0
            PN(J-1) = 0.0

            EXO(J) = 0.0
            EYO(J) = 0.0
            WO(J) = 0.0
            SWO(J) = 0.0
            EFLUX(J) = 0.0
            BZO(J) = 0.0
            PN(J-1) = 0.0

*       Compute absorption.

            WSUM = 0.0
```

```
      DO 55 I = 1, J-2
        SWO(I) = (EFLUX(I)-EFLUX(I+1))/(DLX(I))

        IF (INT(I/2)*2.EQ.I) THEN
          WO(I) = WO(I-1) + DLX(I-1)*(WO(I+1)-WO(I-1))
     +                      /(DLX(I)+DLX(I-1))
        ENDIF

        WSUM = WSUM + WO(I)*DLX(I)

   55 CONTINUE

      DO 999 I = 1, J
        XO(I) = X(I)
        NUCO(I) = AIMAG(1.0/DPC(I))
        VESQRO(I) = VESQR(I)
        DNO(I) = DN(I)
  999 CONTINUE

*.....................................................................*

*     Calculate the absorption of the plasma from boundary.

      WP1SQR = DN(1)

         DPL = DPC(1)
      IF (NLD.EQ.1) THEN
         CALL DAMPL(WP1SQR,DPL)
      ENDIF

      CKTX  = SQRT( 1. - WP1SQR*DPC(1) - KY*KY )

      CKPX = SQRT( (1.- WP1SQR*DPC(1))/(3.0*VESQR(1)*DPL) - KY*KY )

      KTX = REAL(CKTX)
      KPX = REAL(CKPX)
      KT = SQRT( KTX*KTX + KY*KY)
      KP = SQRT( KPX*KPX + KY*KY)

      EXT = EXO(1)
      EYT = EYO(1)

      RDENOM = KY*KY + KTX*KPX

      BR = (KT*(KY*EXT+KPX*EYT) - (KY*KY-KTX*KPX)) / RDENOM

*      BR = EYO(1)/(KTX/KT) + 1.0

      DL = (KP/KT)*( -KTX*KT*EXT + KY*KT*EY
     1               + 2.0*AT*(KY*KTX)      )/RDENOM

      DLSQR = REAL(DL)**2 + AIMAG(DL)**2

      BREAL = REAL(BR)
      BIMAG = AIMAG(BR)

      ALPHAB = 1.0 - BREAL**2 - BIMAG**2
      ALPHAW = WSUM/(KTX/KT)
      ALPHAS = SINIT/(KTX/KT)

*.....................................................................*

*     Find scale length

      II = 0
      I = 1
10    IF (II.NE.1) THEN
         IF (DN(I).GE.1.0) THEN
            XC = X(I)
           IC = I
            II = 1
         ENDIF
        I = I + 1
        GO TO 10
      ENDIF

*      Calculate the analytical absorption fraction
```

```
*       for normal incidence.

        TNUC = AIMAG( 1.0/DPC(IC) )
        TT1 = -32.0/15.0 * TNUC * XC * (KTX/KT)

        ALPHAA = 1 - EXP(TT1)
        SCALEX =  XC/(2*3.141529)

*.....................................................................*

        RETURN
        END

*****************************************************************
        SUBROUTINE CNVOUT(J,NP,LAMDA1,XL3,DM,PLAS1,R3)

        parameter(nmax=80000)

*---------------------------------------------------------------------*

        COMPLEX EXO(nmax), EYO(nmax), BZO(nmax), PN(nmax)
        REAL XO(nmax), WO(nmax), SWO(nmax), EFLUX(nmax), DNO(nmax)
        REAL NUCO(nmax)
        REAL VESQRO(nmax)
        REAL AVEZZ (nmax)
        REAL XL3(151), TXL3(151), DM(151)
        REAL XFLUX(151), XDFLUX(151)
        REAL S1, S2
        REAL R3(151)
        REAL LAMDA1
        REAL TMP(nmax)
        COMPLEX CTMP(nmax)
        COMPLEX BR, DL
        REAL ALPHAA, ALPHAB, ALPHAW, ALPHAS
        REAL SCALEX
        INTEGER JEM
        REAL DD0,DD1,DD2,DLXMX1,DLXMX2

        common/comemb/ XO, EXO, EYO, WO, SWO, EFLUX, DNO, BZO, PN, NUCO,
     +                 VESQRO, BR, DL, ALPHAA, ALPHAB, ALPHAW, ALPHAS,
     +                 SCALEX, JEM , DD0, DD1, DD2,
     +                 DLX1MX, DLX2MX

*---------------------------------------------------------------------*

        JEM = J

*       Make the EMREAB's coordinates system compatible to
*       MEDUSA's.

        DO I = 1, J
          TMP(I) = XO(I)*LAMDA1/(2.0*3.1415926)
        ENDDO
        DO I = 1, J
          XO(I) = R3(NP) - TMP(J-I+1)
        ENDDO

        DO I = 1,J
          CTMP(I) = EXO(I)
        ENDDO
        DO I = 1, J
          EXO(I) = CTMP(J-I+1)
        ENDDO

        DO I = 1,J
          CTMP(I) = EYO(I)
        ENDDO
        DO I = 1, J
          EYO(I) = CTMP(J-I+1)
        ENDDO

        DO I = 1,J
          TMP(I) = EFLUX(I)
        ENDDO
        DO I = 1, J
          EFLUX(I) = TMP(J-I+1)
        ENDDO
```

```
      DO I = 1,J
        TMP(I) = WO(I)
      ENDDO
      DO I = 1, J
        WO(I) = TMP(J-I+1)*PLAS1*(2.0*3.1416)/LAMDA1
      ENDDO

      DO I = 1,J
        TMP(I) = SWO(I)
      ENDDO
      DO I = 1, J
        SWO(I) = TMP(J-I+1)*PLAS1*(2.0*3.1416)/LAMDA1
      ENDDO

      DO I = 1,J
        TMP(I) = DNO(I)
      ENDDO
      DO I = 1, J
        DNO(I) = TMP(J-I+1)
      ENDDO

      DO I = 1,J
        TMP(I) = NUCO(I)
      ENDDO
      DO I = 1, J
        NUCO(I) = TMP(J-I+1)
      ENDDO

      DO I = 1,J
        TMP(I) = PN(I)
      ENDDO
      DO I = 1, J
        PN(I) = TMP(J-I+1)
      ENDDO

      DO I = 1,J
        TMP(I) = VESQRO(I)
      ENDDO
      DO I = 1, J
        VESQRO(I) = TMP(J-I+1)
      ENDDO

      CALL LINE(J,XO,EFLUX,NP,R3,XFLUX,XDFLUX)

      DO I = 1, NP-1
        TXL3(I) = (XFLUX(I+1)-XFLUX(I))
      ENDDO

      DO 15 I = 1, NP-1
        XL3(I) = 0.0
   15 CONTINUE

      DO 30 I = 1, NP
        XL3(I) = PLAS1*TXL3(I)/DM(I)
   30 CONTINUE

*     Calculate Total absorption fraction.


      ALPHAS = 0.0
      DO I = 1, NP-1
        ALPHAS = ALPHAS + XL3(I)*DM(I)
      ENDDO
      IF (PLAS1.GT.0.0) THEN
        ALPHAS = ALPHAS/PLAS1
      ELSE
        ALPHAS = 0.0
      ENDIF

      RETURN
      END

*****************************************************************************
      SUBROUTINE  DAMPL(WPSQR,DPL)
*
*     This routine attempts to calculate the Landau Damping
*     term in the diferential equation: 1 / (1 + i*NUL/W).
```

```
*     NUL is the Landau Damping frequency.

      COMPLEX DPL
      REAL WPSQR, NUL, X, PI

      PI = 3.141592654

      IF (WPSQR.LT.1) THEN
       X = 3.0/(1.0-WPSQR)
      ELSE
       X = 0.0
      ENDIF

      NUL = (0.125*PI)**(0.5)*X**(2.5)*EXP(-X)

      DPL = CMPLX(1.0,0.0) / CMPLX(1.0,NUL)

      RETURN
      END
*****************************************************************
      SUBROUTINE DAMPC(X,WPSQR,DPC,VESQR,AVEZZ)
*
*     This routine computes the collisional damping term:
*     1/(1+i*NUC), where NUC is the collisional damping
*     rate.
*
      REAL X, WPSQR, NUC, LAMBDA, DC
      REAL TEV, ME, VESQR, AVEZZ, T
      COMPLEX DPC

      COMMON/COM1/ LAMBDA, DC, XS

*     TEV is the electron temperature in EV.
*     TK   is the electron temperature in K.
*     Note that VESQR was normalized.  To convert it
*     back to the real Ve**2, we have to multiply it
*     by (speed of light)**2.

      TK =  VESQR/1.684E-10
      TEV = TK*8.6174E-5

*     Note that WPSQR was normalized, To obtain
*           the real density, we have the multiply
*           it by the critical density DC.

*      This is the classical collisional frequency with
*      a polynomial fit to the coulomb log. and clamping
*      and cliping.

*      TWPSQR = WPSQR
*      IF (X.GE.XS) TWPSQR = 0.0
*
*      NUC = 4.73E-13 * TWPSQR
*     1       * ZZLOGL(TEV,AVEZZ,LAMBDA) / VESQR**(1.5)
*     2       / LAMBDA
*
*      IF (NUC.GT.1.0) NUC = 1.0
*

*     This is the CRR model of the collisional frequency.
      ATM = 27.0

      NUC = findnu(WPSQR, DC, VESQR, AVEZZ, ATM,
     +             LAMBDA)


      DPC = CMPLX(1.0,0.0) / CMPLX(1.0,NUC)

      RETURN
      END

*****************************************************
      FUNCTION ZZLOGL(TEV, ZZ, LAMBDA)
*
*     This routine calculates the atomic charge times
*     the coulomb logarithm.
*
```

```
C
C ZZ IS THE ATOMIC CHARGE
C LAMBDA IS THE LASER WAVELENGTH (CM)
C TEV IS ELECTRON TEMPERATURE (EV)

      REAL TEV, ZZ, LAMBDA, ZX, ZY

C
C CALCULATE Z*(SPITZER COULOMB LOGARITHM)
C
      ZX = AMIN1(AMAX1(ALOG10(.01*LAMBDA*ZZ*ZZ) + 4.5,-2.5),2.5)
      ZY = AMIN1(AMAX1(ALOG10(TEV/(ZZ*ZZ)) - 2.,-2.),2.)
C
      ZZLOGL = ZZ * (
     1            (0.126149*ZX + 2.230034)*ZX
     2          + 8.007157
     3          + ZY*(
     4            (0.314866 - 0.078475*ZX)*ZX
     5           + 2.703057
     6           + ZY*(
     7             (0.006118*ZX - 0.120930)*ZX
     8            + 0.103552
     9           )
     1           )
     2         )

        RETURN
        END


*******************************************
      SUBROUTINE PUTAA(JJJ)
      parameter(nmax=80000)
      COMPLEX AA(nmax,6), A(6)
      INTEGER JJJ
      COMMON/COMAA/ AA, A
      DO 10 I = 1, 6
         AA(JJJ,I) = A(I)
   10 CONTINUE
      RETURN
      END

*************************************************
      SUBROUTINE GETAA(JJJ)
      parameter(nmax=80000)
      COMPLEX AA(nmax,6), A(6)
      COMMON/COMAA/ AA, A
      INTEGER JJJ
      DO 10 I = 1, 6
        A(I) = AA(JJJ,I)
   10 CONTINUE
      RETURN
      END

*************************************************
      SUBROUTINE PUTBB(KKK)
      parameter(nmax=80000)
      COMPLEX BB(nmax,3), B(3)
      COMMON/COMBB/ BB, B
      INTEGER KKK
      DO 10 I = 1, 3
         BB(KKK,I) = B(I)
   10 CONTINUE
      RETURN
      END

*************************************************
      SUBROUTINE GETBB(KKK)
      parameter(nmax=80000)
      COMPLEX BB(nmax,3), B(3)
      COMMON/COMBB/ BB, B
      INTEGER KKK
      DO 10 I = 1, 3
        B(I) = BB(KKK,I)
   10 CONTINUE
      RETURN
      END
```

```
*****************************************************
      SUBROUTINE LINE(N,X,Y,N1,X1,Y1,DY1)
*****************************************************
*     This routine uses linear interpolation
*     to obtain interpolated points (X1,Y1)  and
*     (X1,DY1/DX1) from the known data points (X,Y).
*****************************************************

      parameter(nmax=80000)

      REAL X(N),Y(N),X1(N1),Y1(N1),DY1(N1)
      REAL DY(nmax)
      INTEGER  I, N, N1, J
      DOUBLE PRECISION DX

      DO 5 I = 1, N-1
        DY(I) = (Y(I+1)-Y(I))/(X(I+1)-X(I))
    5 CONTINUE
      DY(N) = DY(N-1)

      I = 1
      DO 10 J = 1, N1
   20   IF ( (X1(J).GT.X(I+1)) .AND. (X1(J).LT.X(N)) ) THEN
           I = I + 1
           GO TO 20
        ENDIF
        DX=X1(J)-X(I)
        Y1(J) = Y(I)+DX*DY(I)

*     Assume Y has the same value at the extrapolated pts
*     as the 1st point.

        IF (DX.LT.0.0) THEN
          Y1(J) = Y(I)
          DY1(J) = 0.0
        ENDIF

        DY1(J) = DY(I)
   10 CONTINUE

      RETURN
      END
*****************************************************************
      real function findnu(wpsqr,dc,vesqr,avezz,atw,lambda)

      real wpsqr,dc,vesqr,avezz,atw,lambda
      real ne

      ne = wpsqr*dc
      tev = vesqr*0.512e6
      z = avezz
      aw = atw
      xwavel = lambda/100.0/1e-9
      xintens = 0.0

      call rho (ne,tev,z,aw,xintens,xwavel,cfdh,rhodh,wpe)

      findnu = cfdh*wpe/(1.885e11/lambda)

      end

c     *****************************************************************

      subroutine rho (ne,tev,z,aw,xintens,xwavel,cfdh,rhodh,wpe)
      real me,ni,lei,kei,kd,ldh,ne,mi,k,kmax,kmaxinf,wpe
      real kde2,kdi2,kd2,lee
      external dhfunc,dhcbrd

      common /dhcom/ wra,vr,sqlei,kd2,sq2,sqpi2,epsphi,floorxk
      common /dhcom2/ hbar,terg,me,aion

      dimension rtable(12,12)

      data ndim,nmax,jmax/12,8,7/
      data pi,c/3.141592653589793238,2.99792458e10/
      data amu,esqr,one/1.6605655e-24,2.3068617e-19,1.0/
```

```
      epsphi=1.0e-2
      floorxk=1.0e-5
      me=0.9109534e-27
      hbar=1.05443e-27
      sq2=sqrt(2.0)
c
c     ne      - electron density in cm^-3
c     tev     - electron temperature (= ion temperature) in eV
c     z       - net ion charge (simple number)
c     aw      - atomic weight (simple number)
c     xintens - laser intensity in W/cm^2
c     xwavel  - laser wavelength in nanometers ( if xwavel > 10^6,
c               the resulting frequency, wo, and xintens are set to
c               zero:the problem is static
c
c     cfdh    - collision frequency
c     rhodh   - resistivity
c     vr      - v_E / v_therm ratio
c     xmult   - exact zero-coupling multiplier (divide 1 Sonine result
c               - M_pp - to  get approximate 2 Sonine result
c     omult   - actual multiplier figured from our 2 Sonine result
c
c     Given these params, the subroutine returns cf (electron-ion collison
c     frequency) * wpe and rho (resistivity) in micro-ohm-cm.   See
c     Cauble, Rogers, & Rozmus, SPIE Vol. 1229 (1990), p. 211.
c
c
      ni = ne/z
      aion=(3.0/4.0/pi/ni)**(1.0/3.0)
      mi= amu*aw
      efield = sqrt(xintens*1.0e7*8.0*pi/c)
      terg=tev*1.602021e-12
      xmu=one/(one/me+one/mi)
      gamei=z*esqr/aion/terg
      lei=hbar/aion/sqrt(2.0*pi*xmu)/sqrt(terg)
      lee=hbar/aion/sqrt(pi*me)/sqrt(terg)
      kei=one/lei

      kde2=4.0*pi*ne*aion*aion*esqr/terg
      kdi2=4.0*pi*ni*aion*aion*z*z*esqr/terg
      kd2=kde2+kdi2
      kd=sqrt(kd2)
      ldh=one/kd
      pi22=sqrt(pi)/2.0
      wpe=sqrt(4.0*pi*ne*esqr)/sqrt(me)
      wavel=xwavel*1.0e-7
      wavexa=wavel/aion
      wo=2.0*pi*c/wavel
      woxwpe=wo/wpe

c     vt is thermal speed
c     ve is dc electric field speed
c     vr is ratio ve / vt

      vt=sqrt(terg/me)
      ve=sqrt(esqr)*efield/me/wo
      vr=ve/vt

c     wra is ratio (laser freq*ion sphere radius) / vt

      wr=wo/vt
      wra=wr*aion

c     wra & vr are the competing terms in the theta integral
c     if vr << wra, approx below is bad, set vr = 0 for multiplier only

      if (xwavel .gt. 1.0e6) then
       vr = 0.0
       wra = 0.0
      elseif ((vr/wra) .lt. 0.01) then
       vr = 0.0
      endif
c
c

      co=-ni/wpe*sqrt(2.0*pi)/(8.0*pi**2*sqrt(me)*sqrt(terg))
      c1=-ne/wpe/pi/sqrt(pi*me)/sqrt(terg)
```

```
c     constants in front for DH case
      cc1=4.0*pi*esqr
      cc2=4.0*pi*esqr/terg

      cxdxdh=cc2*z*(-cc1*z)
      cxeexdh=(-cc2)*cc1
      cxeixdh=cc2*z*cc1*z

      cxppxdh=co*cxdxdh

      vrt2=vr/sq2
      vr2=vrt2*vrt2
      vr4=vr2*vr2
      vr6=vr4*vr2

      sqlei=lei*lei
      sqlee=lee*lee
      sqpi2=sqrt(pi/2.0)
      gam2=sqlei*kd2
      gamee2=sqlee*kd2
      wr2=wra*wra

c      Approximate 2 Sonine / One Sonine ratio
      xmult=(13.0-9.0*sq2/(z+sq2))/4.0

c      Calculate static integrals in V_Deutsch, c_Coulomb, and
c      S_Debye-Huckel approximations

c      The delta integral is easy

      bxlamb=-alog(gam2)/(one-gam2)/2.0
      dxdh=cxdxdh*bxlamb

c      Omega_ee adn Omega_ei require corrections for differences
c      between lee & lei

      alfee=one-kd2*sqlee
      alfei=one-kd2*sqlei
      del=sqlee-sqlei
      eitemp= alog(gam2)/alfei
      eetemp=-alog(gamee2)/alfee
      if (abs(del) .gt. 1e-5) then
       exx=alfee*sqlei-alfei*sqlee
       eexeix=alog(gamee2)/alfee+sqlei/exx*alog(sqlei/sqlee)
       eix=kde2*del*eexeix/alfei
       eex=kdi2*del*eexeix/alfei
       eixdh=cxeixdh/2.0*(eitemp+eix)
       eexdh=cxeexdh/2.0*(eetemp+eex)
      else
       eixdh=cxeixdh/2.0*eitemp
       eexdh=cxeexdh/2.0*eetemp
      endif

c     Now get the matrix elements.  Assume that the E field
c     dominates wo term; i.e.,
c     use phi(E=inf).  Here we have exp(-1/2[wo/v_therm/k +
c     v_E/v_therm*cos(theta)]^2)
c     inside statics integral over theta and k. The phi
c     function is the theta integral;
c     phi (E=inf) implies setting the first term to zero.
c     This approximation may NOT
c     be good for high frequencies or small fields individually.
c     zero frequency & zero field    - results below are OK;
c     the problem is static
c     zero frequency & nonzero field - results below are OK;
c     this is the approximation treated explicitly
c     nonzero frequency & zero field - results below are
c     questionable. We will branch around & treat this separately
c     using Cauble & Rozmus (Phys Fluids 28 p.3387, 1985)
c     but with a static  multiplier
c     nonzero frequency & nonzero field - results
c     below are approximate. Compare 2 terms in
c     above exponent and use either static or E=inf
c     multiplier.  M_pp matrix element treated correctly.
c     high field - v_E/v_therm gets large and exp kills integral.
c     No good answer here.
c     The approx used here assumes simple dc electron motion in
```

```
c     electric field; sinusoid disappears under low frequency
c     assumption.  For v_E/v_therm > 1,
c     results cannot be trusted (electrons run away). Best to
c     check zero field
c     result against this one and decide for yourself.


c                 M_pp

      if(vrt2 .lt. 0.1) then
       phiinf=2.0/3.0-0.4*vr2+vr4/7.0-vr6/27.0
      else
       phitemp=sqrt(pi)/2.0*erflocal(vrt2)-vrt2*exp(-vr2)
       phiinf=2.0*sq2*phitemp/vr**3
      endif

      ppxw0xdh=cxppxdh*phiinf*bxlamb


c                 M_rr

      if(vrt2 .lt. 0.1) then
       phiinfrr=433.0/3.0-7339.0/15.0*vr2+69973.0/70.0*vr4
       phiinfrr=phiinfrr-6113142.0/6804.0*vr6
      else
       phirr1=3602.0+2242.0*vr2-28.0*vr4+1320.0*vr6-240.0*vr6*vr2
       phirr2=3602.0-448.0*vr2
       phiinfrr=vrt2*exp(-vr2)*phirr1-pi22*erflocal(vrt2)*phirr2
       phiinfrr=sq2*phiinfrr/vr**3
      endif

      rrxw0xdh=c1*(3.0/28.0*eexdh+eixdh/z/sq2/560.0*phiinfrr)

c                 M_qq

      if(vrt2 .lt. 0.1) then
       phiinfqq=13.0/3.0-131.0/15.0*vr2+753.0/70.0*vr4
       phiinfqq=phiinfqq-2311.0/378.0*vr6
      else
       phiqq1=82.0+54.0*vr2+36.0*vr4
       phiqq2=82.0+8.0*vr2
       phiinfqq=-vrt2*exp(-vr2)*phiqq1+pi22*erflocal(vrt2)*phiqq2
       phiinfqq=sq2*phiinfqq/vr**3
      endif

      qqxw0xdh=c1*(eexdh/15.0+eixdh/z/sq2/20.0*phiinfqq)

c                 M_qr

      if(vrt2 .lt. 0.1) then
       phiinfqr=23.0-71.0*vr2-199.0/14.0*vr4
       phiinfqr=phiinfqr-277.0/5.0*vr6
      else
       phiqr1=360.0+286.0*vr2-120.0*vr6
       phiqr2=360.0
       phiinfqr=vrt2*exp(-vr2)*phiqr1-pi22*erflocal(vrt2)*phiqr2
       phiinfqr=sq2*phiinfqr/vr**3
      endif

      qrxw0xdh=-c1/sqrt(28.0)*(eexdh/5.0+eixdh/z/sq2/20.0*phiinfqr)

c                 M_pq

      if(vrt2 .lt. 0.1) then
       phiinfpq=1.0/3.0-3.0/5.0*vr2+5.0/14.0*vr4
       phiinfpq=phiinfpq-7.0/54.0*vr6
      else
       phipq1=1.0+vr2
       phiinfpq=vrt2*exp(-vr2)*phipq1-pi22*erflocal(vrt2)
       phiinfpq=phiinfpq/vrt2**3
      endif

      pqxw0xdh=-c1/z*3.0/sqrt(5.0)/8.0*(dxdh+eixdh)*phiinfpq

c                 M_pr

      phiinfpr=exp(-vr2)*(one-2.0*vr2)
```

```
      prxw0xdh=c1/z*5.0/sqrt(35.0)/16.0*(dxdh+eixdh)*phiinfpr


c     Put together the combinations

      bigd=  rrxw0xdh*qqxw0xdh - qrxw0xdh*qrxw0xdh

      wosq= woxwpe*woxwpe
      if (wra .eq. 0.0) wosq = 0.0
      Dsqr= (bigd-wosq)**2+wosq*(qqxw0xdh+rrxw0xdh)**2
      bigrr= rrxw0xdh*pqxw0xdh - qrxw0xdh*prxw0xdh
      bigqq= qqxw0xdh*prxw0xdh - qrxw0xdh*pqxw0xdh

      xtemp=(bigd-wosq)/Dsqr*(pqxw0xdh*bigrr+prxw0xdh*bigqq)
      ytemp=wosq/Dsqr*(qqxw0xdh+rrxw0xdh)*(pqxw0xdh**2
     &  +prxw0xdh**2)
      psi=xtemp+ytemp

c *** wo = 0 result
      cfxw0xdh = ppxw0xdh - psi
c ***
      rppw0 = 4.0*pi*ppxw0xdh*9.0e17/wpe
      rhow0dh=4.0*pi*cfxw0xdh*9.0e17/wpe

      omult=ppxw0xdh/cfxw0xdh

      kmax = 10.0 * wra
      npick=nmax+2-jmax
      xl2=sqlei*kmax*kmax


c        No BRD term; V=Deutsch

        if (wra .ne. 0.0) then
         call tromb(nmax,0.0,kmax,dhfunc,rtable,jmax,ndim)
         zerokmax=rtable(npick,jmax)
        else
         zerokmax=0.0
        endif
c          add analyltic part from kmax to inf * phi(l=inf) for DH case
        xtemp=alog((gam2+xl2)/(one+xl2))
        dhlaminf=-xtemp/2.0/(one-gam2)
        kmaxinf=phiinf*dhlaminf
        ppxdh=cxppxdh*(zerokmax+kmaxinf)
        rhoxdh = 4.0*pi*ppxdh/omult*9.0e17/wpe


c        BRD term with V=Coulomb

        if (wra .ne. 0.0) then
         call tromb(nmax,0.0,kmax,dhcbrd,rtable,jmax,ndim)
         zerokmax=rtable(npick,jmax)
        else
         zerokmax=0.0
        endif
c         add analyltic part from kmax to inf * phi(l=inf) for DH case
       balf=hbar/aion/8.0/me/terg/aion*hbar
       sqkda=balf*kd2
       sqkmaxa=balf*kmax*kmax
       dhlaminf=expel(sqkda+sqkmaxa)*exp(-sqkmaxa)/2.0
       kmaxinf=phiinf*dhlaminf
       ppxdhbr=cxppxdh*(zerokmax+kmaxinf)
       rhoxdhbr = 4.0*pi*ppxdhbr/xmult*9.0e17/wpe


c       Put a floor on the rho calculation: use Boercker, Rogers, DeWitt result
c       if in string coupling (GAMMA > 1/2 - this is approximate) and 2 Sonine
c       result in error (omult < 0).  Change to BRD result when our result
passes
c       through BRD result.
c
      if ( (gamei .gt. 0.5 ) .and.
     >    (omult.le.0.0 .or. (rhoxdh .lt. rhoxdhbr))) then
       rhodh = rhoxdhbr
       cfdh = ppxdhbr/xmult
      else
```

```
       rhodh = rhoxdh
       cfdh = ppxdh/omult
      endif

      return
      end

c
*******************************************************************************

      real function phi(k)
      real k,kd2
      common /dhcom/ wra,vr,sqlei,kd2,sq2,sqpi2,epsphi,floorxk
      data one/1.0/
      ratio=vr/(wra/k)
      if(ratio .le. epsphi) then
       phi=2.0/3.0*exp(-wra**2/2.0/k**2)
       return
      endif

      xp=(wra/k+vr)/sq2
      xm=(wra/k-vr)/sq2
      expp2=exp(-xp*xp)
      expm2=exp(-xm*xm)
      phi1=sqpi2*(erflocal(xp)-erflocal(xm))*(one+(wra/k)**2)
      phi2=(expp2-expm2)*wra/k
      phi3=-(expp2+expm2)*vr
      phi=(phi1+phi2+phi3)/vr**3
      return
      end

c
*******************************************************************************

      real function dhfunc(k)
      real k,kd2,me
      common /dhcom/ wra,vr,sqlei,kd2,sq2,sqpi2,epsphi,floorxk
      common /dhcom2/ hbar,terg,me,aion
      data one/1.0/

      if(k .lt. floorxk) then
       dhfunc=0.0
       return
      endif

      dhcVL=k/(one+sqlei*k*k)/(k*k+kd2)
      phitemp=phi(k)
      dhfunc=dhcVL*phitemp
      return
      end

c
*******************************************************************************

      real function dhcbrd(k)
      real k,kd2,me
      common /dhcom/ wra,vr,sqlei,kd2,sq2,sqpi2,epsphi,floorxk
      common /dhcom2/ hbar,terg,me,aion
      data one/1.0/

      if(k .lt. floorxk) then
       dhcbrd=0.0
       return
      endif

      brdexp=-hbar*k*k/aion/8.0/me*hbar/aion/terg
      dhcVL=k/(k*k+kd2)
      phitemp=phi(k)
      dhcbrd=dhcVL*phitemp*exp(brdexp)
      return
      end

c
*******************************************************************************
```

```
      real function expe1(x)

c      returns the value of exp(x) * E1(x)
c      (have to watch out for large x)

       if(x .gt. 50.0) then
        x2=x*x
        x4=x2*x2
        poly=1.0-1.0/x+2.0/x2-6.0/x2/x+24.0/x4
        expe1=poly/x
        return
       endif

       expe1=exp(x)*e1local(x)
       return
       end

c
*************************************************************
      real function e1local(x)
c
c     Returns exponential integral of the first kind.
c     Abramowitz & Stegan p. 231.
c
      dimension a(4),b(4),c(6)

      data c /-.57721566, .99999193,-.24991055,
     >         .05519968,-.00976004, .00107857/
      data a / 8.5733287401,18.0590169730,
     >         8.6347608925,  .2677737343/
      data b / 9.5733223454,25.6329561486,
     >        21.0996530827, 3.9584969228/

      if(x.le. 0.0) then
      write(*,100)
  100 format(' argument of E1 < or = zero)')
      stop
      endif

      if(x.le. 1.0)then
      e=c(6)*x+c(5)
      do 10 i=4,1,-1
      e=e*x+c(i)
   10 continue
      e1local=e - alog(x)
      return
      endif

      enum=x+a(1)
      eden=x+b(1)
      do 20 i=2,4
      enum=enum*x+a(i)
      eden=eden*x+b(i)
   20 continue
      e1local=enum/eden*exp(-x)/x
      return
      end

c
*************************************************************************************

      REAL FUNCTION ERFLOCAL(X)
c
c     RETURNS ERROR FUNCTION.  SEE ABRAMOWITZ & STEGAN.
c
      DIMENSION A1(16),A2(16)
c
c        DOUBLE PRECISION ERROR FUNCTION FOR REAL ARGUMENT
c        RF. A. STREOCK, J COMP PHYS ((??), CIRCA 1966
c
      DATA PI/3.14159265358979238E0/
      DATA A1/0.703225002743775E0,0.330501521916606E0,
     &        0.201339747264706E0,0.108630245022740E0,
     &        0.046775523432484E0,0.015398572615710E0,
     &        0.003801507679852E0,0.000697183792408E0,
     &        0.000094490926881E0,0.000009432811698E0,
     &        0.000000691927520E0,0.000000037225234E0,
```

```
     &        0.000000001466606E0,0.000000000042261E0,
     &        0.000000000000889E0,0.000000000000013E0/
C
      DATA A2/0.247255168140052E0,0.144227226361574E0,
     &        0.086989454995934E0,0.043977338194083E0,
     &        0.017243962588662E0,0.005079069612202E0,
     &        0.001108606453423E0,0.000178228016254E0,
     &        0.000021040458307E0,0.000001820663163E0,
     &        0.000000115330990E0,0.000000005342750E0,
     &        0.000000000180848E0,0.000000000004469E0,
     &        0.000000000000080E0,0.000000000000001E0/
C
      IF(X.GT.6.0)GO TO 9
C
      XPT4=0.4E0*X
      S=SIN(XPT4)
      C=COS(XPT4)
      ALPH=2.0E0*C*C-1.0E0
      SUM=0.0
      DO 1 N=1,16
    1 SUM=SUM+ALPH**(N-1)*(A1(N)+2.0*C*A2(N))
      ERFLOCAL=XPT4/PI+S*SUM
      RETURN
    9 ERFLOCAL=1.0E0
      RETURN
      END

C
*******************************************************************************

      SUBROUTINE TROMB(NMAX,A,B,F,T,JMAX,NRC)
C
C     RETURNS ARRAY T WITH ROMBERG EXTRAPOLATION INTEGRATION OF FUNCTION F
C      WITH LIMITS (A,B).  SEE CARNAHAN, LUTHER, & WILKES.
C
      DIMENSION T(NRC,NRC)
      H=B-A
      T(1,1)=(F(A)+F(B))*H/2.0
      DO 2 N=1,NMAX
      T(N+1,1)=0.0
      FR=H/2.0**N
      IMAX=2**N-1
      DO 1 I=1,IMAX,2
    1 T(N+1,1)=T(N+1,1)+F(FLOAT(I)*FR+A)
    2 T(N+1,1)=T(N,1)/2.0+H*T(N+1,1)/2.0**N
C
      DO 3 J=2,JMAX
      NX=NMAX-J+2
      FOR=4.0**(J-1)
      DO 3 N=1,NX
    3 T(N,J)=(FOR*T(N+1,J-1)-T(N,J-1))/(FOR-1.0)
C
      NMAXP1=NMAX+1
      DO 4 N=1,NMAXP1
      JM=JMAX
      IF(N.GT.NMAXP1+1-JMAX) JM=NMAXP1+1-N
    4 CONTINUE
      RETURN
      END
```